Fire Detection using RF Signals

by

Kai Ma

A thesis
presented to the University of Waterloo
in fulfillment of the
thesis requirement for the degree of
Master of Mathematics
in
Computer Science

Waterloo, Ontario, Canada, 2023

Author's Declaration

I hereby declare that I am the sole author of this thesis. This is a true copy of the thesis, including any required final revisions, as accepted by my examiners.

I understand that my thesis may be made electronically available to the public.

Abstract

Structural fires can be a major threat to life and property. Contemporary smoke alarms suffer from drawbacks such as long response times, lack of penetration through walls, and nuisance (false-positive) alarms. In this thesis, we examine the feasibility of using RF signals for fire detection. We focus on RF signals in the 5 GHz frequency band in the first part of the thesis, which corresponds to the same frequencies that have been used in previous research on Wi-Fi fire detection. We then move on to the 28 GHz frequency band since there is some existing work on fire detection using millimeter wave (mmWave) signals at 77 GHz. We would like to adapt the technique to 28 GHz mmWave 5G signals because, in theory, 28 GHz signals would have better propagation properties than 77 GHz signals and could provide better range and coverage.

For RF signals at 5 GHz, a Virtual Network Analyzer (VNA) is used to study the impact of fire on the signals. The signal strength and phase are recorded in each round of the experiments. We observe only moderate changes in the signal strength and phase from heptane fire when the distance between the two antennas of the VNA is small (1.3 meters). However, the impact of heptane fire becomes imperceptible when we conduct the same experiment with a longer distance between the two antennas (3 meters). We also study the impact of wood fire and smoke at a distance of 3 meters. The fire itself does not have any noticeable impact on the signal strength or phase, but the dense smoke generated after the fire is extinguished results in significant changes in both signal strength and phase. After comparing the magnitude of changes in the signals from the VNA with the fidelity of commodity Wi-Fi devices, we think it is unlikely that the Wi-Fi devices used in previous work could be used to detect fire at a distance that would be practical in real deployments. In a previous study by Zhong et al. [84], the authors only show data from 1 second before to 1 second after the fire starts. We believe that the changes in signals they observe may be caused by the movement of the person who lights the fire. We also conduct some simple experiments to help support this theory.

We examine the feasibility of using mmWave RF signals for fire detection by starting a fire between a 5G base station and a mobile device, both of which operate in the 28 GHz (mmWave) band. We consider several metrics available on the mobile device, including RSRP PRX, RSRP DRX and RSSI. We then conduct experiments using 3 different distances between the base station and the mobile device (3, 28, and 60 meters). Unfortunately, we are unable to observe any patterns in RF signal changes that correspond to the time when the fire is burning in any of the 3 scenarios. Additionally, the RSSI value does not change in any of our experiments due to how it is reported on the mobile device. We conclude that the 5G device used in our experiments may not be suitable for fire detection.

Acknowledgements

Firstly, I would like to express my sincere gratitude to my supervisor, Tim Brecht. His guidance throughout my Master's program and insightful feedback on my thesis have been invaluable. His support has also helped me navigate through the most challenging times in the project. Working with him has undoubtedly been the most enriching experience in my life.

I would like to thank George Shaker not only for his generosity in loaning the equipment for our experiments but also for his expertise and insights in the related research area. I also extend my thanks to Samer Al-Kiswany for taking the time to review my thesis and for hosting the seminar where the thesis was presented.

I am also grateful to Charlie Liu, Kamran Nishat, Manoj Adhikari, and David Radke for their help during the experiments.

Additionally, I thank Rogers Communications Inc. for the 5G equipment and funding that helped with the completion of the thesis.

I would like to thank Beth Weckman and her students for providing us with access to the fire lab facilities and help with experiments.

Lastly, and most importantly, I am indebted to my parents who selflessly supported my studies both mentally and financially over the years. I would also like to thank Qixuan for her company and encouragement throughout this process. I dedicate this thesis to them.

Table of Contents

List of Figures

List of Tables

Chapter 1

Introduction

1.1 Problem Statement

The primary goal of this thesis is to understand the impact of fire on RF signals. In this thesis, we focus on RF signals in two specific frequency bands: 5 GHz and 28 GHz. For each frequency band, we first review the previous work done in the related fields and then conduct experiments to study the impact of fire on RF signals. We evaluate changes in RF signals due to fire by using controlled fires at various distances and compare the changes with those caused by human movement and variability that occurs naturally in different environments.

1.2 Background and Motivation

Structural fires can be a major threat to life and property. According to the National Fire Protection Association, each year in the United States, structural fires cause over 2,500 deaths and $7.2 billion in property damage [5] even though smoke alarms have been installed in 96% of all households [4]. Contemporary smoke alarms still suffer from high response time, lack of penetration, and nuisance (false-positive) alarms. The response time for a typical home smoke alarm is 150 seconds in a kitchen environment [24] since it takes time for the smoke to reach the alarm. It may take even longer if the fire starts in a different room than where the smoke alarm is installed, or if there are obstacles like walls and closed doors between the fire and the alarm. Such delays in alarms leave less time for people to exit the building. Moreover, the major cause of casualties in structural

fires is smoke inhalation rather than contact burns [31]. This is because the smoke may contain toxic gas generated by furniture burning and the high temperature of the air can cause permanent damage to the respiratory system. Since typical smoke alarms can only be triggered when the smoke reaches the sensor [24], when a smoke alarm goes off, the fire and smoke in the rest of the building may pose a significant threat to the life of the occupants. Therefore, a faster, reliable indoor fire detection method is needed to help identify fire earlier and promptly activate alarms to alert occupants.

Fire detection using radio frequency (RF) signals has been studied over the last few decades [84, 47, 63, 51, 32]. An advantage of this method is that it does not require fire or smoke to reach the detector before triggering the alarm, which may reduce the response time and improve coverage. This type of device regularly polls one or more metrics of the RF signals and triggers an alarm whenever it identifies a pattern of variation that is possibly caused by fire. RF signals at a certain frequency range can also penetrate walls, making it possible to detect non-line-of-sight (non-LoS) fires behind some occlusions [63]. In this thesis, we examine the possibilities of using RF signals to detect fires at two frequency bands (the 5 GHz Wi-Fi band and the 28 GHz millimeter wave 5G network band). Our work is inspired by previous work on Wi-Fi fire detection [84, 47] and mmWave fire detection [63, 51, 32]. We conduct a series of experiments to examine the feasibility of using RF signals for fire detection at these frequency bands.

In 2017, Zhong et al. [84] used commodity Wi-Fi access points to detect fire between transmitting and receiving devices by monitoring the Channel State Information (CSI) of the Wi-Fi network on the receiver side. The CSI measures the signal strength and phase for all the subchannels in the Wi-Fi network, which contains more information than other commonly used signal strength indicators like RSSI. However, due to the absence of a universal standard for how CSI is calculated and reported, the interpretation of CSI is manufacturer specific and thus it remains unclear precisely how and why fire affects Wi-Fi signals. After reviewing the experiments in their work, we find some inconsistencies in the experimental results. The CSI amplitude, which is the main indicator used in their work, decreases after the fire starts in one scenario but increases when the Wi-Fi devices are moved farther apart. Such inconsistency seems odd since it seems unlikely that the fire would have a different impact on the CSI when the only variable changed in the experiment is the distance between the fire and the detection device. More importantly, the figures in their work only show 2 seconds of data (1 second before the fire starts and 1 second after), which does not seem like enough time for the person to leave the FoV of the device after lighting the fire. Therefore, there is some concern that the changes they observe may be caused by the movement of the person who lights the fire instead of the fire itself. In this thesis, we use a Vector Network Analyzer (VNA) to directly measure the changes in signal

during the transmission of RF signals in the 5 GHz Wi-Fi band. We create a controlled fire between the transmitter and the receiver to capture and study variations in the signal strength and phase. Since the VNA device can directly report the values of the signal strength and phase with much higher precision than the CSI values obtained from a Wi-Fi device, we expect to obtain more details and insights into the impact that fire has on the propagation of RF signals in the 5 GHz Wi-Fi band. In addition, we create a methodology for running experiments that minimizes the unrelated factors that might affect RF signals (e.g., changes due to the person who lights the fire).

Besides fire detection with Wi-Fi devices, millimeter wave (mmWave) technology has also been widely used in object detection and wireless sensing. Radke et al. [63] introduce a fire detection method using a 77 GHz mmWave radar device. It is worth noting that the mmWave radar device was not designed for fire detection but rather for object detection. Radke et al. extract the received signal strength from the radar device and use changes in the signal as the main indicator of fire. A neural network is trained with data collected from the radar device in both fire and non-fire environments. The resulting model is then used to determine the presence of fire. Our interest in this work is in trying to determine if RF signals may be impacted by fire in ways that could be detected on devices that operate in the mmWave range. A question we study is whether or not it might be possible to leverage changes in the cellular signals to detect fire that occurs between the base station and the mobile device. In particular, we explore the potential of using 5G mobile devices that operate in the 28 GHz band for fire detection.

1.3 Contributions

The contributions of this thesis are as follows:

Reviewing Previous Work on Wireless Fire Detection

We examine the previous work done in wireless fire detection with RF signals at various frequency bands, including microwave, Wi-Fi, and mmWave. The frequency of the RF signals that the device uses influences the potential coverage and penetration capabilities. Fire detection devices can be classified into two categories: receive-only devices and transmit-receive devices. The former detects fire by receiving RF signals emitted by fire and triggers the alarm when the received signal strength exceeds the threshold. The latter actively transmits and receives RF signals and monitors any changes in the properties of received signals. A fire detection algorithm is then needed to distinguish any changes due

to fire from those due to other factors (e.g., the movement of a person). We describe the advantages and disadvantages of each type of device in Chapter 2. The focus of our experiments is the signal strength and phase of RF signals because we find that they are the key indicators commonly used in previous work.

Examining the Impact of Fire on RF Signals

Since the Wi-Fi access points proposed in previous work [84, 47] were not initially designed for fire detection, there is a lack of understanding of the underlying cause of the changes in the RF signals in the presence of fire. We conduct experiments with heptane fire and measure the changes in the signal strength and phase of RF signals in the 5 GHz frequency band using a VNA device with much higher fidelity than a Wi-Fi access point. Our experiment results indicate that for the specific frequency range (5.166 - 5.168 GHz), moderate changes can be observed due to fire but only at a relatively close range (1.3 meters). The changes become insignificant when we increase the distance between the transmitter and the receiver to 3 meters. Given the fidelity of commodity Wi-Fi access points and the VNA device used in our experiments, it would be difficult for commodity Wi-Fi devices to detect fire at longer distances. We also suggest some methods that could be used to mitigate drawing false conclusions due to unrelated factors and to improve the reliability of the results when designing fire experiments.

Examining the Impact of Smoke on RF Signals

In addition to the heptane fire experiments, we also use the VNA device to measure changes in RF signals with wood-burning fires. Compared to heptane fires, wood can generate more smoke while it is burning and even after the fire is extinguished. Although fire and smoke from burning wood have no observable impact on RF signals, we discover that a high concentration of smoke after the fire is smothered has a significant impact on RF signals. We observe a decrease in the signal strength and a phase shift when signals travel through the smoke. Therefore, wireless signals may be useful for detecting fires from materials that can generate dense smoke in households (e.g., mattress and couches).

Exploring Fire Detection with mmWave 5G Signals

We design and conduct experiments with controlled fires to explore the feasibility of fire detection with 5G mobile devices in the 28 GHz frequency band. Similar to Wi-Fi fire

detection studies, the question being explored is whether it might be possible to detect fire that occurs on the direct path between the base station and a mobile device by observing changes in the RF signals. We first select several available signal metrics from the documentation of the 5G device we use. We then narrow those metrics down to RSRP PRX and RSRP DRX based on the results of experiments with a person's movement. The changes in these two metrics match the pattern of the movement. We also notice that one potential metric, RSSI, is not useful due to how it is reported. The RSSI is mapped to the same value when the signal is stronger than a threshold. We record the changes in each metric with controlled fire and analyze the data. However, we are unable to identify any significant changes in these metrics when the fire is burning. There are also no consistent changes across multiple trials of the same experiment with fire.

1.4 Thesis Outline

The rest of the thesis is structured as follows. In Chapter 2, we present and review the related work on wireless fire detection. We study the impact of fire on RF signals in the 5 GHz frequency band using experiments with a VNA device in Chapter 3. We then conduct more experiments with a 5G device to explore the feasibility of using a mmWave 5G device operating at 28 GHz to detect fires in Chapter 4. Finally, we conclude the thesis and introduce possible future work in Chapter 5.

Chapter 2

Related Work

2.1 Fire Detection using Wireless Signals

The process of fire detection is essentially monitoring some indicators of fire and triggering the alarm when they reach a certain threshold. The selection of indicator(s) will determine the level of difficulty and accuracy for fire detection. For example, smoke can be used as an indicator of fire since it is generated in most structural fires. Smoke alarms are the most common fire detection device for households, with 96% of all US households having at least one smoke alarm installed [4]. Other types of fire detectors based on infrared and visible light have also been used to monitor forest fires [81]. However, they are not as popular as smoke detectors in households due to high costs and the inability to penetrate obstacles like walls [14]. Despite the high installation rate of smoke alarms, there are still some drawbacks that constrain their performance:

- **High response time:** Contemporary smoke alarms usually consist of one or multiple types of sensors that measure the density of particles produced by fire [4]. Thus, a smoke alarm can only be activated when enough particles reach the sensor. Typical smoke alarms have an average response time of 150 seconds [24] in a kitchen environment. However, by that point the fire may have already spread beyond the room where the alarm was triggered, leaving less time for the occupants to escape from the building.
- **Lack of penetration:** In structural fires, smoke inhalation is a major threat to people's lives [31] due to the high temperature and the toxic gas produced during the

combustion process [70]. Smoke can be blocked by walls and closed doors, making it harder to detect fires that start in another room when the door is closed. Thus, each room with potential fire hazards must have at least one detector to ensure proper coverage for the building. Radio signals have the potential to better penetrate obstructions [28], which would improve alarms in environments with occlusions and could reduce the cost of installing multiple detectors.

- **Nuisance alarms:** A nuisance (false-positive) alarm occurs when the alarm goes off when there is actually no fire in the room. These alarms not only disturb daily life but they also degrade the urgency felt by occupants when a real fire occurs. A survey from 2010 shows that 43% of the households in the United States have experienced their fire alarms going off in the previous year, with 73% of them being nuisance alarms caused by cooking [4]. Furthermore, nuisance alarms can also put stress on the local fire department if they have to search through the building and verify that there is no fire while these resources could have been dispatched to other locations with real fires. Therefore, a more reliable fire detection solution is needed to distinguish structural fires from daily activities.

Apart from typical indicators of fire like smoke [22], toxic gas [35], infrared rays (IR) [73, 14], and visible light [23, 53], wireless signals at microwave [12, 11, 45, 54] and millimeter wave (mmWave) [63, 51, 32] frequencies have also been proposed for use in fire detection.

The use of wireless signals and devices to detect fire can be roughly classified into two categories: receive-only devices [12, 11, 45, 66] and transmit-receive devices [54, 84, 47, 63]. The former is based on the thermal radiation generated from high-temperature objects and measures the RF signals emitted by fire in the surrounding environment [26]. The latter is based on the fact that fire attenuates [55, 79] and/or reflects [68] electromagnetic waves. The fire detection devices constantly monitor changes in the received signals and search for any abnormal patterns that could be attributed to fire.

2.2 Microwave Fire Detection

Previous work on fire detection with microwave signals has revealed that fire may emit [45] and/or reflect [54] RF signals in the microwave band. Based on these findings, microwave radiometers have been built for detecting fires on moving trains and in forests by receiving the signals generated by fire at 12 GHz [11] and 30 GHz [12, 45]. In addition, Masoumi et al. [54] propose an alternate method that uses a pair of transmitting and receiving antennas

and a Vector Network Analyzer (VNA) to analyze and detect the reflection of microwave signals on the ionized electron cloud from the combustion of plant leaves. The device is able to observe changes in the reflected signal in the 0.1 to 0.5 GHz spectrum. It is worth noting that these experiments are either conducted outdoors [12, 45] or inside a laboratory environment [11, 54]. It is unclear whether their method will work in a home or office environment to replace typical fire and smoke detectors. However, they provide hope that one may be able to detect fire with other devices that transmit and receive RF signals like Wi-Fi access points or 5G mobile devices. The key is to measure the changes in the signal and identify any abnormal patterns related to the presence of fire. In this thesis, we focus on trying to understand if fire changes the signal used by 5 GHz Wi-Fi devices and 28 GHz 5G devices in ways that could demonstrate the suitability of these devices for use in fire detection.

2.3 Wi-Fi Fire Detection

Wi-Fi Subcarriers

The 802.11 Wi-Fi standards use channels to allow more devices to operate in the allocated frequency band without interfering with each other. More recent Wi-Fi networks like 802.11a/n/ac networks use Orthogonal Frequency Division Multiplexing (OFDM) [49, 40] technology to further split a channel into subchannels (subcarriers) to increase the total throughput and to help improve tolerance of interference from other devices communicating using nearby frequencies. Each subcarrier is linearly spaced in the channel with a narrow frequency bandwidth. For example, a channel with a 20 MHz bandwidth in the 802.11ac network can have 64 subcarriers. Thus, the width of each subcarrier is 0.3125 MHz (or 312.5 KHz), which is much smaller than the total bandwidth of the channel. Later in Chapter 3, we will use subcarriers to study the impact of fire in the 5 GHz Wi-Fi frequency bands.

RSSI and CSI

The Received Signal Strength Indicator (RSSI) [58] is a widely-used indicator for signal strength in wireless communication systems, including Wi-Fi and cellular networks. RSSI is a measure that indicates the signal strength between the the transmitter and receiver. It can also sometimes be used as a rough estimate of the distance between transmitter and receiver since the power of the signal decreases exponentially as the distance between the two devices increases [74]. The value of RSSI is often reported in decibel-milliwatts (dBm),

which means the power level in decibels (dB) relative to one milliwatt (mW). The formula for converting the power P in mW to power level x in dBm is:

$$x = 10 \log_{10} \frac{P}{1 \text{ mW}}$$

Thus, a 10 dBm change in the power level corresponds to a 10-fold increase in power and a -10 dBm change in the power level corresponds to a reduction to $\frac{1}{10}$ of the original power.

RSSI is reported as a single value that represents the overall signal quality in 802.11 networks. To get more information about the quality of the network, Channel State Information (CSI) [52, 48] is sometimes available to provide more insights into the status of each subchannel (subcarrier) in the network. Compared to RSSI, CSI contains both the signal strength and phase information for each subchannel. The signal strength in CSI represents the power level of the received signal in dBm on the Wi-Fi device. Since Wi-Fi signals are sinusoidal, the phase information represents the angular position of the signal at a particular time. In CSI, the phase information measures the phase shift (difference in angular positions) of the signal when propagating from the transmitter to the receiver. Depending on the complexity of the environment, the signal may reflect off different surfaces (e.g., walls, windows) before reaching the receiver. Thus, the phase shift of the signal can provide useful insights into the reflection and multi-path effects that the signal has experienced during propagation.

Fire Detection

In some recent studies using Wi-Fi signals [84, 47], the signal strength of 5 GHz networks has been reported to be affected by fire, which makes it possible to detect fire between an access point and a device that connects to the network. CSI is used as a main indicator of fire in both papers.

In work conducted by Zhong et al. [84], the CSI information is collected using an Intel Link 5300 Wi-Fi network card [25], which has a resolution of 1 dB [48]. The authors use a TP-Link DWR 7500 Wi-Fi router as the transmitting device. The router is configured to operate in 802.11n [30] AP mode in the 5 GHz band. The exact channel index and frequency range are not specified in their paper. The raw data for signal strength is then recorded and processed to obtain the CSI amplitude by running a series of feature extraction algorithms including Principal Component Analysis (PCA) [3]. The authors observe changes in the CSI amplitude right after the fire is started. A Random Forest [17] machine learning model is then trained using the CSI amplitude along with changes in

phase information to determine whether there is fire occurring in the FoV of the device. The maximum coverage tested in their work is 4 meters in an office environment. The fire is started in a container approximately halfway between the transmitter and receiver. The container is at the same height as the transmitting and receiving devices. The exact size of the fire and fuel type are not provided in the paper. However, from the pictures, the fire burns in a container with a diameter of about 50 cm. Unfortunately, the authors only show 2 seconds of data for the CSI amplitude (1 second before the fire starts and 1 second after). The short time shown only near the start of the fire is not long enough for the environment to stabilize from the perturbation that would be caused by the person who lights the fire. Furthermore, across the four rounds of experiments they mention in their work, the CSI amplitude decreases in one scenario after the fire starts but increases in the others. There is a lack of explanation in their work about why fire would influence the signals differently, while the only variable that changes in their experiments is the relative positions (distance and angle) between the fire and the Wi-Fi devices.

Li et al. [47] also introduce a method for detecting fire between a pair of Raspberry Pi 4B [59] devices. The Wi-Fi signals are transmitted and received by the built-in wireless chip (Broadcom BCM43455 [18]) on the Raspberry Pi devices. The Wi-Fi devices are configured to operate in 802.11ac [30] mode on channel 36 centered at 5180 MHz with a bandwidth of 80 MHz. The resolution of the signal strength obtained from the wireless chip is reported to be 3 dB [18]. Similar to Zhong's work [84], the authors also use the CSI amplitude as an indicator of fire, which is collected by the Nexmon CSI tool [67, 33] on the receiver. Instead of using a feature extraction algorithm on all subcarriers, they examine the changes in each subcarrier separately and find that there is an increase in the variability of the CSI amplitude after the fire is started. The authors conduct two sets of experiments with different types of fuels. Both experiments are conducted in an indoor environment. In the former experiment, the transmitter and receiver are placed 60 cm apart, with a butane stove in the middle with the fire and both devices at the same height. The diameter of the fire on the butane stove is not given by the authors, but it appears to be about 10 cm (judging by the photos in their paper). Although the authors claim that they observe differences in the mean values of CSI amplitude during the period of time before and as the fire is burning, the estimation errors of the two mean values overlap with each other. Therefore, their findings differ from the work by Zhong et al. [84] as they were not able to see significant changes in CSI when using the butane stove. In the latter experiment, the two Wi-Fi devices are placed 90 cm apart, with an Aluminium Composite Panel (ACP) in the middle at the same height. There is also a torch lighter aimed at the ACP to start the fire. The authors show the changes in CSI in each subcarrier of the Wi-Fi network while the ACP is burning. A potential problem with using this material for fire experiments is

that the ACP deforms while it is burning, which may change the CSI since the occlusions and signal paths between the transmitting and receiving device may be altered as the ACP deforms. Therefore, it is unclear how much of the changes they observe are from fire or the deformation of the material. Also, this experiment does not show the CSI information for the environment without fire since the torch lighter is burning throughout the experiment. So an open question is how fire changes the signal relative to when there is no fire.

The tests conducted in the papers discussed above [84, 47] only cover situations where the fire is near (up to 4 meters) the Wi-Fi devices and there are no occlusions between the two Wi-Fi devices despite the fact that Wi-Fi access points could operate at larger distances and the signals can penetrate obstacles like walls. It would be helpful to test the maximum coverage of fire detection using Wi-Fi signals, which is an important factor to consider when comparing the performance of different fire detectors. Most importantly, neither of these studies examines the reliability of the system in a non-static environment (e.g., with the movement of people). This is critical because it is an important factor that affects the CSI of Wi-Fi signals. In fact, in other research [78, 85], CSI has been used for indoor localization of people. Since both fire and people (and their movement) can affect the signal, an important component missing in their work is to distinguish fire from daily activities in households. Therefore, some open questions left from previous work on Wi-Fi fire detection are as follows:

- Is the change observed in their work really from the fire?
- What coverage is possible when using Wi-Fi devices for fire detection? Is it sufficient to make the use of such devices practical in households?
- Is it possible to distinguish the changes due to fire from those caused by the movement of the person who starts the fire?

In Chapter 3, we examine the first two questions. We use a VNA device to formally study the feasibility of using Wi-Fi signals in fire detection because it has much higher fidelity than Wi-Fi devices. If changes in the RF signals at 5 GHz are successfully observed in the presence of fire, we will then examine the range at which Wi-Fi signals are affected and the suitability of using Wi-Fi signals for fire detection.

2.4 Millimeter Wave Fire Detection

Millimeter Wave Sensing

In recent years, mmWave technology has been widely used in wireless sensing. There are two main types of mmWave radar devices in general: pulsed wave radar [29] and Frequency-Modulated Continuous Wave (FMCW) radar [44]. Pulsed wave radar devices send a short pulse and measure the round trip time to locate an object. This mechanism limits the sample rate of pulsed wave radar devices since they have to wait for the arrival of the reflected pulse (or reach the pre-defined timeout period) before the next transmission. FMCW radar devices resolve the problem by transmitting a continuous signal with varied frequencies (e.g., linearly increasing over time) and comparing the frequency differences in the transmitted and received signals [42]. This allows FMCW radar devices to achieve much higher sample rates and accuracy than traditional pulsed wave radar devices [44]. Recent work on mmWave radar object sensing [51, 32] and fire detection [63] have focused on using FMCW radars over pulsed wave radars.

Various applications have been built based on mmWave radar devices, including human detection [39] and gesture recognition [50]. They have also been used in autonomous vehicles [43, 72, 76]. Compared to optical sensors like video cameras [19, 8] and LiDAR [75, 20], mmWave radar devices can detect objects through smoke [51] and even walls [32], making them potential candidates for indoor fire detection. When travelling through smoke and fog, the attenuation of mmWave is much smaller than infrared rays and visible light [83, 7].

Fire Detection

In 1998, Sadovnik et al. [66] discovered that flames emit mmWave signals that can be captured by a specifically designed radiometer operating in the 90 to 94 GHz bands, which indicates the potential for using mmWave sensors in fire detection. Their work also discovered the patterns in received signal strength for fires started by various materials. The prototype device used in their research can detect a $0.3\,\text{meter} \times 0.3\,\text{meter}$ fire at $91.4\,\text{meters}$ even in the fog. Since the device is passively receiving signals from fire, the fire detector is unable to determine how far the fire is from the device. There is also a lack of indoor experiments to test the performance of the fire detector for indoor scenarios with obstacles in the FoV.

Besides mmWave radiometers, Radke et al. [63] observe changes in the received signal strength using a commodity 77 GHz mmWave radar device [41]. A neural network is

trained using days of data collected in environments with and without fire to detect fire in the device's FoV. Since the device can distinguish signal strength at different distances, in theory, one could use the distance from the fire to the radar device to determine the location. The device achieved a maximum detection range of 7 meters. The average response time for tests at distances of 4 - 7 meters was 26 seconds and the average response time over all tested distances (1 - 7 meters) was 24 seconds. These times are much faster than contemporary smoke detectors [24] at similar ranges (147 and 128 seconds respectively [63]). The device also successfully detected non-LoS fires behind drywall in the same detection range (7 meters from the fire to the device). Although this mmWave radar approach shows promising results, the idea of using a neural network to determine the presence of fire does not provide any insights into how or why the RF signals change with fire. Another important question is the area that could be covered by a single device. This information is useful for determining how many devices need to be installed (e.g., in a house). The advertised detection range from the manufacturer of the 77 GHz mmWave radar device claims a range of 20 to 80 meters [69] depending on the configuration and range resolution.

It is also worth noting that, in general, the atmospheric attenuation of RF signals increases as the frequency increases [83, 37]. Figure 2.1 shows the relationship between the signal frequency and average atmospheric absorption in the mmWave range at sea level and 9150 meters altitude [1]. The x-axis indicates the frequencies and the corresponding wavelengths of the signals and the y-axis is the attenuation in dB per kilometer caused by the absorption of the atmosphere. It is worth noting that the y-axis is log-based. As one would expect, the overall trend of attenuation is increasing as the frequency increases. Thus, one might expect a better detection range when using devices at lower frequencies. However, there are some peaks near 23, 63, 130, 200, and 360 GHz due to the absorption characteristics of H_2O and O_2 in the atmosphere. For example, the peak at 63 GHZ means oxygen has a large contribution to the increase in attenuation of mmWave signals at that frequency. The attenuation of mmWave signals also depends on the altitude (e.g., the attenuation at 9150 meters altitude is significantly lower than attenuation at sea level for the same frequency) since air is thinner at higher altitudes. A larger gap between the two lines means the attenuation level is more sensitive to the change in altitude (i.e., the density of air). Although the experiments in this work are all conducted at similar altitudes in the same city (at an altitude of about 329 meters), it is worth noting that fire consumes oxygen and vaporizes water in the burning material during the combustion process. As a result, we suspect that there may be a change in the density of O_2 and H_2O in the area above the fire, which might cause similar attenuation changes as a change in altitude (but to a smaller degree). These previous results provide some evidence that perhaps fire detection could work with mmWave devices using a lower frequency (and possibly with larger range)

and motivates our study of 5G signals at 28 GHz frequency. In Chapter 4, we will examine the feasibility of using mmWave 5G signals in fire detection.

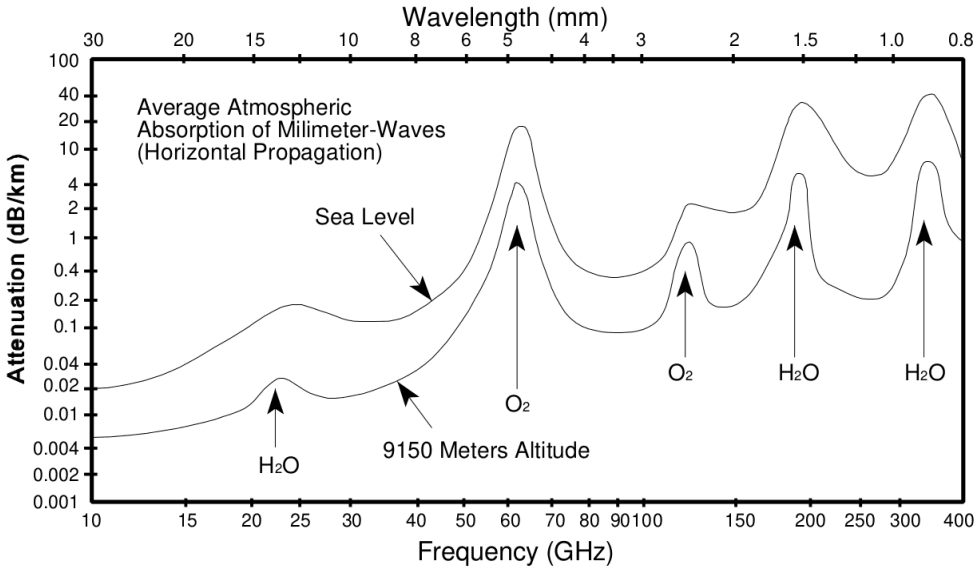

Figure 2.1: Atmospheric absorption of signals (Source: Naval Air Warfare Center, 1999, p. 5-1.1 [1]).

2.5 Physical Explanation of Wireless Fire Detection

In contrast with Section 2.4, the attenuation properties in a wildfire are different from atmospheric attenuation. Studies of forest fires conducted by Belcher et al. [15] and Mphale et al. [56] provide possible explanations for how fire could affect the propagation of RF signals. Both studies use transmit-receive devices to analyze the changes in RF signals from vegetation fuels. In Belcher's work [15], the authors use an oscilloscope and place the transmitter and receiver on different sides of the burning chamber, while Mphale et al. [56] use a network analyzer with a similar setup. Both studies conduct experiments with only a small sample of the vegetation fuel to study the attenuation properties of RF signals. They explain that the various kinds of metallic salt (e.g., Potassium and Calcium salt) in vegetation produce ions during a wildfire, which intensifies the attenuation of electromagnetic waves. Their experiments also indicate that the attenuation is inversely proportional to the square of frequency. Thus, signals with higher frequencies will be impacted by fire to a smaller degree than signals with lower frequencies. These findings provide theoretical

support for wireless fire detection applications. They also seem to indicate that RF signals at lower frequencies may work better in fire detection. We conduct experiments with both 5 and 28 GHz RF signals to examine their suitability for fire detection.

2.6 Fire Detection with 5G Networks

As the next generation of cellular communication technology, fifth-generation (5G) networks are expected to provide high-bandwidth and low-latency network access for mobile devices [6]. Recent studies using 5G networks have focused on adapting channels in the mmWave spectrum to achieve unprecedented bandwidth of up to several Gbps [16, 2]. When it comes to fire detection, 5G networks are usually used to broadcast the information collected from other sensors with low latency [82]. Motivated by the previous work done on mmWave fire detection in Section 2.4 and the large changes in atmospheric attenuation at different altitudes shown in Figure 2.1 for the 28 GHz spectrum, we believe it would be interesting to examine the possibility of using mmWave 5G signals at 28 GHz to detect changes in signals due to fire. If possible, 5G base stations and mobile devices could be used as both fire detectors and alarms that notify people when a fire occurs between the base station and mobile device. To the best of our knowledge, our research is the first to focus directly on using 5G 28 GHz signals in fire detection.

Chapter 3

Understanding RF Signals in Fire Detection

3.1 Motivation

3.1.1 5 GHz Wi-Fi Fire Detection

Apart from fire detection with RF signals at mmWave bands, previous work [84, 47] also proposes some methods for detecting fires using 5 GHz 802.11n and 802.11ac Wi-Fi networks. In those papers, changes in Channel State Information (CSI) [36] are used as the main indicator of fire. Unlike RSSI which only provides the signal strength, CSI reports both the signal strength and phase information for each subcarrier in the network. In this chapter, we use a Vector Network Analyzer (VNA) to provide an in-depth examination of changes in signal strength and phase in the 5 GHz band when fire is present between the transmitter and receiver. We use a VNA instead of a Wi-Fi access point in our experiments because a VNA can capture both the signal strength and phase information with much higher fidelity and finer granularity than Wi-Fi devices.

3.2 Methodology

Experiment Facility

The fire lab where we conduct all of the experiments in this chapter is located on the outskirts of town and is at a fair distance from any other buildings as shown in Figure 3.1. To minimize other signals that could be generated by Wi-Fi devices communicating on the same frequency band, we also turn off the Wi-Fi access point in the lab and disable Wi-Fi on all nearby mobile devices (e.g., smart phones, laptops, etc.). We use a Wi-Fi analyzer application to ensure that there are no Wi-Fi devices using the 5 GHz frequency band before we start the experiments.

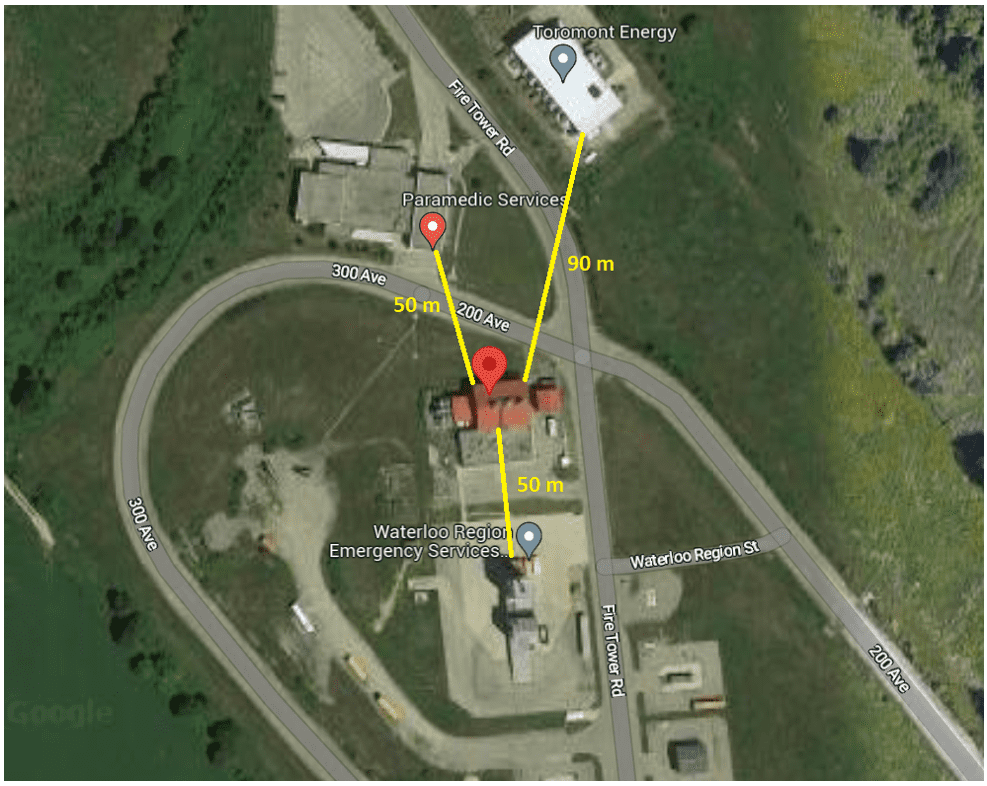

Figure 3.1: Satellite view of the experiment facility (Source: Google Maps). The red pin locates the facility where all experiments are conducted. It is at least 50 meters away from the building at the top of the image.

3.2.1 Experiment Setup

Hardware Setup

Figure 3.2 provides a high-level overview of the hardware devices and connections used. The VNA device is an Agilent E5071C ENA Vector Network Analyzer [46]. Two custom-made wideband dual-polarized Vivaldi antennas (0.5 to 18 GHz) are connected to the VNA using coaxial cables. The VNA device can achieve an accuracy of 0.01 dBm after calibration [46], which is much higher than commodity Wi-Fi devices (typically 1 dB [48]). Signals are transmitted from the antenna on the left side of Figure 3.2 to the antenna on the right. The position and direction of the antennas are calibrated before each set of experiments to ensure the signals are strong and stable on the VNA. A laptop is connected to the VNA through a USB port to monitor and collect data during the experiments. The VNA is configured to transmit signals by sweeping through frequencies in the range of 5.14 - 5.22 GHz. We specifically choose this frequency range to resemble the experiments conducted by Li et al. [47]. In their work, they claim to successfully detect fire using wireless signals on channel 36 using a bandwidth of 80 MHz in an 802.11ac network.

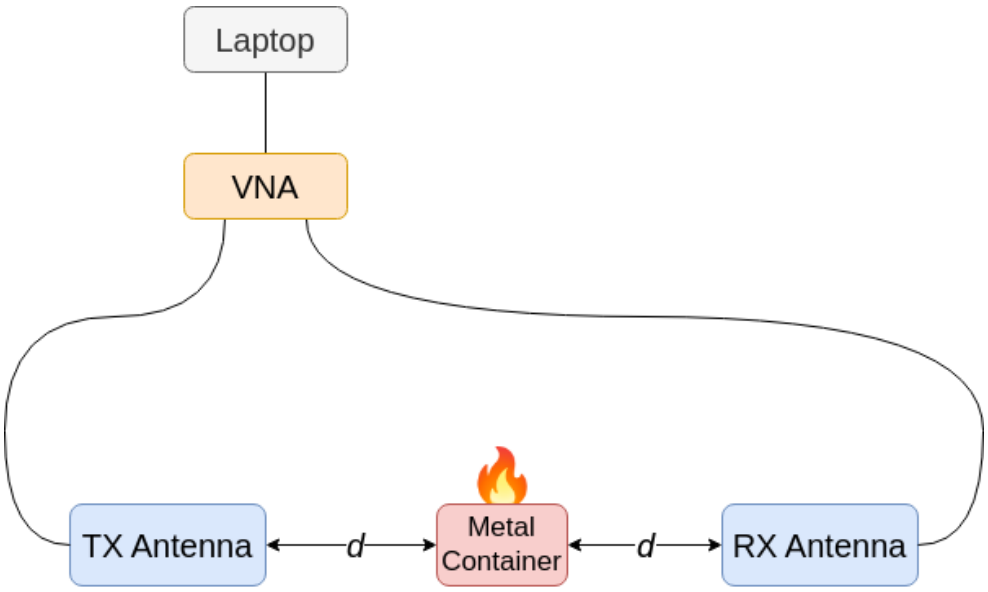

Figure 3.2: Hardware connection overview with the VNA. The distance d is from the fire to each antenna. We vary d for different experiments.

To start the fire, we use a 12 cm diameter metal pan with a 6 cm depth which is placed

halfway between the two antennas. The duration of the experiment is controlled by the amount of fuel placed in the metal pan. We use 100 milliliters of heptane for each round of the experiment. This burns at a height of around 50 cm above the pan. The fire lasts for approximately 3 minutes before the fuel runs out. Heptane is a highly flammable liquid that generates relatively low amounts of smoke while burning. We use a 1.5-meter metal pole with a match taped to the end to start the fire. This approach ensures the safety of the person who lights the fire and minimizes the movement of the person inside the FoV of the antennas. To start the fire in the metal pan, the person first lights the match on the long metal pole and then walks slowly toward the metal pan. After the person successfully ignites the fire in the metal pan, they immediately walk outside FoV. The above process may take approximately 5 - 10 seconds to finish. We use a timer to record the time when the person starts walking toward the metal pan and when the fire starts. However, the time could be off by a few seconds since the person starts from a location far from the metal pan and it is difficult to measure the exact time when the person enters and leaves the FoV of the antennas.

3.2.2 Baseline Experiments

To better understand and distinguish changes due to small variations in signals that occur naturally from those caused by fires, two rounds of baseline measurements are recorded before each fire experiment, each lasting for 1 minute. The baseline measurements use the same setup as the fire experiments, except without the presence of fire or the person who lights the fire. The averaged signal strength and phase from the baseline experiment are then subtracted from the raw data of the fire experiments to show the relative changes in the signals. This is done to test if changes due to fire are larger than those that occur naturally in the environment.

Within each set of fire experiments, two windows of time are also recorded before and after the fire. This allows us to again identify any natural variations in the environment before and after the fire and ensures that the changes we observe are actually caused by fire. Table 3.1 provides a list of events recorded during each experiment where fire is used along with their corresponding timestamps. We start recording signals on the laptop at time t_0 and wait for about 30 seconds to record some baseline data. Then at t_1, a person walks toward the metal pan with the 1.5-meter pole that helps to reach the liquid fuel. They light the fire as described in Section 3.2.1. The fire finishes burning at t_3 and we stop recording at t_4, providing some time to record and examine the signal after the fire is out.

Time	Event
t_0	Recording starts
t_1	Fire starts
t_2	Fire burning finishes
t_3	Recording stops

Table 3.1: Events during the VNA experiments with corresponding timestamps.

3.2.3 Data Collection and Processing

The VNA is configured to sweep through the frequency range approximately 10 times per second and to collect both signal strength and phase information. The VNA samples 201 data points for each sweep (frame), with each data point evenly spaced in the frequency band. Since the total sweeping range is 80 MHz (5.14 - 5.22 GHz), the spacing between two data points is 0.4 MHz. We implement a MATLAB script with the Virtual Instrument Standard Architecture (VISA) library [71] to record and store raw data on the laptop in the form of an $m \times n$ matrix, where m is the number of frames in the experiment and n is the number of data points in each frame. Each recording consists of two $m \times n$ matrices, one for the signal strength (M_{ss}) and the other for the phase (M_p). For example, for a 60-second recording with the current VNA configuration, the dimension of each matrix will be $(60 \times 10) \times 201 = 600 \times 201$. The total number of data points in this recording will be $600 \times 201 \times 2 = 241,200$ since there is one matrix for the signal strength and one for the phase. Then a separate MATLAB script is implemented to visualize the data using various graphs.

Data Normalization and Visualization

Since the environment changes for each experiment setup, the absolute values for signal strength and phase obtained from one experiment may change for another experiment. For example, the distance and alignment of the antennas may affect the magnitude and variation of the received signal strength. It is infeasible to compare the absolute values of the received signal strength across two experiments with different hardware setups. Therefore, if we want to measure the impact of fire at various distances, we need to record a baseline at each distance and subtract the baseline data from the raw data obtained from fire experiments to obtain the relative changes. Then we can compare the relative changes in the RF signal to determine the relationship between the distance from the fire to the antennas and the impact of the fire. We call the process of calculating relative changes to

the baseline, data normalization.

Recall from the previous section that the signal strength and phase are represented by two $m \times n$ matrices, namely M_{ss} and M_p. To normalize the raw data, we first calculate the average values for signal strength and phase over time in the baseline matrices, which gives two vectors of length n: V_{ss} and V_p. Thus, each element in the vector is the average signal strength (phase) at that frequency over the entire period of the recording. Then for fire experiments, we subtract V_{ss} from M_{ss} and V_p from M_p column-wise to obtain the normalized matrices M'_{ss} and M'_p. We use the normalized matrices for data visualization.

Example Experiment

In this section, we apply the data normalization process to two different rounds of recording under the same hardware setup. There are no fires involved in this experiment, but a person walks into the FoV twice during the experiment to introduce some known variations during the experiment. The goal of this section is to walk through the data normalization process with a concrete example and show the importance of data normalization in our analysis.

In this experiment, the distance d is 1.5 meters from the metal pan to both antennas. A 1-minute baseline is recorded for the environment with the same hardware setup. There is no fire involved in the experiment, but a person walks into the FoV of the antennas at 25 and 45 seconds and each time stays there for about 5 seconds to create some perturbations in the signal strength and phase.

The results of the two experiments are shown in Figure 3.3. Figure 3.3a shows the raw data for the baseline recording. The received signal strength is represented by a negative value in dBm and values closer to 0 represent stronger signals. We display the phase data for the baseline recording in Figure 3.3b. The phase is recorded on the VNA as values between $[-\pi, \pi]$. However, a data point near the boundary may be wrapped around to the other side of the interval even if there is only a minor change. For example, a data point at 0.99π with a 0.02π phase shift in the positive direction, results in a new data point at -0.99π. Thus, the change may look like 1.98π in the graph although the real phase shift is merely 0.02π. The vertical lines near 5.16, 5.19, and 5.21 GHz between the blue and yellow areas in Figure 3.3b are caused by small changes and the wrapping mentioned above. Although the signal strength and phase are quite consistent over time at the same frequency (because the environment is fairly static during the experiment), the values are clearly different across the frequency spectrum, which can be seen by the vertical stripes in the graphs. For example, the signal strength is generally weaker between 5.14 and 5.15 GHz than between 5.18 and 5.19 GHz. The exact value at each frequency depends on

the environment and hardware setup (e.g., the position and alignment of antennas, the placement of other objects in the room, and multi-path effects on RF signals).

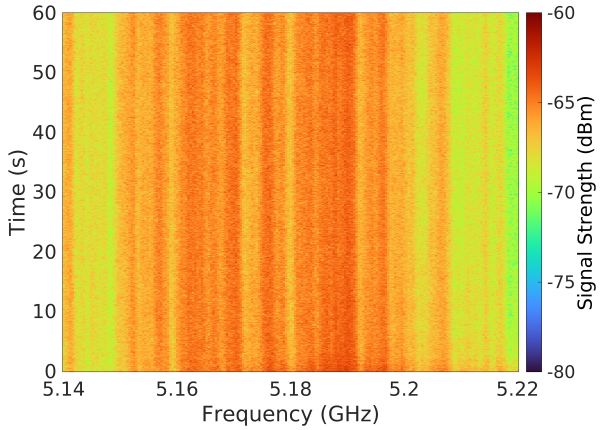

(a) Signal strength of baseline recording.

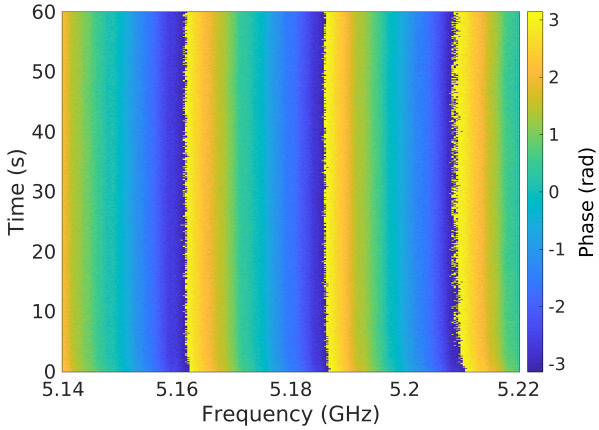

(b) Phase of baseline recording.

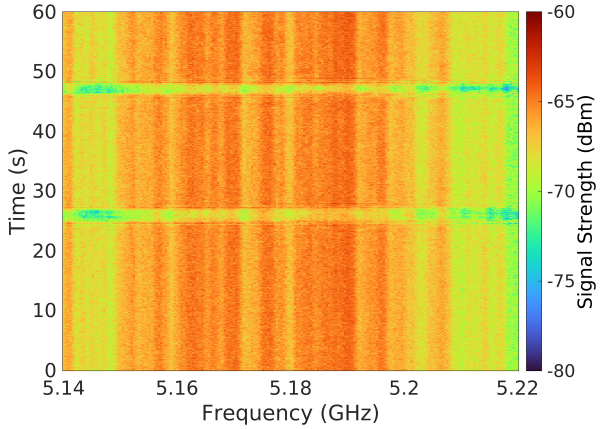

(c) Signal strength with person walking in and out of the FoV at 25 and 45 seconds.

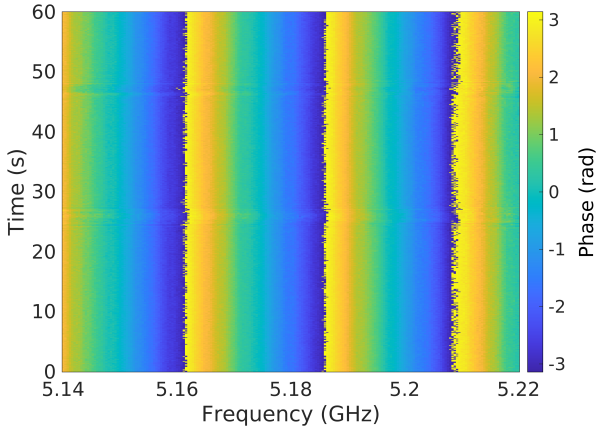

(d) Phase with person walking in and out of the FoV at 25 and 45 seconds.

Figure 3.3: Signal strength and phase data before normalization.

Similarly, the recorded raw data for the signal strength and phase are presented in Figure 3.3c and 3.3d respectively. We can clearly see the variations in the signal strength caused by the movement as horizontal bars near 25 and 47 seconds in Figure 3.3c. Similarly, there are slight changes in phase that are faintly visible during the same time periods in Figure 3.3d.

Figure 3.4a and 3.4b show the results after normalization with respect to the baseline data. The vertical stripes disappear after data normalization since the differences between

frequencies are mitigated by their average values from the baseline recording. The ranges of signal strength and phase data are now both centered around 0 with a smaller span. Thus, the changes in phase are more noticeable now on the heatmap since the span of the color map is $[-1, 1]$ (i.e., the variation of phase is between -1 and 1 radians compared to the baseline). This will allow us to compare the relative changes between experiments and reduce the changes seen from natural variations in the environment.

Since the VNA records 201 different frequencies over the spectrum and 10 frames per second, the size of each data point in the heatmaps is relatively small. It is also difficult to observe the overall trend of the data during different periods of the experiment. As a result, we aggregate multiple nearby data points to create more visible points on the graph. In Figures 3.3c and 3.3d, to mimic the data analysis in the work of Zhong et al. [84], we divide the frequency spectrum into 30 subcarrier groups, each with 2.8 MHz width in frequency. We then choose the size of time intervals according to the total duration of the experiment so that each data point is more visible in the heatmap and the variation patterns are preserved from the raw data heatmap. In this experiment, we calculate the average of every 7 consecutive frequencies (2.8 MHz) along the x-axis and then calculate the average of every 10 consecutive frames (1 second) along the y-axis. We will refer to the value averaged over windows of frequencies and time as a *block*. We can also calculate the 95% confidence interval of all the data points within each block for statistical analysis. Figure 3.4c and 3.4d show the heatmaps with blocks using the above groupings of frequency and time. Now each block is the average value from 7×10 data points from the previous heatmap. We can still observe the changes in the average values of normalized signal strength and phase when the person is walking within the FoV at 25 and 45 seconds.

In this section, we have illustrated the data normalization process and how it helps us compare the results from different rounds of experiments. This process also eliminates the difference across the frequency spectrum by highlighting the real changes we are interested in. In the following sections, we will use these techniques to investigate the changes caused by fire and smoke.

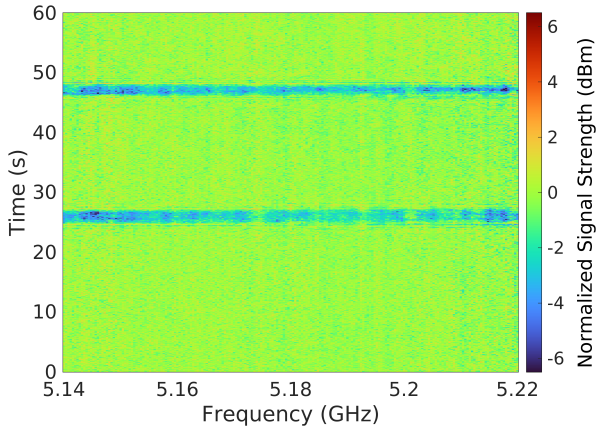

(a) Signal strength after normalization. Colormap is fixed to the range of $[-6, 6]$. All data points fall inside this interval.

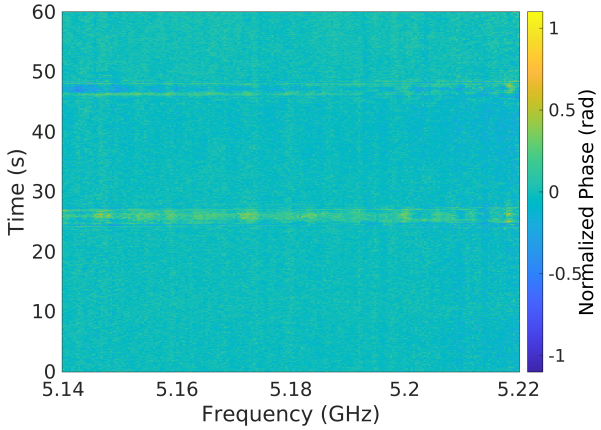

(b) Phase after normalization. Colormap is fixed to the range of $[-1, 1]$. All data points fall inside this interval.

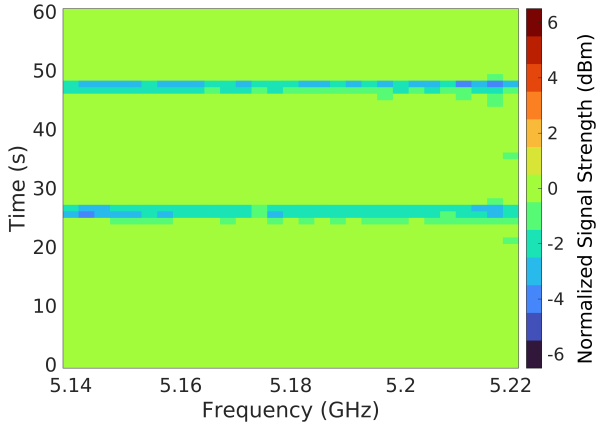

(c) Signal strength after normalization and averaging. Data points are averaged over a window of 2.8 MHz along the x-axis and 1 second along the y-axis.

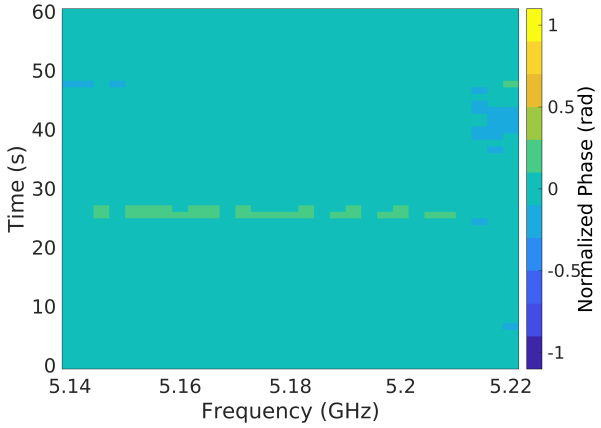

(d) Phase after normalization and averaging. Data points are averaged over a window of 2.8 MHz along the x-axis and 1 second along the y-axis.

Figure 3.4: Signal strength and phase data after normalization.

Time (s)	Event
0	Recording starts
35 - 46	Person walks into FoV and starts fire
160	Fire burning finishes
240	Recording stops

Table 3.2: Events during the close-range experiment with corresponding timestamps.

3.3 Impact of Fire on RF Signal Strength and Phase

3.3.1 Close-Range Experiment: 1.3 meters

Methodology

To better understand the impact of fire on RF signals, we conduct a series of experiments by starting real fires in the fire lab. Figure 3.5 shows the setup of the experiment. The TX and RX antennas are placed 1.3 meters from each other and the metal pan is halfway between the two antennas (0.65 meters from each antenna). Notice that the distance from the TX antenna is measured from the left side (the base) of the horn-shaped antenna to the center of the pan. So although they are the same distance from the pan, the TX antenna may look closer to the pan than the RX antenna. Both antennas are placed slightly higher than the pan so that signals will travel through the fire to reach the receiving side. The pan is filled with 100 milliliters of heptane fuel before each experiment. Table 3.2 consists of a list of events during the experiment and the corresponding timestamps. The total duration of the experiment is 240 seconds. A person walks towards the pan and starts the fire using a match attached to a 1.5-meter metal pole between 35 and 46 seconds. The fire ends at 160 seconds.

Experiment Results

Data collected from the experiment is shown using two heatmaps in Figure 3.6. Both signal strength and phase are normalized with respect to the baseline by subtracting the average value of the corresponding frequency in the 1-minute baseline experiment as described in Section 3.2.3. Figure 3.6a shows the normalized signal strength during the experiment with the colormap fixed to $[-6, 6]$ dBm. Figure 3.6b shows the normalized phase information with colormap fixed to $[-1, 1]$ radians. All data points are inside the selected intervals. Figure 3.6c and 3.6d shows the heatmaps averaged by every 2.8 MHz along the x-axis and

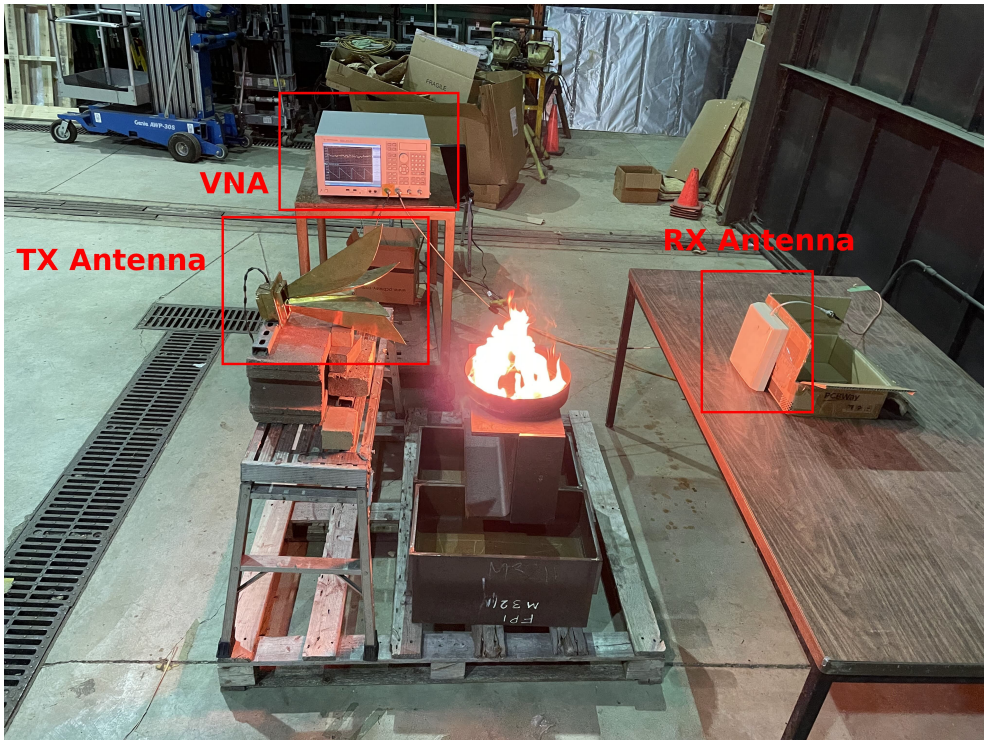

Figure 3.5: Photo of close-range experiment showing the position of VNA and antennas. Fire is placed between the two antennas with equal distance ($d = 0.65$ meters) to both antennas.

every 3 seconds along the y-axis. The averaging window of time is longer than those in Figure 3.4c and 3.4d since the total duration of this experiment is longer than previous experiments and we want the blocks in the heatmap to remain visible in these graphs.

It is worth noting that the patterns for changes in the signal strength are different when we look at different frequencies. In Figure 3.6a, most of the changes occur within the frequency range of 5.15 and 5.18 GHz, which is indicated by orange colors in the heatmap. As for phase, we also observe changes during the same time periods in Figure 3.6b between 5.15 and 5.16 GHz as the fire burns. The differences indicate that the propagation of RF signals at these frequencies is more affected by fires than other frequencies.

In Figure 3.6c, the signal strength increases at some frequencies as the fire burns, with a maximum increase of 1.37 dBm (with a 95% confidence interval of [1.25, 1.49] dBm) at 5.18 GHz and 140 seconds compared to the average value at that frequency in the baseline recording. There is also a slight decrease in the normalized signal strength during the

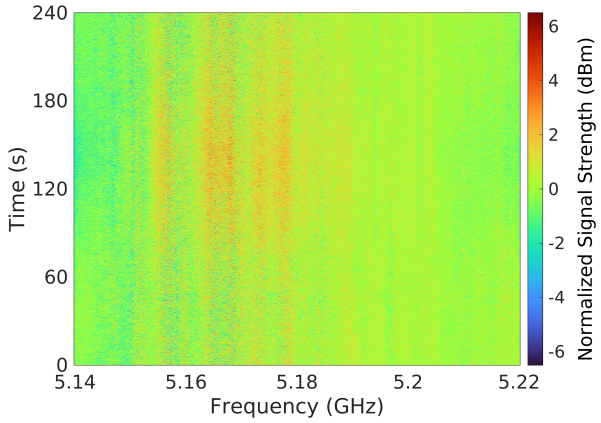

(a) Signal strength after normalization. Colormap is fixed to $[-6, 6]$. All data points fall inside this interval.

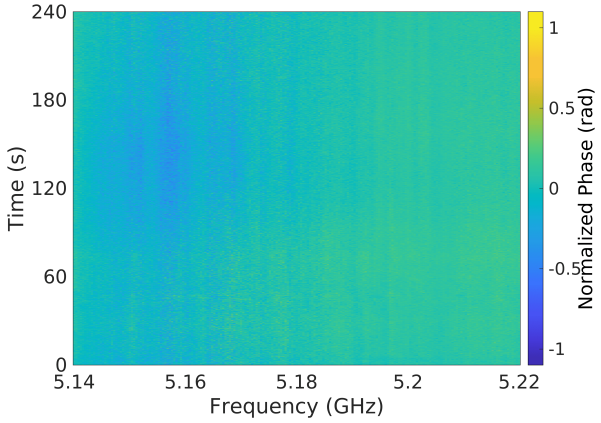

(b) Phase after normalization. Colormap is fixed to $[-1, 1]$. All data points fall inside this interval.

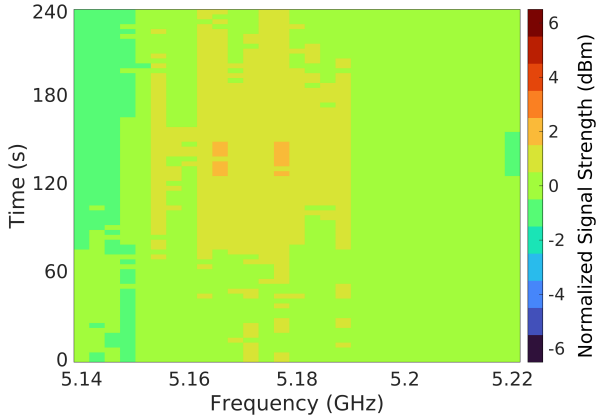

(c) Normalized signal strength plot produced from Figure 3.6a by averaging the data points within every 2.8 MHz along the x-axis and every 3 seconds along the y-axis.

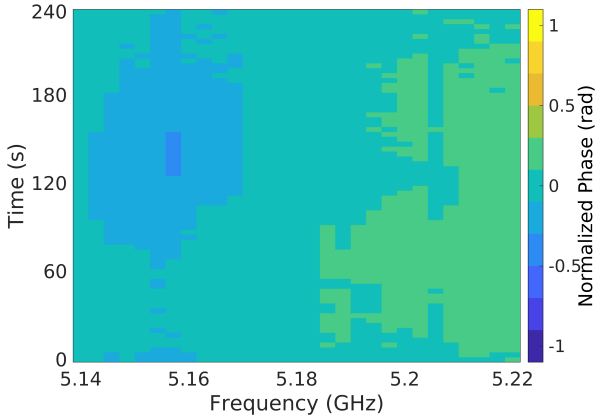

(d) Normalized phase plot produced from Figure 3.6b by averaging the data points within every 2.8 MHz along the x-axis and every 3 seconds along the y-axis.

Figure 3.6: Heatmaps for the close-range experiment. The fire starts at $t_1 = 46$ seconds and ends at $t_2 = 160$ seconds. The total duration of the experiment is $t_3 = 240$ seconds.

same time period at lower frequencies, with a maximum decrease of 1.32 dBm (with a 95% confidence interval of [1.24, 1.40] dBm) at 5.14 GHz and 150 seconds compared to the baseline recording. We also observe changes in the normalized phase during the same time period in Figure 3.6d, with the largest magnitude of phase change being -0.34 radians (with a 95% confidence interval of [-0.36, -0.32] radians) at 5.16 GHz and 156 seconds. Although the fire is burning between 46 and 160 seconds, changes in signal strength and phase are visible between 70 and 210 seconds. Thus, there appears to be a 24-second delay between the start of the fire and the time when we observe changes in the signals. This is still much faster than smoke alarms, whose average response time is 150 seconds [24] (as mentioned in Section 1.2). Note that the first 46 seconds of normalized data for signal strength and phase look quite static and mostly match the baseline recording. Although the heptane ignites and appears to reach full strength immediately, we believe the delay after the fire starts is because the magnitude of change may be positively correlated with the heat generated during combustion. We suspect that the delay after the fire stops burning is because of the heat above the pan, which may take some time to dissipate after the fire goes out.

Examining Subcarrier Groups at 5.14 and 5.18 GHz

While the heatmap is an intuitive format to visualize all of the recorded data, it is difficult to identify the exact value at a given frequency and time. In Figure 3.7, we look specifically into the normalized signal strength for the subcarrier groups at 5.14 GHz (the red line) and 5.18 GHz (the green line). These two subcarrier groups are selected since the changes in these groups are more visible in the heatmap, with the subcarrier group at 5.14 GHz having a decreasing trend after the fire starts, and the subcarrier group at 5.18 GHz having an increasing trend after the fire starts. The amount of change for each subcarrier group is determined by summing the absolute values of all blocks within the frequency range of that subcarrier group. Recall from Section 3.2.3 that each subcarrier group consists of 7 data points with a span of 2.8 MHz in the frequency spectrum. Thus, the exact frequency ranges for the subcarrier groups are 5.1428 - 5.1456 GHz and 5.1772 - 5.1800 GHz. We calculate the mean values of the normalized signal strength data over windows of 2.8 MHz and 3 seconds. The 95% confidence intervals corresponding to each mean value are plotted with a lighter color in the same graph. Thus, each line in Figure 3.7 is essentially showing a single column of data from Figure 3.6c where large changes occur. Furthermore, each data point in Figure 3.7 corresponds to a block in the heatmap.

In Figure 3.7, we can see that the normalized signal strength for the subcarrier group near 5.14 GHz (the red line) decreases slightly after the fire starts. The lowest point of

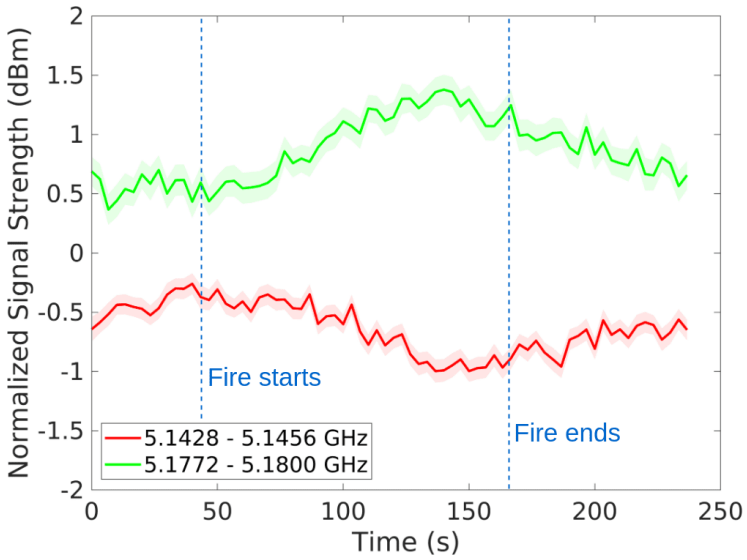

Figure 3.7: Normalized signal strength for subcarrier groups near 5.14 and 5.18 GHz for the close-range experiment. The x-axis is the time in seconds. The y-axis is the normalized signal strength in dBm over the selected frequency range. Each data point corresponds to the average value over a window of 2.8 MHz and 3 seconds from the raw data.

the red line is at -0.99 dBm (with a 95% confidence interval of [-1.08, -0.90] dBm) at 150 seconds. However, since the pre-fire mean value of the red line is -0.49 dBm (with a 95% confidence interval of [-0.55, -0.43] dBm), the real change in the signal strength is only around -0.5 dBm. Then the signal strength slowly moves back to the pre-fire level after the fire ends. As for the subcarrier group near 5.18 GHz (the green line), the changes in normalized signal strength are somewhat symmetric to the other group. It slowly increases after the fire is lit at 46 seconds and gradually approaches the pre-fire level after the fire finishes burning at 160 seconds. The average value of the normalized signal strength before the fire starts is 0.63 dBm (with a 95% confidence interval of [0.57, 0.69] dBm). The largest change relative to the baseline recording is the same as in Figure 3.6c at 1.37 dBm (with a 95% confidence interval of [1.25, 1.49] dBm) at 140 seconds, which is clearly higher than the average before the fire starts without any overlap in the confidence intervals. However, since the signal strength in this experiment is generally higher than those in the baseline recording (i.e., the pre-fire level is greater than 0), the real change caused by fire is less than 1 dBm after subtracting the average value during the pre-fire period. Therefore, the changes in signal strength are statistically significant in this experiment (the confidence interval of the peak does not overlap with those before the fire starts), but the

magnitude of the changes seems relatively small, especially if one was to use commodity Wi-Fi devices, which will not have the high fidelity of the VNA device used for these experiments. Although the combustion process ends at 160 seconds when the heptane has all burned, the signal strength does not return to the same value as the pre-fire level at that moment. We believe this is because there is still heat in the area which can also impact the environment, which takes some time to dissipate.

Summary

In this section, we see that the signal strength and phase of RF signals in the 5 GHz band can be affected by fire when the transmitting and receiving antennas are 1.3 meters from each other. The signal strength on the receiver side increases in frequencies between 5.15 and 5.18 GHz, but decreases around 5.14 GHz in the presence of fire. There are also phase shifts occurring between 5.15 and 5.16 GHz during the time period when the fire is burning. However, those changes are quite small in magnitude. Recall that the previous work on Wi-Fi fire detection by Zhong et al. [84] mentioned in Section 2.3, instead of showing the raw CSI information for each subcarrier, applies some feature extraction algorithms like PCA on the raw data. The output is a single value called CSI amplitude that indicates the overall status of the Wi-Fi signals. Unfortunately, in their work, the CSI amplitude decreases after the fire starts for one experiment but increases in another (at a longer distance). It may be the case (as seen in our experiments) that the fire impacts different subchannels differently (e.g., increasing signal strength in some frequencies and decreasing in others). Therefore, we look into each subcarrier group and examine the frequency range where the largest change occurs. After inspecting the subcarrier group with the largest changes (5.1772 - 5.1800 GHz), the variation in signal strength is statistically significant, but it is unlikely to be captured by commodity Wi-Fi devices given the magnitude of the changes (less than 1 dBm in signal strength). Furthermore, the impact of fire also varies for different frequencies. RF signals within the 5.15 - 5.18 GHz frequency range seem more sensitive to fires than the other frequencies studied in this experiment.

3.3.2 Longer-Range Experiment: 3 meters

Methodology

After seeing the results from the close-range experiments, we would like to study the potential changes in signal strength and phase at a longer distance and examine the feasibility of using RF signals for fire detection using 5 GHz signals. The results of such experiments

can help us understand the possible coverage of a potential fire detection device using RF signals, which is an important factor to consider when installing fire detectors. Intuitively, one might expect the fire to have a weaker impact on the propagation of RF signals as we move the transmitter and receiver farther apart since the fire occupies a smaller proportion of the FoV. The experiment setup is similar to the close-range experiment, except that the distance between the two antennas is now 3 meters. Figure 3.8 shows the setup for this experiment. The metal pan for starting the fire is again halfway between the antennas (1.5 meters from each). Table 3.3 presents the events and their timestamps chronologically. The total duration of the experiment is 180 seconds. A person walks towards the pan and starts the fire using a match attached to a 1.5-meter metal pole between approximately 35 and 45 seconds. Then the fire finishes burning at 130 seconds. The duration is shorter than the close-range experiment in Section 3.3.1 because the metal pan still has residual heat from the previous experiments, which speeds up the vaporization of the liquid fuel.

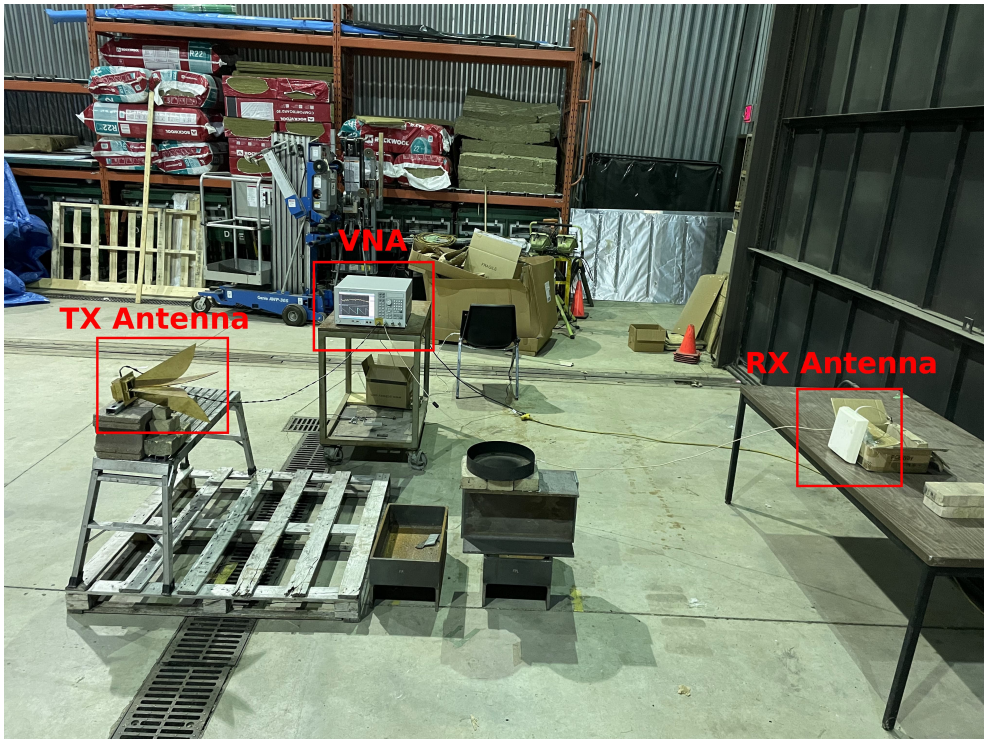

Figure 3.8: Photo of longer-range experiment showing the position of the VNA and antennas. The metal pan is placed between the two antennas with an equal distance ($d = 1.5$ meters) to each antenna.

Time (s)	Event
0	Recording starts
35 - 45	Person walks into FoV and starts fire
130	Fire burning finishes
180	Recording stops

Table 3.3: Events during the longer-range experiment with corresponding timestamps.

Experiment Results

The experiment results are visualized as heatmaps in Figure 3.9. Figure 3.9a and 3.9b show the raw data from the experiment. We then group the data points by every 2.8 MHz along the x-axis and every 3 seconds along the y-axis to generate the heatmaps averaged over these windows in Figure 3.9c and 3.9d.

The results are different from those we obtained in the short-range experiment. We visualize them in the same format in Figure 3.6. For both signal strength and phase, the data is quite uniform during the time when the fire is burning in Figure 3.9a and 3.9b. The maximum change in the normalized signal strength after we start the fire is 0.30 dBm (with a 95% confidence interval of [0.24, 0.36] dBm) at 5.15 GHz and 83 seconds in Figure 3.9c and the maximum change in phase is 0.12 radians (with a 95% confidence interval of [0.11, 0.13] radians) at 5.22 GHz and 150 seconds in Figure 3.9d, both are much smaller in magnitude than the changes we observe in the close-range experiment. The same experiment is repeated twice in a row to ensure the results we observe are reliable. In both trials, the changes in signal strength and phase are not visible while the fire is burning. The horizontal area with a different color near 35 seconds is caused by the person walking toward the metal pan to light the fire. (Recall that they light the fire using a match on a 1.5-meter metal pole so they are approximately 2 meters from the pan). The horizontal bar is not observed in the close-range experiment. This is because the antennas are placed closer in the previous setup, so the region covered by the FoV of both antennas is smaller and the movement of the person that starts the fire is not captured by the receiver. With a longer distance between the antennas, the person walks into the FoV of the antennas and only briefly interferes with the propagation of the signals.

Examining Subcarrier Group at 5.21 GHz

Similar to Section 3.3.1, Figure 3.10 provides a closer look at the changes in signal strength for the subcarrier group near 5.21 GHz where the largest variation is observed. The specific

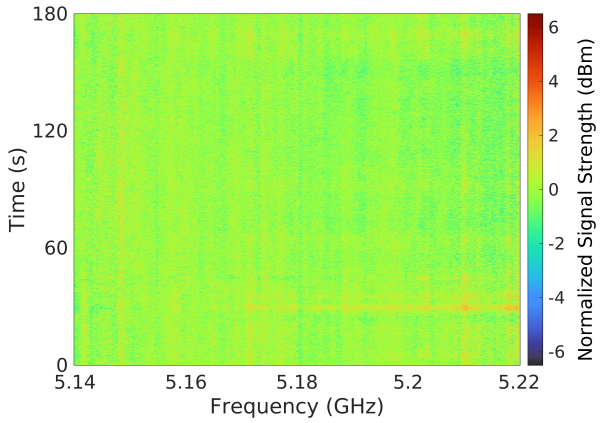

(a) Normalized signal strength (in dBm). Colormap is fixed to $[-6, 6]$. All data points fall inside this interval.

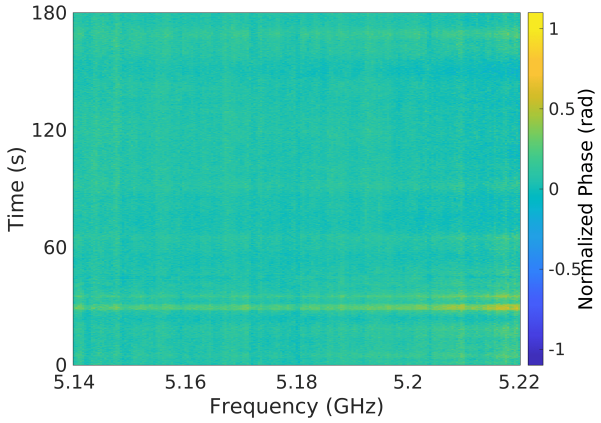

(b) Normalized phase (in radians). Colormap is fixed to $[-1, 1]$. All data points fall inside this interval.

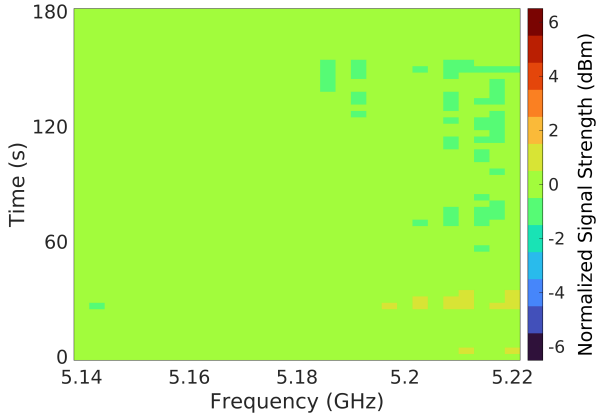

(c) Normalized signal strength plot produced from Figure 3.9a by averaging the data points within every 2.8 MHz along the x-axis and every 3 seconds along the y-axis.

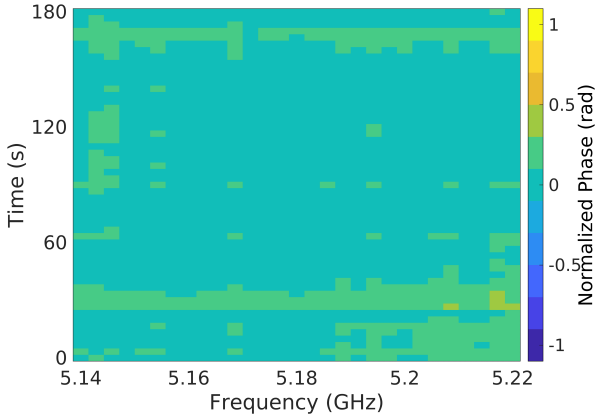

(d) Normalized phase plot produced from Figure 3.9b by averaging the data points within every 2.8 MHz along the x-axis and every 3 seconds along the y-axis.

Figure 3.9: Heatmaps for the longer-range experiment. The fire starts at $t_1 = 45$ seconds and ends at $t_2 = 130$ seconds. The total duration of the experiment is $t_3 = 180$ seconds.

frequency range for the subcarrier group is 5.2086 - 5.2114 GHz. We hypothesize that the spike near 35 seconds is caused by the person walking into the FoV since the person is inside the FoV between 35 and 45 seconds to light the fire. Note that the changes are relatively small because the person uses a match on a pole to reduce the impact of entering the FoV. The changes in the longer-range experiment are much smaller in magnitude than those from the close-range experiment. While the fire is burning between 45 and 130 seconds, the changes in the normalized signal strength are always within 0.5 dBm compared to the pre-fire level. Such small changes are too small for most commodity Wi-Fi devices to distinguish and utilize for fire detection given the coarse granularity of Wi-Fi devices compared to the VNA used in our experiments (as mentioned in Section 3.2.1). Most importantly, it is not possible to distinguish when the fire starts and ends in the plot in Figure 3.10.

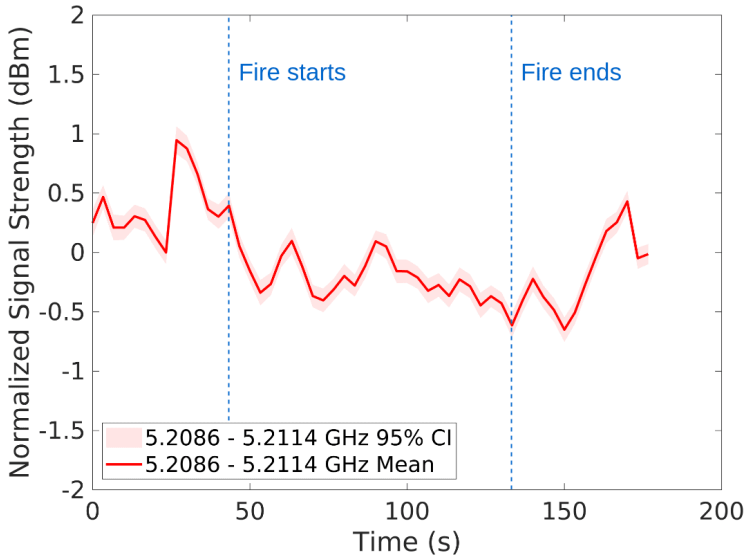

Figure 3.10: Normalized signal strength over a narrow part of the spectrum (5.2086 - 5.2114 GHz) for the longer-range experiment. The x-axis is the time in seconds. The y-axis is the normalized signal strength in dBm over the selected frequency range. Each data point corresponds to the average value over a window of 2.8 MHz and 3 seconds from the raw data.

Summary

Results from the longer-range experiment indicate that the changes in the magnitude of the signal strength and phase diminish quickly in magnitude as we increase the distance between the two antennas. It seems unlikely that we can detect fire by comparing the signal strength and phase data with those before the fire starts since the changes are too small at this distance. In previous work on Wi-Fi fire detection [84], the maximum distance that the Wi-Fi device was able to detect fires is 4 meters. Since our data is recorded with a much more sensitive device, it seems unlikely that a Wi-Fi device could detect changes given the accuracy and fidelity of the device. Thus, this fire detection method may only work when the fire is near the transmitter and/or receiver. We do not conduct additional experiments with occlusions since the changes are quite small at a distance of 3 meters.

3.4 Impact of Smoke on RF Signal Strength and Phase

So far in this chapter, we have explored how RF signals are affected by heptane fires when they travel through the flames. The experiments are conducted with TX and RX antennas aiming directly at the fire and the fuel source is limited to heptane. We observe statistically significant changes in the signal strength and phase when the antennas are close to the fire, but those changes soon become unnoticeable as the distance between the two antennas increases. However, the flame itself is not the only indicator of the presence of fire. The combustion process usually produces smoke, which can be detected by a smoke alarm [4]. In this section, we examine the impact of smoke from the fire on RF signals since smoke consists of particles generated during the combustion process [80]. The goal is to examine the feasibility of using wireless signals to detect smoke generated by fire. A wireless detector is expected to react faster than ordinary smoke alarms since it can detect and activate the alarm before the smoke reaches the detector sensors.

Li et al. [79] previously observe that smoke generated by fire can attenuate RF signals in the 350 MHz to 400 MHz frequency range. Furthermore, the intensity of attenuation is positively correlated with the concentration of smoke. In this section, we focus on the impact of smoke generated by fire on the signal strength and phase of RF signals in the 5 GHz frequency band. The amount of smoke generated during the experiment is controlled by the type of fuel. We start with heptane as a cleaner fuel that generates little smoke and then move on to wood, which produces denser smoke. By comparing the results obtained from experiments using these two types of fuels, we hope to gain insights into the impact of smoke on RF signals.

3.4.1 Heptane Smoke Experiment

Methodology

Figure 3.11 provides an overview of the experiment setup. We place the metal pan on the floor so the signal now travels through the smoke above the fire. The VNA and the two antennas are at the same positions as in the longer-range experiment from Section 3.3.2. The fire is halfway between the two antennas (with distance d being 1.5 meters from the fire to each antenna). Table 3.4 consists of a list of events with corresponding timestamps during the experiment. The total duration of the experiment is 180 seconds. A person walks towards the pan and starts the fire using a match attached to a 1.5-meter metal pole between approximately 30 and 50 seconds. The fire burns until 165 seconds.

Figure 3.11: Photo of heptane smoke experiment setup. The hardware setup is the same as the longer-range experiment in Figure 3.8 except that the metal pan is placed on the floor.

Time (s)	Event
0	Recording starts
30 - 50	Person walks into FoV and starts fire
165	Fire burning finishes
180	Recording stops

Table 3.4: Events during the heptane smoke experiment with corresponding timestamps.

Experiment Results

Figure 3.12 shows the results of this experiment. The two subfigures on the top are raw data for the normalized signal strength and phase. The two subfigures at the bottom are averaged data over a window of 2.8 MHz along the x-axis and 3 seconds along the y-axis for better visualization. There is a slight increase in the normalized signal strength in Figure 3.12c while the fire is burning compared to the baseline recording. The largest change in the normalized signal strength is 0.77 dBm (with a 95% confidence interval of [0.70, 0.84] dBm) at 5.20 GHz and 120 seconds. The phase of the RF signal is fairly stable during the entire period of the experiment. Overall, the impact of smoke from the heptane fire is quite small. The magnitude of change in signal strength is not large enough to make reliable detections with any Wi-Fi devices. One possible explanation is that heptane is a relatively clean burning fuel that generates only a small amount of smoke, which is not enough to result in noticeable changes in the signal strength or phase of the RF signals.

3.4.2 Wood Smoke Experiment

Motivation

Since the heptane does not generate a lot of smoke in the previous experiment, we conduct another experiment using chopped wood since it generates more smoke during combustion. Intuitively, denser smoke is expected to have a stronger impact on the signal strength and phase since it contains more particles that can attenuate the signal. Previous work on forest fire detection [11, 45, 54] has shown that RF signals at microwave bands can be used to detect fire from vegetation. Wood is also a complex composite that contains a wider variety of chemicals than heptane [55]. The metallic elements like Potassium and Calcium in vegetation fuel produce a cloud of ions when it is burning, which in turn increases the attenuation of RF signals [15, 56]. Wood is also commonly used as a construction material

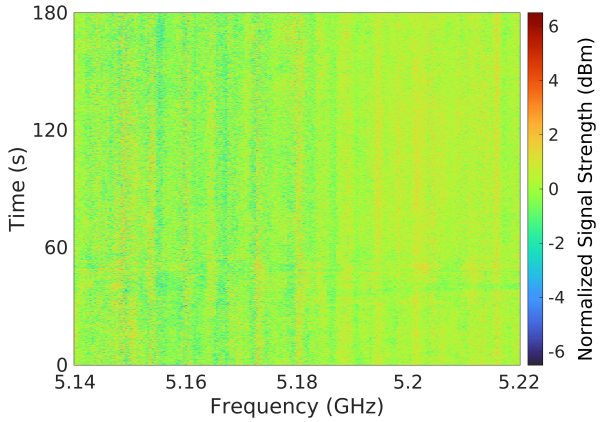

(a) Normalized signal strength (in dBm). Colormap is restricted to $[-6, 6]$. All data points fall inside this interval.

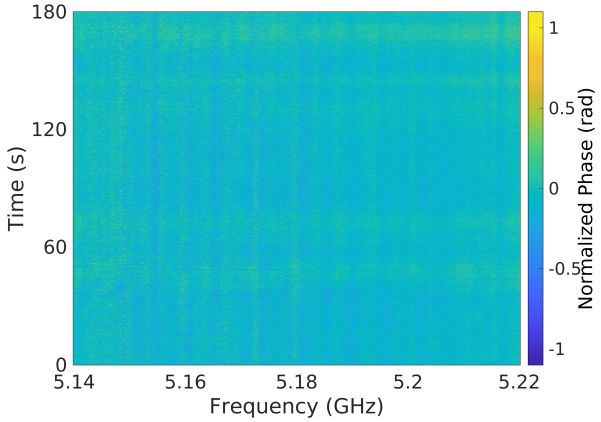

(b) Normalized phase (in radians). Colormap is restricted to $[-1, 1]$. All data points fall inside this interval.

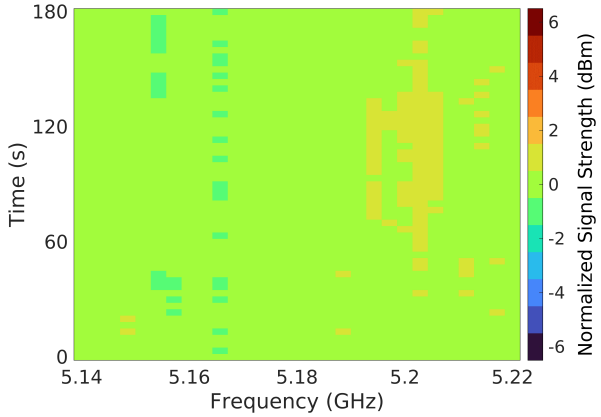

(c) Normalized signal strength plot produced from Figure 3.12a by averaging the data points within every 2.8 MHz along the x-axis and every 3 seconds along the y-axis.

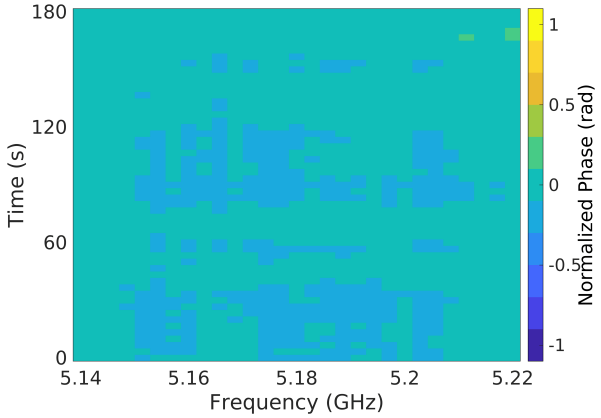

(d) Normalized phase plot produced from Figure 3.12b by averaging the data points within every 2.8 MHz along the x-axis and every 3 seconds along the y-axis.

Figure 3.12: Heatmaps for the heptane smoke experiment. The fire starts at $t_1 = 50$ seconds and ends at $t_2 = 165$ seconds. The total duration of the experiment is $t_3 = 180$ seconds.

Time (s)	Event
0	Recording starts
50	Fire starts
120	Person walks to the metal pan and returns
225	Person walks to the metal pan and extinguishes the fire with a concrete plate
230	Person leaves the FoV
300	Recording stops

Table 3.5: Events during the wood smoke experiment with corresponding timestamps.

in houses. Thus, we believe that wood is an interesting fuel to use when analyzing the impact of smoke on RF signals.

Methodology

We build a small fire from chopped wood inside a 45×20 cm metal container with a depth of 15 cm (as shown in Figure 3.13a). We also pour 30 milliliters of heptane on top of the wood so that it will catch fire more quickly. The container is placed halfway between the antennas (1.5 meters to each antenna). The metal container is placed slightly lower than the two antennas to ensure the signals will travel through the fire and smoke. Since the fire takes a long time to completely burn itself out, we use a concrete plate to cover the container 180 seconds after the fire starts. In this way, the fire can be extinguished in about 5 seconds due to the lack of oxygen inside the container, at which point dense smoke is generated. It is also worth noting that the amount of smoke generated when the wood is burning with large flames is significantly lower than after the fire is suffocated. The differences can be seen in Figures 3.13b and 3.13c.

Table 3.5 shows the timestamps for each event during the experiment. The experiment lasts for 300 seconds in total. A person walks towards the container and lights the fire at 40 seconds using a match attached to a 1.5-meter metal pole. To ensure the changes we see are actually caused by fire or smoke, a person walks up to the metal container at 120 seconds in the same way as they would extinguish the fire later in the experiment and walks back (but does not do anything with the fire). At 225 seconds, the person walks to the metal pan again and covers it with a concrete plate. The fire is suffocated in about 5 seconds and starts generating dense smoke. The person then removes the concrete plate to release the smoke from the container and walks out of the FoV.

(a) Wood pile layout (b) Wood fire (c) Smoke generated by wood after the fire is extinguished

Figure 3.13: Photos of wood smoke experiment.

Experiment Results

Figure 3.14 shows the results of this experiment. Again, Figures 3.14a and 3.14b present the raw data for signal strength and phase recorded during the experiment. We then average the raw data for every 2.8 MHz and 3 seconds window and plot the averaged data in Figures 3.14c and 3.14d for better visualization. The patterns of variation for the signal strength and phase are similar to each other.

There is a horizontal bar near 120 seconds in the heatmaps due to the movement of the person. The largest change in the normalized signal strength caused by the movement is 1.26 dBm (with a 95% confidence interval of [1.13, 1.38] dBm) at 5.17 GHz and 122 seconds in Figure 3.14c. As for phase, the largest change is 0.52 radians (with a 95% confidence interval of [0.51, 0.53] radians) at 5.20 GHz and 120 seconds for the phase in Figure 3.14d. We can see that the signal strength and phase quickly fall back to values around 0 after the person leaves the FoV, which indicates that the movement of the person does not have a persistent effect on the signal strength or the phase after the person has moved away.

Overall, we are unable to observe any significant changes in signal strength and phase while the fire is burning from 40 to 225 seconds. A significant change (dark blue horizontal bar in the heatmaps) in both the signal strength and phase is observed at 225 seconds. This is because the concrete plate blocks most of the signals when the person lifts and covers

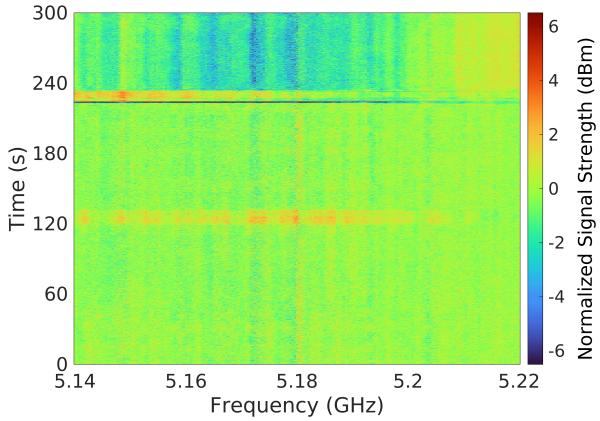

(a) Normalized signal strength (in dBm). Colormap is restricted to $[-6, 6]$. All data points fall inside this interval.

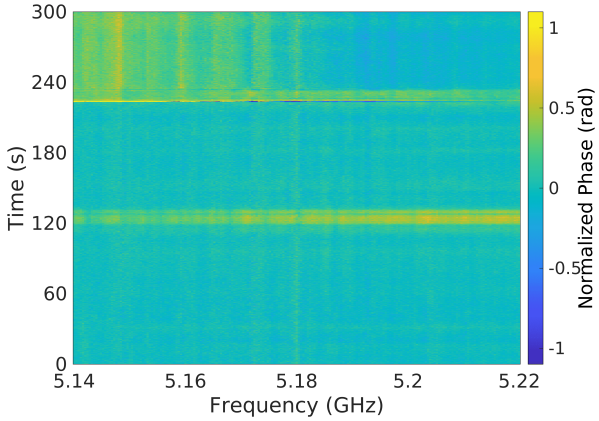

(b) Normalized phase (in radians). Colormap is restricted to $[-1, 1]$. All data points fall inside this interval.

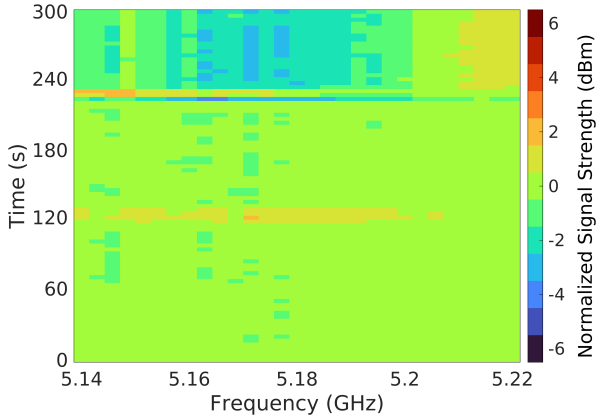

(c) Normalized signal strength plot produced from Figure 3.14a by averaging the data points within every 2.8 MHz along the x-axis and every 3 seconds along the y-axis.

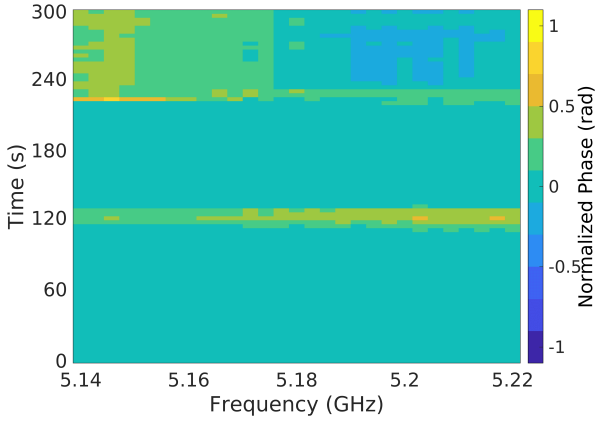

(d) Normalized phase plot produced from Figure 3.14b by averaging the data points within every 2.8 MHz along the x-axis and every 3 seconds along the y-axis.

Figure 3.14: Heatmaps for the wood smoke experiment. The fire starts at 40 seconds and ends at 230 seconds. The total duration of the experiment is 300 seconds.

the container. The blue bar soon disappears once the cover is placed on the container and changes color to red and yellow since the person is still inside the FoV. The largest change in the normalized signal strength caused by the movement of the person during this period is -3.58 dBm (with a 95% confidence interval of [-4.08, -3.08] dBm) at 5.17 GHz and 225 seconds in Figure 3.14c. As for phase, the largest change is -0.78 radians (with a 95% confidence interval of [0.76, 0.80] radians) at 5.15 GHz and 225 seconds in Figure 3.14d.

After the person leaves the FoV at 230 seconds, there is a clear decrease in the signal strength and positive phase shift. The largest change in the normalized signal strength after the fire is extinguished is -3.21 dBm (with a 95% confidence interval of [-3.37, -3.05] dBm) at 5.17 GHz and 280 seconds in Figure 3.14c. The largest change in the normalized phase is 0.44 radians (with a 95% confidence interval of [0.43, 0.45] radians) at 5.15 GHz and 293 seconds in Figure 3.14d. We believe the changes after the fire is extinguished are caused by the dense smoke generated. When the wireless signal travels through the smoke, it collides with the particles in the smoke and is attenuated. Therefore, we observe a weaker and phase-shifted signal on the receiver side. The variations in the signal strength and phase are also frequency-dependent. The impact of smoke is unnoticeable while the fire is burning since the wood used in our experiment does not generate enough smoke when the fire is burning (120 - 225 seconds). The frequencies that are more likely to be affected by smoke are indicated by the vertical bars with blue color in Figure 3.14c and yellow color in Figure 3.14d after 225 seconds. Most of the changes are centered between 5.16 and 5.19 GHz for signal strength. As for phase, signals between 5.14 and 5.15 GHz have a larger phase shift than the others.

Examining Subcarrier Group at 5.17 GHz

In this section, we take a closer look at the subcarrier group that has the largest change due to smoke. Figure 3.15 shows the normalized signal strength for the subcarrier group near 5.17 GHz in this experiment, specifically in the frequency range 5.1700 - 5.1728 GHz. Each data point is the average over a window of 3 seconds within the selected frequency range, with the 95% confidence interval drawn in a lighter color. The values in this graph are the same as a single column at 5.17 GHz in the heatmap in Figure 3.14c since they use the same window of time to calculate the averages.

In Figure 3.15, the two peaks near 120 and 230 seconds are both caused by the movement of the person. The largest change caused by the movement is 1.26 dBm (with a 95% confidence interval of [1.13, 1.38] dBm) at 122 seconds. There is also a sudden drop to -3.58 dBm (with a 95% confidence interval of [-4.08, -3.08] dBm) at 225 seconds. This is likely because the concrete plate used to extinguish the fire attenuates the signals. After the

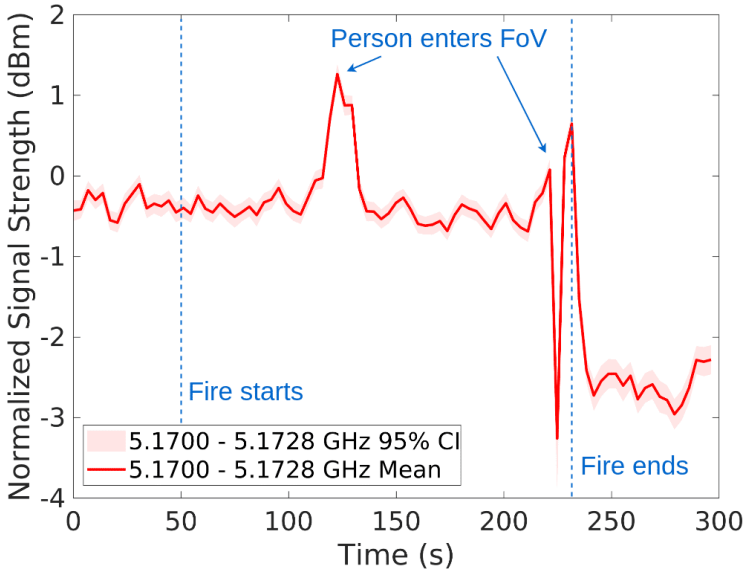

Figure 3.15: Normalized signal strength over a narrow part of the spectrum (5.1700 - 5.1728 GHz) for the wood smoke experiment. The x-axis is the time in seconds. The y-axis is the normalized signal strength in dBm over the selected frequency range. Each data point corresponds to the average value over a window of 2.8 MHz and 3 seconds from the raw data. Fire is burning between 50 and 225 seconds. A person walks into the FoV at 120 and 225 seconds.

fire is extinguished at 230 seconds, the wood starts to generate dense smoke that attenuates the signal. There is a significant decrease in the average values of the normalized signal strength from 230 seconds to the end of the experiment. The largest change is -3.21 dBm (with a 95% confidence interval of [-3.37, -3.05] dBm) at 280 seconds. The changes caused by smoke are significant since the confidence intervals do not overlap with any confidence intervals before the fire starts or while the fire is burning.

Summary

From the results of these experiments, we may conclude that wood fire does not have a significant impact on the RF signals. One may argue that the wood fire used in our experiment is not large enough to impact the propagation of RF signals. However, when compared to the previous work on Wi-Fi fire detection [84, 47] where the fires are started by a butane stove, we believe the size of fire we are using is likely as large or larger. The changes due to smoke are not noticeable while the fire is burning since there is only

a moderate amount of smoke during this time period. After we extinguish the fire by depriving it of oxygen, the wood generates a large amount of smoke, which significantly attenuates the RF signals. The dense smoke impacts both the signal strength and the phase after the fire is extinguished. It shows the potential of detecting smoke using RF signals. For the wood used in this experiment, this fire detection method may not be very useful since it does not generate a lot of smoke when the fire is burning. However, for indoor fires, material in some furniture (e.g., mattress or couch) may generate dense smoke that may be used to trigger an alarm. Therefore, it is unlikely that we can utilize 5 GHz RF signals to detect fires, but it is potentially feasible to detect dense smoke in structural fires.

3.5 Variations Introduced by Movement

Motivation

In addition to the impact of fire and smoke on RF signals, we notice that the movement of the person lighting the fire affects the received signal strength and phase. The signal strength and phase change whenever the person walks into the FoV to start the fire. The pattern and magnitude of the variation are also different from those caused by fire or smoke. In the previous work conducted by Zhong et al. [84], the authors claim to be able to detect fire by observing changes in the CSI of a Wi-Fi network. After seeing the results from the previous sections, we suspect that the changes in their work might have been caused by the movement of the person who starts the fire rather than the fire. The VNA device we are using has much better fidelity than commodity wireless network cards. The variations in signal strength and phase due to fire are not noticeable on the VNA when the distance between the transmitter and the receiver is 3 meters. However, in the previous work [84], the authors note that they are able to see changes in the CSI at up to 4 meters with the Wi-Fi device.

We include one of the figures from their paper (Fig. 1 [84]) and present it in Figure 3.16. It shows the changes in the CSI amplitude moments before and after the fire starts. The x-axis indicates the packet index and packets are transmitted at a constant rate of 1000 packets per second. Since the x-axis goes from 0 to 2000, each graph only contains 2 seconds of data from the experiments, with 1 second before the fire starts and 1 second after. It is worth noting that to light the fire, a person has to walk to and from the container, which could take more than 1 second. Therefore, the authors would need to show data well beyond the 2 seconds of data around the fire starts since the person may still be within

the FoV of the devices and impact the RF signals. The y-axis is the CSI amplitude of the signal strength on the receiver side (in dB). The 4 subfigures correspond to different scenarios varied by whether the fire is in the direct path between the transmitting and receiving devices, as well as the distance between the two devices (2 and 4 meters). We can see that the CSI changes in all 4 scenarios immediately after the fire is started. It decreases in the first scenario (LOS with distance = 2 meters), and increases in the others. It seems odd that the fire would have affected the CSI in two different directions when we change the locations of the Wi-Fi devices. There is a lack of explanation for this finding in the original paper. We suspect that the changes are actually caused by the person who lights the fire.

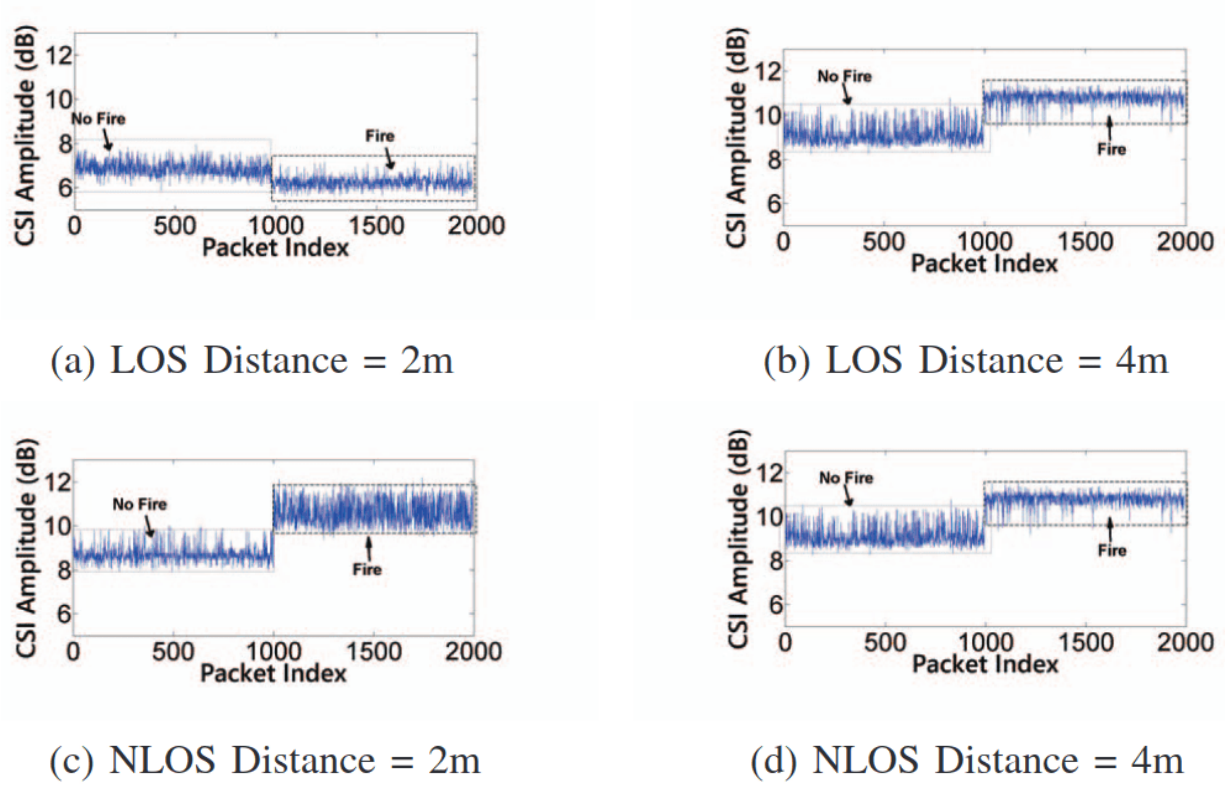

Figure 3.16: CSI amplitude before and after fire starts from the Wi-Fi fire detection paper by Zhong et al. [84].

As a result, we design a set of experiments to examine the impact of a person's movement on RF signals and try to approximate similar results as in the Wi-Fi fire detection paper [84] by conducting some simple experiments without fire. If we can produce similar

results without fire, we may conclude that the changes observed in their experiment are more likely due to movement than fire. We would also like to show the importance of collecting the baseline data before and after the fire as well as minimizing the movement inside the FoV of the antennas during fire-related experiments. We propose some methods that can improve the reliability of the conclusions drawn from the experiment results.

Methodology

The experiment setup is the same as the close-range experiment in Section 3.3.1, except that there is no fire in this experiment. Figure 3.17 shows an overview of the experiment setup. The metal pan is placed halfway between the TX and RX antennas with the distance d being 0.65 meters. Each round of the experiment lasts 60 seconds. At the beginning of each experiment, a person stands outside the FoV of both antennas, far from the metal pan. Then the person walks to the metal pan and stays in the FoV for about 5 seconds before returning to the starting point. Table 3.6 shows the list of events and corresponding timestamps during the experiment. The long metal pole is not used since we want to observe the changes caused by the person's movement. We use two different paths, one perpendicular to the direct path of the two antennas and one on a 45° angle to the direct path, in two separate rounds of experiments.

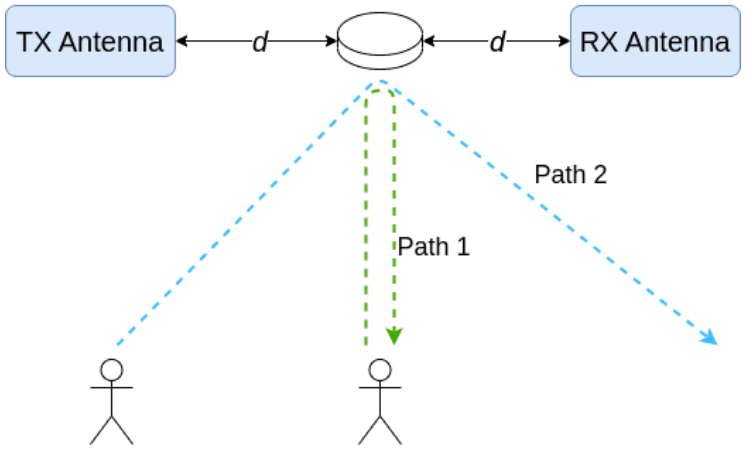

Figure 3.17: Walking paths relative to the TX and RX antennas. Path 1 is perpendicular to the direct path between the TX and RX antennas. Path 2 is on about a 45° angle to the direct path between the two antennas. The distance d is 0.65 meters. The metal pan is placed halfway between the two antennas but no fire is started in this experiment. The VNA device and laptop are omitted in this figure.

Time (s)	Event
0	Recording starts
22 - 27	Person enters and leaves the FoV
41 - 46	Person enters and leaves the FoV again
60	Recording stops

Table 3.6: Events during the movement experiment with corresponding timestamps for both paths.

Name (unit)	Path	Min (with 95% CI)	Max (with 95% CI)
Normalized Signal Strength (dBm)	1	-2.69 [-2.90, -2.48]	1.37 [1.19, 1.55]
	2	-4.24 [-4.79, -3.69]	2.73 [2.69, 2.77]
Normalized Phase (radians)	1	-0.22 [-0.24, -0.20]	0.24 [0.22, 0.26]
	2	-0.36 [-0.38, -0.34]	0.46 [0.43, 0.48]

Table 3.7: Ranges of the normalized signal strength and phase during the movement experiment for both paths. Average values and confidence intervals are calculated based on blocks over windows of 2.8 MHz in frequency and 0.5 seconds in time.

Experiment Results

In both scenarios, we observe significant changes in the normalized signal strength and phase when the person walks into and out of the FoV. We present the normalized signal strength and phase in heatmaps with similar format to those used in the previous sections. The normalized data is shown in Figure 3.18 for Path 1 and Figure 3.19 for Path 2. The signal strength and phase vary as soon as the person enters the FoV of the antennas at 22 and 41 seconds. Table 3.7 shows the minimum and maximum values in the normalized signal strength and phase for both paths. The average values and confidence intervals are calculated based on the data points within each block in the heatmaps. The size of each block is 2.8 MHz in frequency and 0.5 seconds in time. The magnitude of the changes in signal strength and phase is larger than those we observe from fire in Section 3.3.1. The changes caused by the person's movement in the previous experiments are not comparable with this experiment since we use a metal pole to reduce the movement within the FoV.

It is worth noting that the changes caused by movement can be positive or negative in the heatmaps depending on the direction of the movement and it appears to be different across the frequency spectrum. For example, after the person walks into the FoV following Path 1 (as shown in Figure 3.18a), the normalized signal strength is generally decreasing

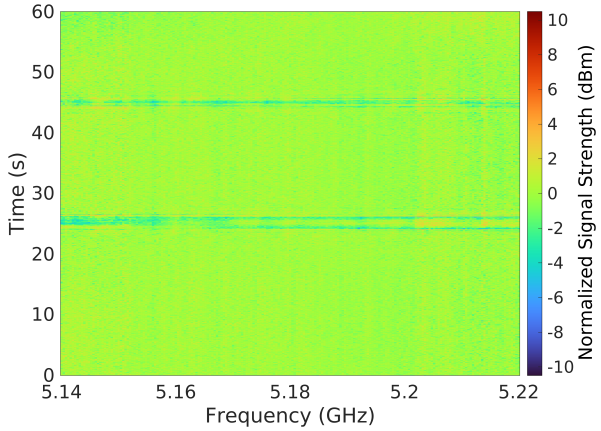

(a) Normalized signal strength (in dBm) for Path 1. Colormap is restricted to $[-10, 10]$. All data points fall inside this interval.

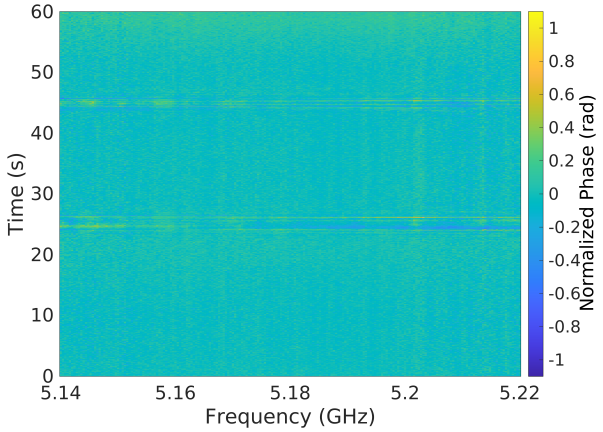

(b) Normalized phase (in radians) for Path 1. Colormap is restricted to $[-1, 1]$. All data points fall inside this interval.

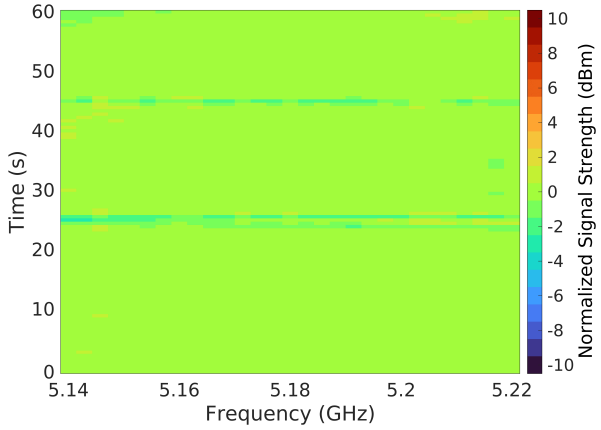

(c) Normalized signal strength plot produced from Figure 3.18a by averaging the data points within every 2.8 MHz along the x-axis and every 0.5 seconds along the y-axis.

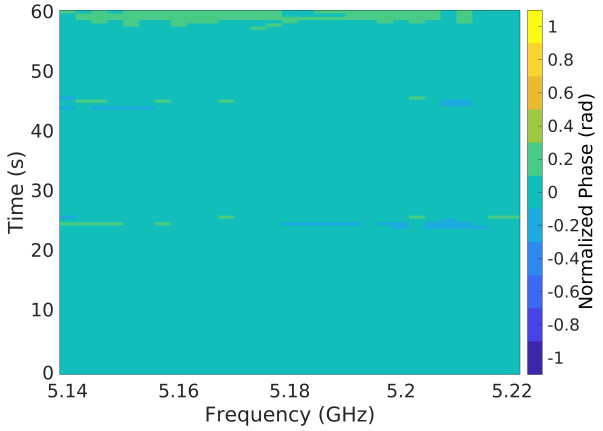

(d) Normalized phase plot produced from Figure 3.18b by averaging the data points within every 2.8 MHz along the x-axis and every 0.5 seconds along the y-axis.

Figure 3.18: Heatmaps for Path 1 in the moving experiment. A person walks into the FoV of the two antennas at approximately 22 and 41 seconds.

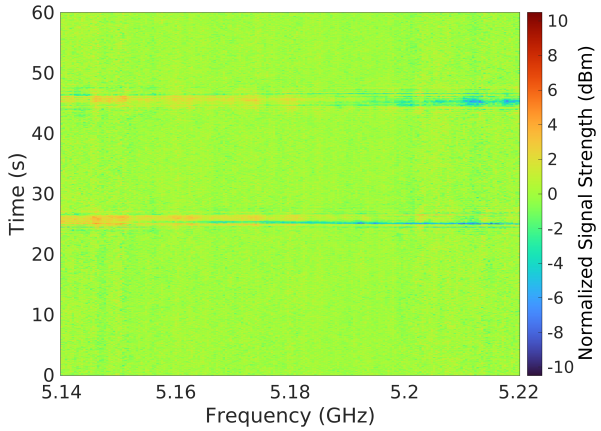

(a) Normalized signal strength (in dBm) for Path 2. Colormap is restricted to $[-10, 10]$. All data points fall inside this interval.

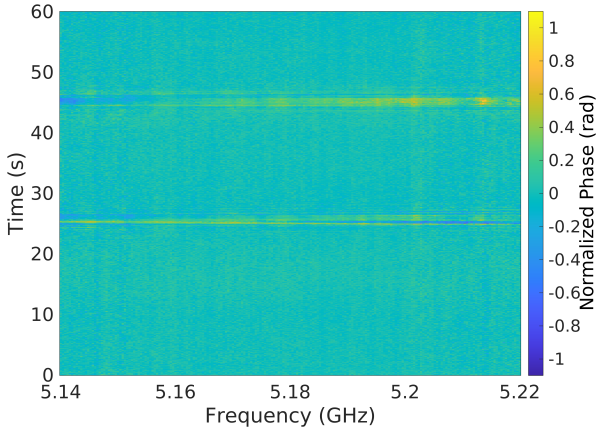

(b) Normalized phase (in radians) for Path 2. Colormap is restricted to $[-1, 1]$. All data points fall inside this interval.

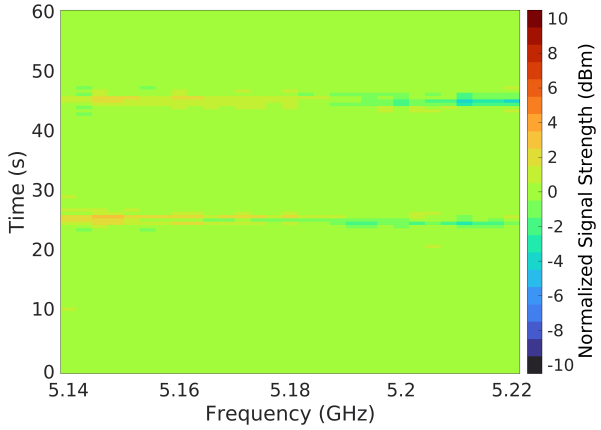

(c) Normalized signal strength plot produced from Figure 3.19a by averaging the data points within every 2.8 MHz along the x-axis and every 0.5 seconds along the y-axis.

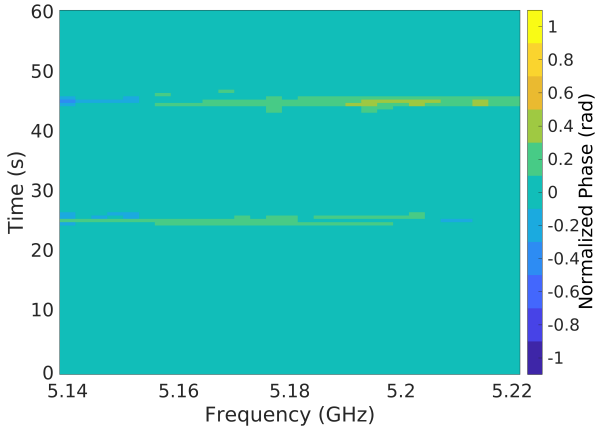

(d) Normalized phase plot produced from Figure 3.19b by averaging the data points within every 2.8 MHz along the x-axis and every 0.5 seconds along the y-axis.

Figure 3.19: Heatmaps for Path 2 in the moving experiment. A person walks into the FoV of the two antennas at 22 and 41 seconds.

between 5.14 and 5.20 GHz with relatively rare increases in values at some frequencies between 5.20 and 5.21 GHz. As for Path 2, the normalized signal strength is mostly increasing on the frequency spectrum below 5.18 GHz and decreasing in the other half of the spectrum. The magnitude of the phase change with Path 1 (as seen in Figure 3.18b) is smaller than the phase change in Path 2 (as seen in Figure 3.19b).

Furthermore, the magnitude of these changes is similar to those from the fire and smoke experiments. Therefore, if the experiment procedures are not designed carefully to avoid or minimize such interference from the movement of the person, it is possible for researchers to draw false conclusions about the impact of fire and smoke on RF signals.

Examining Subcarrier Groups at 5.14 and 5.21 GHz

To better visualize the difference in the variations of signal strength, we consider the normalized signal strength over 3 categories: the full spectrum and two subcarrier groups near 5.14 and 5.21 GHz. The full spectrum means the entire frequency range (5.14 - 5.20 GHz) that the VNA sweeps through in each frame. The specific frequency ranges for the subcarrier groups are 5.1457 - 5.1485 GHz and 5.2114 - 5.2142 GHz. These two subcarrier groups are selected because the changes are most visible in these two groups while they behave differently when the person enters the FoV following two different paths. The average of all data points within the corresponding frequency range over 0.5 seconds of data is plotted in Figure 3.20. The 95% confidence intervals for each data point are plotted with a lighter color. The results for Path 1 and Path 2 are shown in Figures 3.20a and 3.20b respectively.

For Path 1, the normalized signal strength fluctuates across the full spectrum as well as for the two subcarrier groups while the person is walking within the FoV. In Figure 3.20a, the magnitudes of the variations are similar (between about -2 and 1 dBm) for all 3 categories when the person is moving inside the FoV. However, the changes in signals are different during the period of time between 55 and 60 seconds. The signal strength for the subcarrier group near 5.14 GHz (the green line) decreases slightly, while the signal strength of the subcarrier group near 5.21 GHz (the blue line) increases slightly compared to the signal strength of the full spectrum. These small changes are most likely natural variations in the environment since there is no movement after the person leaves the FoV at 46 seconds.

However, when the person walks into the FoV along Path 2, the changes in the signal strength are different for the 3 categories. In Figure 3.20b, when the person is moving within the FoV, the normalized signal strength increases for the subcarrier group near

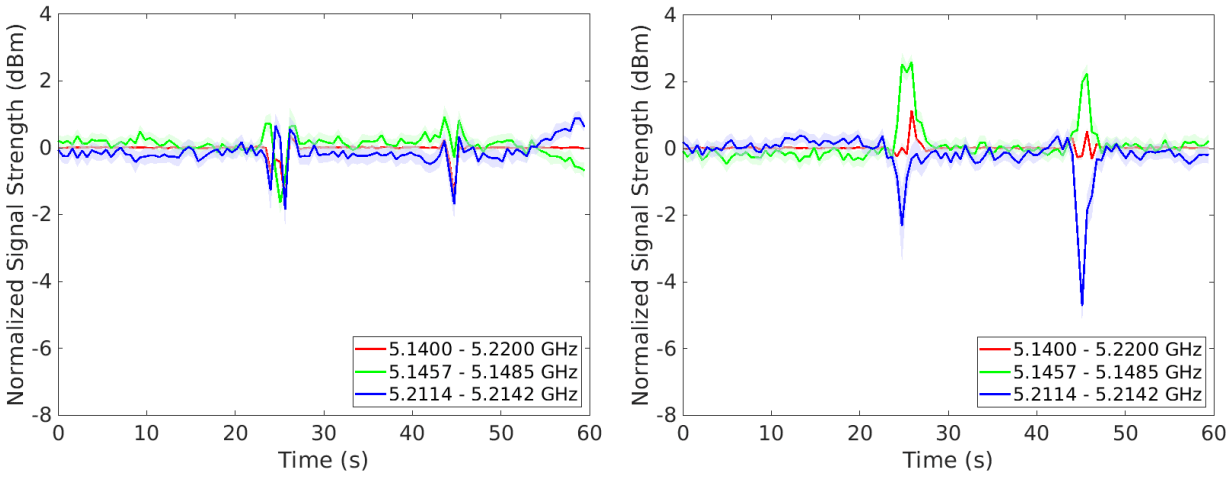

(a) Normalized signal strength over different parts of the spectrum for Path 1 after averaging over 0.5 seconds of data.

(b) Normalized signal strength over different parts of the spectrum for Path 2 after averaging over 0.5 seconds of data.

Figure 3.20: Normalized signal strength over different parts of the spectrum for Path 1 and Path 2. The x-axis is the time in seconds. The y-axis indicates the average values of the normalized signal strength in dBm over the selected frequency range. Each graph shows the averaged signal strength after normalization for the full spectrum (the red line) and two partial spectrums (the green and blue lines).

5.14 GHz (the green line) and decreases for the subcarrier group near 5.21 GHz (the blue line), while the full spectrum (the red line) lies between those two lines. It is interesting to observe that the signal strength goes up for one subcarrier group and goes down for the other. The largest difference between the signal strength within the two subcarrier groups is 4.85 dBm at 24 seconds and 6.71 dBm at 45 seconds. For the overall spectrum, the largest change in the normalized signal strength is 1.14 dBm (with a 95% confidence interval of [1.07, 1.21] dBm) at 26 seconds. For the subcarrier group near 5.14 GHz (the green line), the largest change is 2.60 dBm (with a 95% confidence interval of [2.36, 2.84] dBm) at 26 seconds. For the subcarrier group near 5.21 GHz (the blue line), the largest change is -4.74 dBm (with a 95% confidence interval of [-5.28, -4.20] dBm) at 45 seconds. Therefore, the changes caused by the movement of the person are statistically significant for all 3 frequency ranges.

It is worth noting that all 3 lines in Figure 3.20b are from the same recording. However, the movement of the person has a completely different impact on the signal strength when we look at different parts of the spectrum. Even for the same frequency range, the signal

strength may react differently when the person walks into the FoV following two different paths. For example, after the person enters the FoV at 22 seconds, the signal strength for the subcarrier group near 5.14 GHz (the green line) decreases in Figure 3.20a but increases in Figure 3.20b. Thus, one may draw completely opposite conclusions about the changes in the signal strength if only looking at a particular range of the spectrum.

Recall the plots from the previous Wi-Fi fire detection work [84] (Figure 3.16), since each figure only contains 2 seconds of data, it is possible that the changes we see in those graphs may be caused by the movement of the person lighting the fire and not the fire. We now examine a similar time period in Figure 3.21 by only showing 1 second before and after the person enters the FoV from Figure 3.20b with finer granularity. Each data point in Figure 3.21 is the average value of the raw data within the corresponding frequency range in a single frame (sweep). We also calculate the 95% confidence intervals for each data point. The normalized signal strength is fairly stable near 0 dBm for all 3 groups before 44 seconds and varies immediately after 44 seconds (when the person starts to enter the FoV). The signal strength for the subcarrier group near 5.14 GHz (the green line) increases after the person enters the FoV, with the largest change being 2.86 dBm (with a 95% confidence interval of [2.45, 3.27] dBm). Meanwhile, the signal strength for the subcarrier group near 5.21 GHz (the blue line) decreases after the person enters the FoV, with the largest change being -5.41 dBm (with a 95% confidence interval of [-7.02, -3.80] dBm). Although the changes in signal strength for the blue line seem larger than the other subcarrier group (the green line), the signal strength is also more variable in this group, resulting in a wider confidence interval. The signal strength for the full spectrum remains almost unchanged during the same time period. The difference in the green and blue lines corresponds to situations where the CSI amplitude goes up after the fire starts in some cases and goes down in others (e.g., in the work by Zhong et al. [84] as shown in Figure 3.16). If one was to only look at 2 seconds of data, as was done in the work by Zhong et al. [84], the changes in signal strength for the two subcarrier groups may be interpreted as being caused by fire. However, all changes we observe in Figure 3.21 are caused only by the movement of the person. These results again emphasize the importance of including more data before and after the fire starts and waiting until the signal strength stabilizes after the person leaves the FoV of the device.

Summary

The results of these experiments show that the movement of a person inside the FoV can lead to variations in signal strength and phase. Such variations, if not properly recognized and accounted for, could be mistakenly treated as the effects of fire or smoke. The

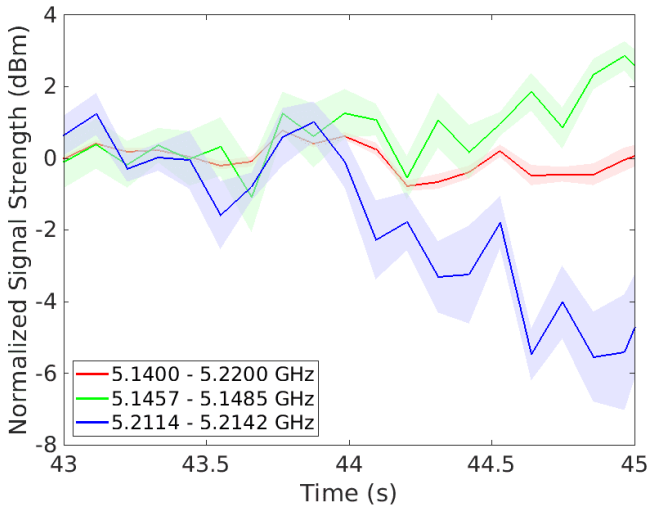

Figure 3.21: Normalized signal strength for Path 2 between 43 and 45 seconds (1 second before and after the person enters the FoV). Each data point represents the average value of all data points within the corresponding range in the spectrum for a single frame (sweep) of the VNA. The frame rate of the VNA device is 10 frames per second.

real effects of fire or smoke may also be overwhelmed by variations caused by movement. Therefore, it is important to avoid or minimize variations from unrelated causes during the experiment process to ensure the conclusions are correct and reliable.

Here is a list of measures we have taken and can be used as guidelines for others to use to improve the reliability of the findings:

- Turn off all nearby Wi-Fi access points that operate at similar frequencies.
- Minimize the movement inside the FoV of the antennas (e.g., we use a match attached to a 1.5-meter metal pole to light fires).
- Record a separate 1-minute baseline to understand the degree of variation that occurs naturally in the environment and normalize the fire experiment data against the baseline.
- Record some period of baseline data before we start the fire as well as after the fire goes out to understand the changes before and after the experiment (possibly natural changes in the environment).

- Repeat the same experiment multiple times and use statistical methods to draw conclusions.

Although it is impossible to eliminate all unrelated variations (e.g., changes brought by the movement of the metal pole) from the experiment, we should always be extra cautious about the possible influential factors from the environment when designing and conducting the experiments.

3.6 Conclusions

We observe that butane fire can moderately affect the propagation of RF signals near 5 GHz frequency bands with a limited distance (1.3 meters). Fire from heptane fuel appears to reduce the attenuation of RF signals and thus increases the signal strength at the receiver. We also observe phase shifts at the same time when the signal strength changes. Interestingly, the signal strength in some range of frequencies seems to decrease after the fire is lit (as shown in Figure 3.7). Recall from Section 2.4 and 2.5 that the attenuation of RF signals can be affected by the amount of oxygen and moisture in the atmosphere, as well as the ionization above the fire. However, the experiment results do not consistently align with either of the theories.

The changes in signals become very small when the distance between the two antennas is 3 meters. As for a larger fire with wood at a distance of 3 meters, we are unable to observe any changes while the fire is burning. After we extinguish the fire, the wood generates a lot of smoke that attenuates the RF signals. Thus, we can only observe changes in RF signals when the smoke is dense enough. Although it may not seem useful for detecting wood fires, it shows the potential of detecting smoke in structural fires for materials that generate a large amount of smoke when burning. The magnitude of changes in received signal strength and phase varies across the frequency spectrum. Some of the frequency bands seem to be impacted more by fire and smoke than the other frequencies. Therefore, one possible avenue for future work is to study the difference in the impact of fire for different frequencies in the spectrum.

As a result of our experiments, it seems difficult for commodity Wi-Fi access points to detect such small variations in signal strength or phase with the capabilities and limited accuracy of these devices. We suspect that the variations reported in the previous Wi-Fi fire detection paper [84] are likely caused by movement rather than fire due to the limited time window they used to collect data. The VNA used in our experiments has a much

higher frequency resolution than the Wi-Fi device in their work [84] (with 7 readings on the VNA per subcarrier group). It is also worth noting that unrelated factors like the movement of people nearby during the experiment may introduce extra variations in the recorded data. Thus, it is important to strictly control the environment and minimize the unrelated variations in the experimental procedures.

Chapter 4

Fire Detection using 5G Devices

4.1 Motivation

As described in Section 2.2 and 2.4, previous work on fire detection with RF signals has shown that fire can affect millimeter wave (mmWave) signals at 90 GHz [66] and 77 GHz [63]. Additionally, researchers have built radiometers for capturing the microwave signals emitted by fire at 12 GHz [11] and 30 GHz [12, 45]. These fire detection methods all rely on laboratory equipment or utilize devices that are originally designed for purposes other than fire detection. In this chapter, we examine the feasibility of using 28 GHz mmWave 5G cellular devices for fire detection. The 28 GHz mmWave 5G band is designed to provide high-throughput, low-latency network connection for indoor use cases [6]. If such devices can be used for fire detection, there will be no need for additional devices other than 5G base stations and mobile devices that communicate with the base station (e.g., a 5G mobile phone).

The hypothesis is that if the fire impacts wireless signals across a wide enough part of the RF spectrum or in different parts of the spectrum more than others, we may be able to observe changes in signals correspondingly on a 5G device. Thus, if we can collect useful information about signals received on the 5G device and those signals change enough to be noticed, one may be able to tell if there is a fire between the base station and the 5G device. Among the various frequency bands in 5G networks, the 28 GHz mmWave band is chosen in our experiment since previous work on wireless fire detection covers similar frequencies near the 30 GHz frequency band [12, 45] and because this is an emerging technology that can be used in the high-throughput, low-latency communication. We believe this frequency band may be affected by fire as well. Therefore, we use a 5G device to see if the fire between the

device and the base station affects the signals. Since the information about signal strength is also available on the 5G device, we would like to conduct fire experiments with this device and identify changes that are most likely due to fire.

4.2 Equipment

In this experiment, we use a Quectel RM510Q-GL [62] 5G modem (shown in Figure 4.1a) as the mobile device. The modem is configured to use the n261 mmWave 5G band [27] in the frequency range from 27.50 to 28.35 GHz with a bandwidth of 850 MHz. It is worth noting that the n261 band is not licensed in Canada at the time of this study. Thus, there are no mobile phones available for use with this band. The information related to the 5G network is easily accessible on the modem and we can connect it to a laptop for data collection and processing. Once we find the key metrics available on the 5G device that may help with fire detection, we can transfer that knowledge to other types of mobile devices and use the same metrics to implement fire detection applications on different platforms. To support Multiple-Input Multiple-Output (MIMO) technology [21] in modern 5G networks, the Quectel device has 2 transmitting antennas and 2 receiving antennas (4 antennas in total as shown in Figure 4.1a). The MIMO technology allows mobile devices to use multiple physical antennas to transmit data in parallel and achieve higher bandwidth. The n261 band used in this experiment is one of the 5G bands that supports MIMO technology. The base station used in the experiment is a local station installed by Rogers. A photo of the base station is shown in Figure 4.1b, with Figure 4.1c providing a distant view of the base station showing where it is mounted on the wall. It is mounted indoors on a wall between the second and third floors of the Davis Center at the University of Waterloo. The 5G SIM card used by the modem is also provided by Rogers to access the local station.

The modem is connected to a laptop using a USB 3.0 cable and an Ethernet cable. The USB cable is used to collect signal information and the Ethernet cable is used to access the network. We send AT commands [61] to the modem and receive output from those commands through the USB port to collect information about the 5G signals. We transmit data over the Internet through the Ethernet port to keep the modem active. Although it is possible to collect information and transmit data at the same time with a single USB cable, we separate the use of the Ethernet and USB ports to ensure that the data sampling rate is not throttled by the data transmitted.

Since the building is not dedicated to fire experiments, we cannot use the same fire source as in Chapter 3. As a result, a butane stove is used to create controlled fires during the experiments (shown in Figure 4.1d). The size of the fire is 10 cm in diameter on the

(a) Quectel RM510Q-GL 5G modem.

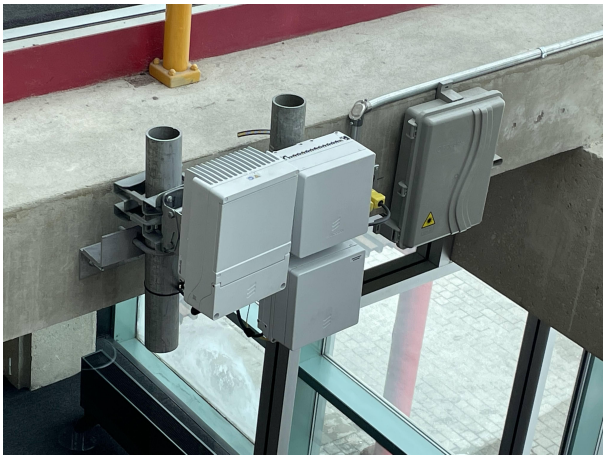

(b) Rogers 5G base station.

(c) Rogers 5G base station (distant view).

(d) Butane stove.

Figure 4.1: Photos of equipment used in 5G fire detection experiments.

butane stove. Since the fuel source is butane gas, we can easily control the combustion by turning the stove on and off.

Table 4.1 provides a list of potentially useful information available on the 5G devices we use along with descriptions. A subset is chosen from the available data because they seem to be related to the signal quality in the documentation of the modem [61]. However, not all metrics related to the signal strength can be effective indicators of fire and we narrow down the scope as we conduct experiments. To improve the readability of the table, we merge the cells with similar names and display the names in a hierarchy. For example, the RSRP PRX and RSRP DRX are two metrics both related to RSRP, so we merge RSRP in their names and display it in the first column. Since the 5G device we use in this experiment has 2 receiving antennas, they are identified as primary and diversity receivers (i.e., PRX and DRX). The metrics for PRX are usually considered first when selecting the best base station to communicate with. We include the metrics for both PRX and DRX for better coverage of the potential candidate metrics.

Metric Name		**Description**
RSRP	PRX	Reference Signal Receive Power for primary receiver
	DRX	Reference Signal Receive Power for diversity receiver
RSRQ	PRX	Reference Signal Receive Quality for primary receiver
	DRX	Reference Signal Receive Quality for diversity receiver
SINR	PRX	Signal to Interference and Noise Ratio for primary receiver
	DRX	Signal to Interference and Noise Ratio for diversity receiver
RSSI		Received Signal Strength Indicator

Table 4.1: Names and descriptions of 5G network metrics collected in experiments.

RSRP

The Reference Signal Receive Power (RSRP) measures the power level of the reference signal received by the mobile device. The reference signal is a special type of signal transmitted by the base station that provides useful information about the network [60]. The signal is transmitted at constant power for all base stations. Thus, mobile devices can use the quality of the received reference signal as an indicator of the channel conditions for nearby base stations. The RSRP is a negative value measured in dBm and an RSRP value closer to zero indicates a stronger signal. Since the transmission power of the reference signal is known and fixed on the base station, the RSRP can be used as an estimation of the transmission quality. In 5G networks, the RSRP is a primary factor for determining

the best base station to communicate with [65, 10, 38] when there is an overlap in the coverage of multiple base stations or cellular towers. The range of possible RSRP values is from -140 to -44 dBm on the 5G modem we use in our experiments [61].

RSRQ

The Reference Signal Received Quality (RSRQ) is defined as the ratio of the power level of the received reference signal to the power level of all received signals, including interference and noise. Thus, it can be viewed as an indicator of signal-to-noise. The RSRQ value is measured as a negative value in dB and values closer to zero correspond to signals with better quality. The RSRQ is a second factor used when choosing the best base station to communicate within 5G cellular networks [77], preceded by RSRP. The range of possible RSRQ values is from -20 to -3 dB on the 5G modem we use in our experiments [61].

SINR

The Signal to Interference and Noise Ratio (SINR) is the ratio between the power level of the signal of interest to the power level of interference and noise signals. The SINR is measured in dB, with possible values ranging from -23 to 40 dB on the 5G modem [61] we are using. A larger SINR value means better signal quality in the 5G network.

The difference between SINR and RSRQ is that the numerator in SINR is a measure of the signal quality for any wireless signals of interest in general, while RSRQ specifically measures the signal quality of the reference signal. The SINR is also an important factor that helps determine the maximum throughput of the 5G network [64, 9, 34].

RSSI

The Received Signal Strength Indicator (RSSI) is a measurement of the power level of the received signal on the mobile device. It is a common indicator of the received signal strength in many wireless communication systems (e.g., cellular networks, Wi-Fi, and Bluetooth). The RSSI is a negative value in dBm and a larger RSSI value means the signal is stronger. The 5G device in our experiments uses an integer between 0 and 31 to represent the RSSI. Table 4.2 shows the relationship between the returned values from the AT command and the real RSSI values [61]. The granularity of the RSSI is 2 dBm on the 5G device, which is much coarser than the VNA device used in the previous chapter. This should obviously make it more difficult to detect small changes in signal strength (e.g., if changes caused by

fire are smaller than 2 dBm). It is worth noting that the RSSI values of -113 dBm or less are all represented by 0 in the AT command response and values of -51 dBm or greater are all represented by 31. Therefore, this measure is only useful when the signal strength is in the intermediate range. We cannot distinguish changes in the signal strength using this metric when the signal strength is too strong or too weak.

Return Value	**RSSI**	**Signal Strength**
0	-113 dBm or less	Weak
1,2, ... ,30	-111 dBm to -53 dBm	Intermediate
31	-51 dBm or greater	Strong

Table 4.2: Conversion from the AT command return values to the RSSI values. The granularity of RSSI is 2 dBm on the 5G device. The last column shows the signal strength levels.

4.3 Methodology

The experiments we conduct in this section consist of two stages. In the first stage, we conduct some preliminary experiments with the movement of a person in the FoV without fire. The goal of this stage is to determine a set of potential indicators in 5G networks that can help us detect fire between the base station and mobile devices. The idea is that if a metric does not change significantly due to the movement of a person in the FoV, it is unlikely that this metric will change when the fire is present, since movement will cause more variations in the signal than fire (as we have seen previously). The second stage is used to observe the changes in the selected set of metrics with fire in the FoV. This set of experiments will help us to understand the impact of fire on the metrics related to RF signals available on the 5G devices we use.

Figure 4.2 shows a high-level overview of the experiment setup. The 5G device is connected to the laptop as described in Section 4.2. The distance between the 5G device and the base station is d as shown in the figure. In the experiments with fire, the butane stove is placed next to the 5G device to ensure that the FoV of the antennas on the device is covered by the fire. The center of the fire is about 30 cm from the antennas of the 5G device. The initial goal is to try to maximize the impact of fire on the 5G signals. If the signal is changed, we can later examine issues related to range of detection and fire locations (i.e., coverage).

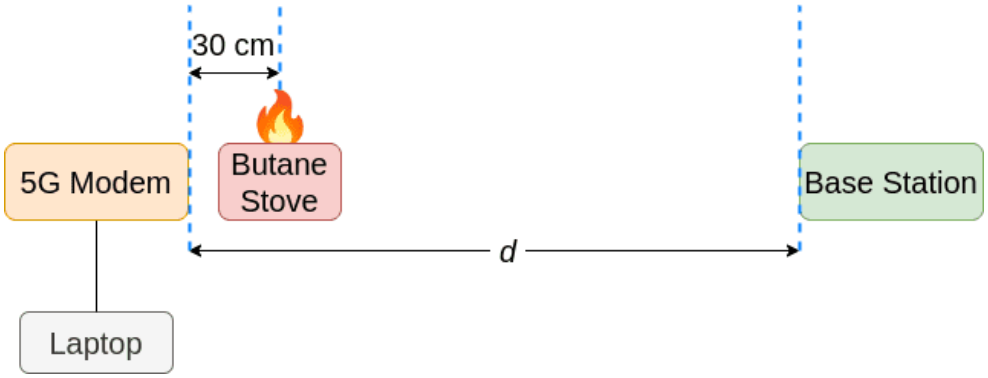

Figure 4.2: Experiment setup for fire detection with 5G devices. The distance d is measured from the mobile device to the base station. The center of the fire is about 30 cm from the antennas of the device.

4.4 Data Processing and Baseline Experiment

We created a Python script that uses AT commands to query all of the candidate metrics and store the data in a CSV file when the experiment is completed. This provided an average of approximately 20 readings for each metric per second. The raw data collected from each experiment is then processed and visualized in graphs. Figure 4.3 shows an example of the raw data for each metric from a baseline recording. The plot of the raw data is suitable for showing instantaneous changes during the experiment. However, it is difficult to compare the density of the points when they are close together and overlapping with each other (e.g., points between 0 and 10 seconds in the RSRP PRX raw data plot). As a result, we plot the average values over 3 seconds in Figure 4.4. We also include the 95% confidence intervals for the average using a lighter color for the background.

Even if the data is recorded in a static environment without any movement or fire, there will still be some variations in the metrics due to natural variations in the environment. It is important to understand the natural variations before we start any fire-related experiments to help distinguish the changes that happen naturally in the environment from those due to fire. We plot each 5G metric separately in its own graph for better visualization. The x-axis indicates the time in seconds and the y-axis indicates the value of the metric. The recording is 60 seconds long and the distance d between the 5G device and the base station is 3 meters. We keep the environment as static as possible during the experiment to minimize any unrelated factors that might cause changes in the 5G signals. All personnel stay behind the 5G device (outside the FoV) and remain stationary throughout the recording. There

is no fire involved in this experiment.

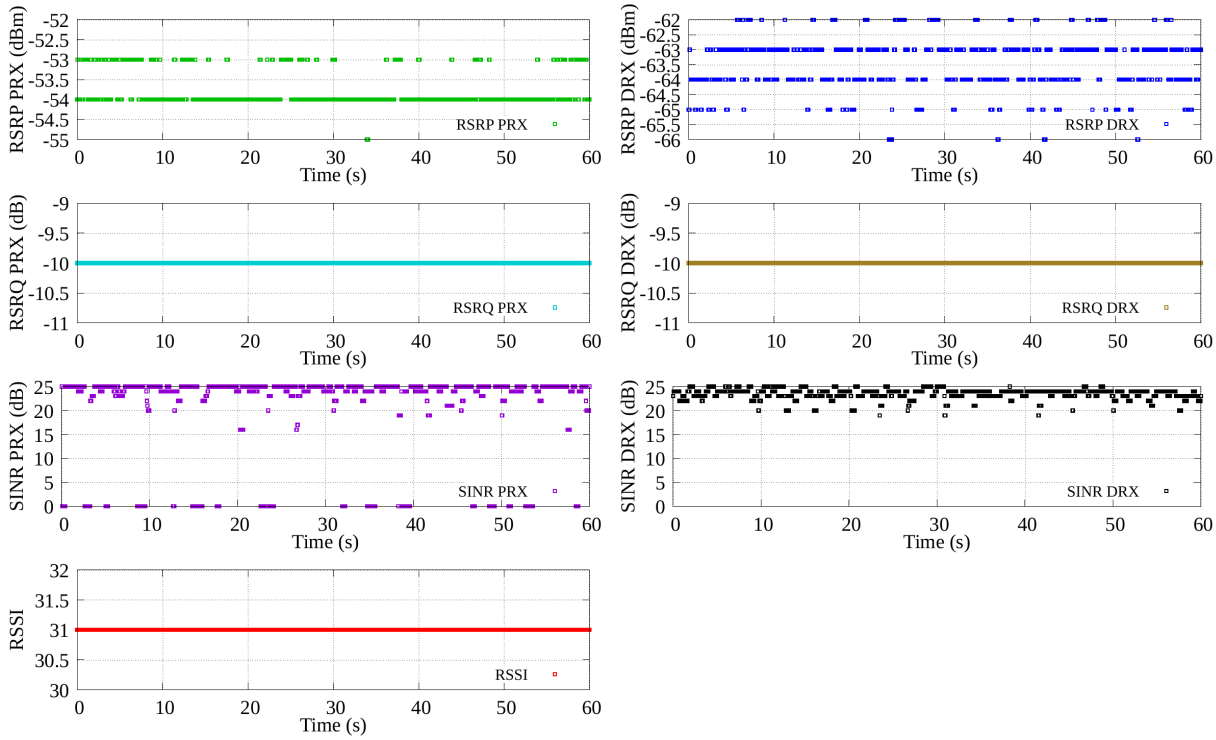

Figure 4.3: Raw data for each metric from the baseline experiment. The distance d between the 5G device and the base station is 3 meters. The x-axis indicates time in seconds and the y-axis contains values for the metrics.

In Figure 4.3, the RSRP PRX values are mostly at -54 and -53 dBm, with one outliner at -55 dBm at 33 seconds. The RSRP DRX values range from -66 to -62 dBm, with the majority of data points at -64 and -63 dBm. The range of the 3-second average is 0.5 dBm for RSRP PRX and 1.1 dBm for RSRP DRX in Figure 4.4. The RSRQ is also quite stable during the baseline experiment and the values are unchanged for both RSRQ PRX and RSRQ DRX. The variation in SINR PRX is larger than SINR DRX, with an 8 dB range for the former and 1.2 dB for the latter. As for SINR PRX, most of the data points are near the extreme values (0 dB and 20 - 25 dB). The SINR DRX values are mostly between 20 and 25 dB. For plots showing averages and confidence intervals, the SINR DRX also seems more stable than SINR PRX with smaller spans for the mean values and narrower confidence intervals. It is worth noting that the granularity for RSRP, RSRQ, and SINR is 1 dBm (dB) on the 5G device due to hardware limitations. Thus, there may be some minor

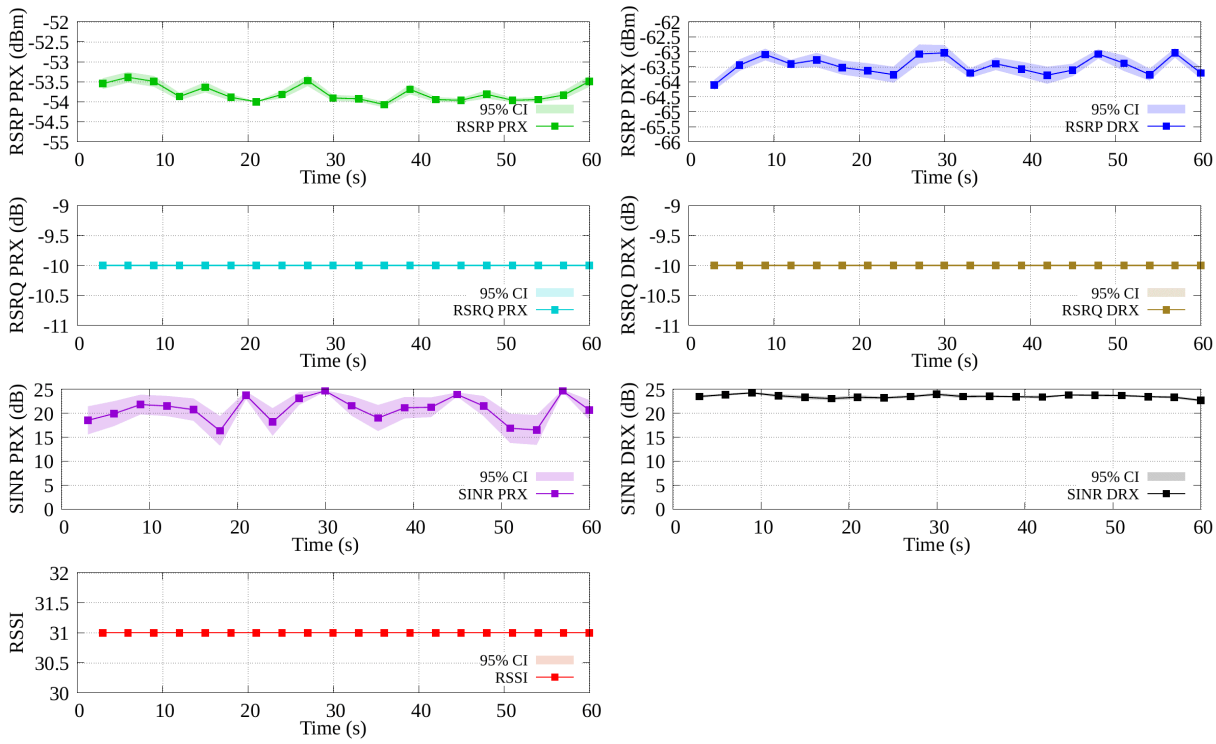

Figure 4.4: Average values for each metric over windows of 3 seconds from the baseline experiment. The distance d between the 5G device and the base station is 3 meters.

variations in RSRQ that are not reflected in the reported values. The RSSI is a flat line in the baseline experiment due to the poor mapping between real and reported RSSI values. The signal is strong at such a close range and thus the RSSI value is always reported as 31 on the 5G device (recall Table 4.2). We are not able to determine the variation in RSSI since the signal strength is above the threshold. Now that we have established a baseline for the natural variations for each metric of interest on the 5G device, we will be able to examine if there are additional variations due to fire by comparing the variations when there is fire with those seen in the baseline recording.

4.5 Movement Experiment

Motivation

In the previous section, we established a baseline for the changes of the selected metrics in the environment when there is no movement. Some metrics are quite stable in the baseline recording (e.g., RSRQ PRX and RSRQ DRX), while others have more variability (e.g., SINR PRX). In this section, we study the variations of each metric while a person is moving within the FoV of the device and further narrow the number of candidate metrics for fire detection. The idea is that if we cannot see any obvious changes due to the movement of the person for some metric, it is unlikely that we will be able to detect fire with the metric since the person is expected to introduce more changes in RF signals.

Methodology

The setup for the movement experiment is similar to Figure 4.2 except that the butane stove is not used in this experiment. The distance between the base station and the mobile device is $d = 25$ meters. The total duration of the experiment is 150 seconds. Table 4.3 shows a timeline for the events that occur during the movement experiments. The person walks into the FoV twice (at 30 and 90 seconds respectively) during the experiment. Each time the person stays in the FoV for about 30 seconds and walks back and forth along the direct path between the base station and the mobile device.

Time (s)	Event
0	Start recording
30 - 60	Person moves within the FoV
90 - 120	Person moves within the FoV again
150	End recording

Table 4.3: Events during the 5G movement experiment with corresponding timestamps.

Experiment Results

Figure 4.5 shows the raw data of the movement experiment for each candidate 5G metric from Table 4.1, namely RSRP, RSRQ, SINR, and RSSI. We plot each metric separately for better visualization, but they are all from the same experiment. We also calculate the

average values for every 3 seconds and show the results in Figure 4.6. Each data point in the graph is the mean value of the raw data over 3 seconds. The 95% confidence intervals for the means are shown with a lighter color. The x-axis indicates the time in seconds and the y-axis indicates the values of the metrics. We denote the name and unit of each metric beside the y-axis. The values for RSRQ and RSSI are quite stable during the experiment, but we can see some variations for RSRP and SINR.

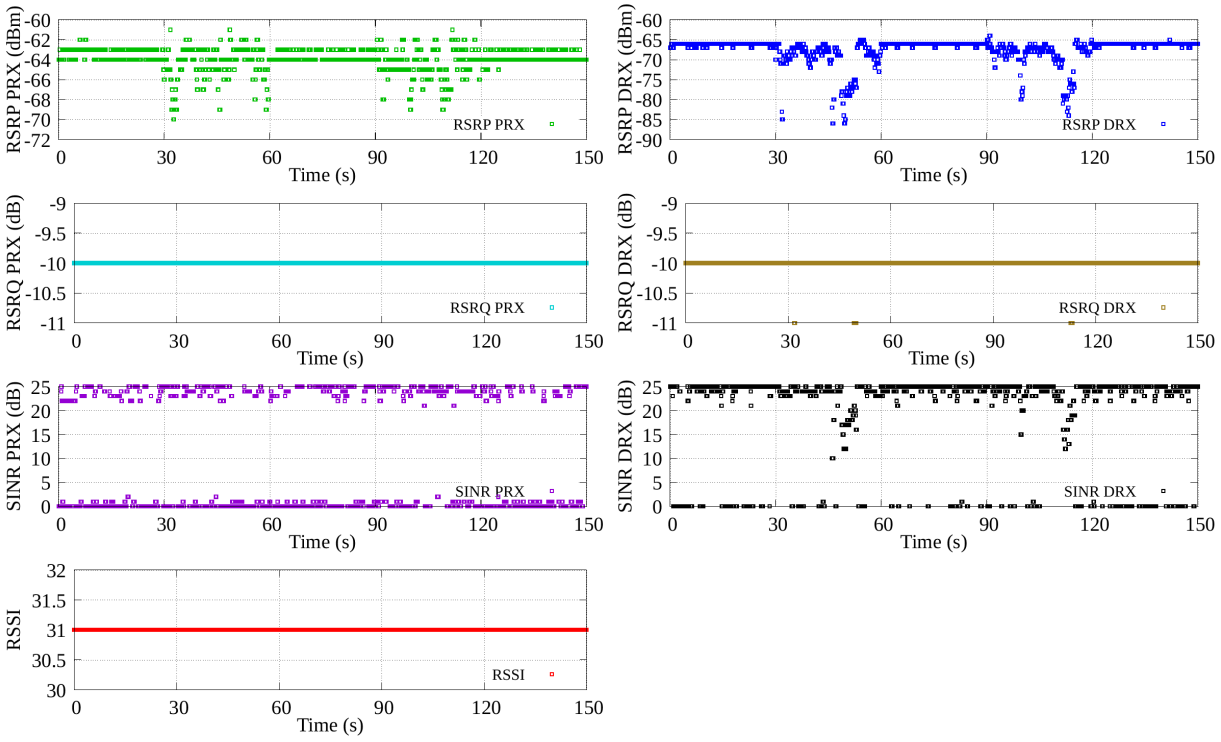

Figure 4.5: Raw data for each metric from the movement experiment. The distance d between the 5G device and the base station is 25 meters. The x-axis indicates time in seconds and the y-axis contains values for the metrics.

The two subfigures in the first row of Figure 4.5 show the values for RSRP PRX and RSRP DRX respectively, with the average values over 3 seconds shown in Figure 4.6. The periods of larger variations for both metrics match with the period of time when the person is walking within the FoV. In Figure 4.5, the values of RSRP PRX range from -64 to -62 dBm when the person is not in the FoV. We can observe large variations in RSRP PRX immediately after the person enters the FoV. The values of RSRP PRX vary from -70 to -61 dBm when the person is walking within the FoV (i.e., during the periods of 30 - 60 and

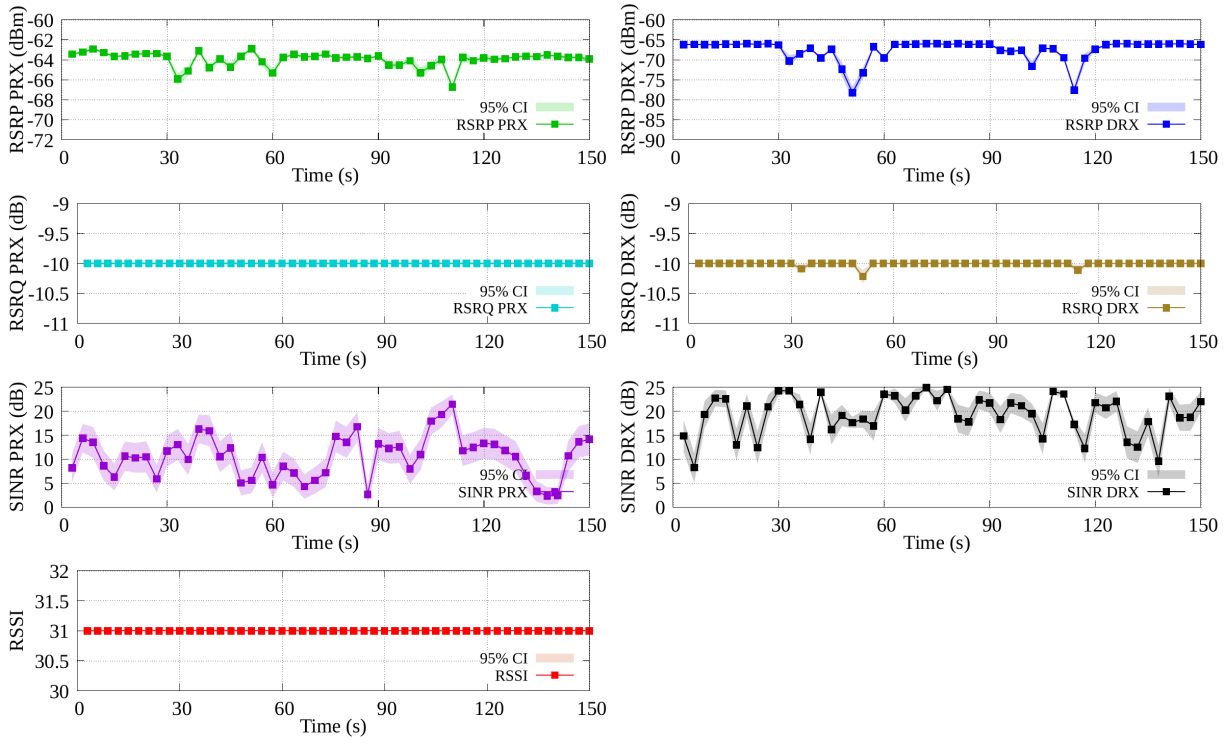

Figure 4.6: Average values for each metric over windows of 3 seconds from the movement experiment. The distance d between the 5G device and the base station is 25 meters.

90 - 120 seconds). As for RSRP DRX, the raw data is fairly stable before the person enters the FoV (between -67 and -66 dBm). Then the values of RSRP DRX range from -86 to -64 dBm after the person enters and moves within the FoV. In Figure 4.6, when comparing the values between 0 to 30 seconds with the largest change in a 3 seconds window is 3.3 dBm lower (with a 95% confidence interval of [2.9, 3.7] dBm) at $t = 111$ seconds for RSRP PRX and 12.1 dBm lower (with a 95% confidence interval of [10.6, 13.6] dBm) at $t = 51$ seconds for RSRP DRX. In general, the values for RSRP drop as the person enters the FoV since RSRP measures the signal strength of the reference signal and the person's body can attenuate the signal. However, there are some exceptions in RSRP PRX with slightly higher values when the person walks within the FoV than those before 30 seconds. In Figure 4.6, the values increase slightly at $t = 39$ and 54 seconds compared to the time periods when the person is outside the FoV. We believe the increase in signal strength is due to the additional reflection of signals from the person or because their movement changes the environment in ways that enhance multipath effects.

The results for RSRQ PRX and DRX are shown in the second row of Figure 4.5, with average values in Figure 4.6. In both figures, the RSRQ PRX is completely unchanged with a value of -10 dB during the experiment. There are only some slight variations for RSRQ DRX when the person is walking within the FoV. As for RSRQ DRX, the values are mostly -10 dB with some rare drops to -11 dB when the person is moving within the FoV (during the time periods of 30 - 60 and 90 - 120 seconds). In Figure 4.6, the largest change in a 3-second window is -0.2 dB (with 95% confidence interval of [0.1, 0.3] dBm) at 51 seconds, which is too small to reliably detect fire. It is worth noting that the changes caused by fire are likely smaller than those due to movement since the person's body can interfere more with the RF signals. Therefore, the RSRQ values will not be useful for fire detection given the small changes we observe in this experiment.

The third row of Figure 4.5 shows the results for SINR PRX and SINR DRX, with average values in Figure 4.6. In Figure 4.5, the SINR PRX data seems quite random and alternates near the extreme values (0 and 25 dB) even when there is no movement within the FoV. Although the values for SINR PRX vary throughout the whole experiment, we are unable to see a correlation between the variations and the movement of the person in the raw data plot or average data plots. Thus, the changes are just as likely to come from the natural variations in the environment rather than the movement of the person. This is similar to the characteristics of the value in the baseline experiment (as seen in Figure 4.3). Similarly, the values for SINR DRX range from 0 to 25 dB and follow a fairly bimodal distribution as well; where most of the points reside near the extreme values when there is no movement within the FoV. In Figure 4.5, when the person is moving within the FoV, some data points fall in the range of 10 to 20 dB. Although the changes in SINR DRX correspond with the time periods of movement, they are not as prominent as those in RSRP DRX (notice that the variations are visible right after the person enters the FoV at 30 and 90 seconds in RSRP DRX). The 3-second average values of SINR PRX and SINR DRX are generally lower and more variable than those in the baseline recording (as shown in Figure 4.4). The average values for SINR PRX are mostly between 0 and 20 dB in the movement experiment, while they are between 15 and 20 dB in the baseline recording. The average values for SINR DRX are mostly between 5 and 25 dB in this experiment, while they are between 20 and 25 dB in the baseline recording. Recall from Section 4.2 that SINR is the ratio between the signal strength and noise, higher SINR values indicate better signal quality. Thus, weaker signals are expected with more variations at the receiver side since the 5G device is placed farther from the base station in this experiment. There are no patterns in SINR PRX and SINR DRX in Figure 4.6 that reliably correspond to the movement of the person. As a result, we will not consider SINR in the analysis of the following experiments with fire.

The last row of Figure 4.5 shows the results for RSSI, with average values in Figure 4.6. The RSSI values remain constant during the experiment because (as mentioned in Table 4.2) the 5G device always reports the RSSI value as 31 when the signal is stronger than a threshold (-51 dBm). Therefore, even if the movement of the person introduces some variation in the RSSI, we will not observe any changes in the reported value if the value does not go below -51 dBm. However, we still include the RSSI in the next set of experiments since some of the experiments will have a larger distance between the base station and the mobile device, resulting in weaker signals at the receiver side. There is a chance that the RSSI may drop below the threshold and then visible changes may be observed.

Summary

The results of these experiments show that the movement of the person clearly affects the RSRP on the 5G device. The RSRQ is not useful since it is mostly constant during the experiment and the changes are not large enough to detect any movement (or fire). There are also variations seen in the SINR DRX values. However, the variations in SINR DRX are not as prominent as those in RSRP DRX. The changes in SINR DRX are not reflected in the average value plot since the values alternate near the extreme values (0 and 25 dB) due to natural variations in the environment. Thus, we believe that the RSRP DRX is a better metric than SINR DRX and we will not include SINR in the following sections. The movement may have an impact on the RSSI as well, but the changes are not visible due to how the RSSI is reported by the device. A possible way to utilize RSSI is to conduct the experiments at a longer distance where the signal is weaker so that the real RSSI value falls into the intermediate range and the variation can be observed in the converted RSSI value. Therefore, we will include RSRP and RSSI as the candidate metrics in the fire-related experiments and further examine their feasibility for fire detection.

4.6 Fire Experiments

Methodology

After identifying the potential metrics from our 5G device that may help with fire detection, we conduct experiments by starting a butane stove fire between the 5G device and the base station. The hardware setup for the fire experiment is shown in Figure 4.2. We conduct the experiments at 3 different distances: $d = 3, 28, \text{and } 60$ meters. The duration of each

experiment is 360 seconds. This is longer than the movement experiment in Section 4.5 since we want the fire to fully heat the surrounding air after we turn it on and provide some time for the environment to recover to the original state after we turn off the stove. The fire created by the butane stove is smaller than those we use in Chapter 3. Thus, it might take longer for the fire to create noticeable changes, if there are any. Table 4.4 shows the list of events during each round of experiments and their corresponding timestamps. At 60 seconds, a person reaches over to the stove but does not turn it on. This helps us distinguish any changes caused by the movement of the person while turning on the stove from those caused by the fire (as we have seen in Section 4.5). The person only reaches over to the stove for a short time (less than 5 seconds) and moves back behind the 5G device (outside the FoV of its antennas) immediately after pretending to operate the stove. We repeat the same experiment twice to ensure the results are consistent and reliable.

Time (s)	Event
0	Start recording
60	Reach over to the stove and pretend to turn it on
120	Turn on stove
240	Turn off stove
360	End recording

Table 4.4: Events during the 5G fire experiment with corresponding timestamps.

Experiment Results

Figure 4.7 shows the results for the experiments conducted at 3 meters. The raw data of the two trials are shown in Figure 4.7a and 4.7b. We then calculate the average values over a 5-second window and show the results in Figure 4.7c and 4.7d. Because of the longer time scales, each data point in the graph is the average value over 5 seconds instead of 3 seconds. The formats of the plots are similar to those in the movement experiment in Section 4.5. The x-axis indicates the time in seconds and the y-axis is the value for each metric.

In general, the RSRP PRX is quite stable throughout the experiment with some drops when the person reaches over to the stove at 60, 120, and 240 seconds. The raw data of RSRP PRX is mostly at -56 and -55 dBm in the first trial and at -54 and -53 dBm in the second trial. The values of RSRP PRX are generally higher in the second trial (likewise for RSRP DRX) because the laptop behind the 5G device (as shown in Figure 4.2) moved

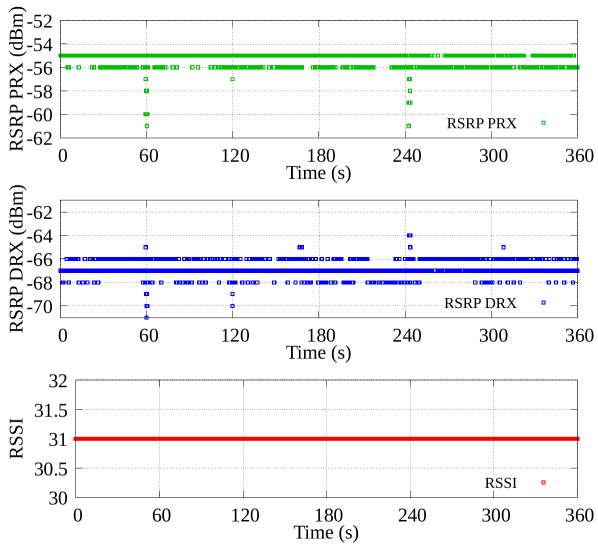

(a) Raw data for the first trial.

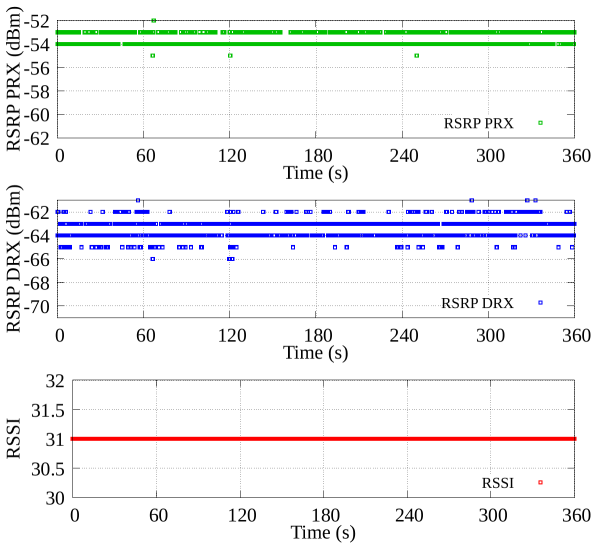

(b) Raw data for the second trial.

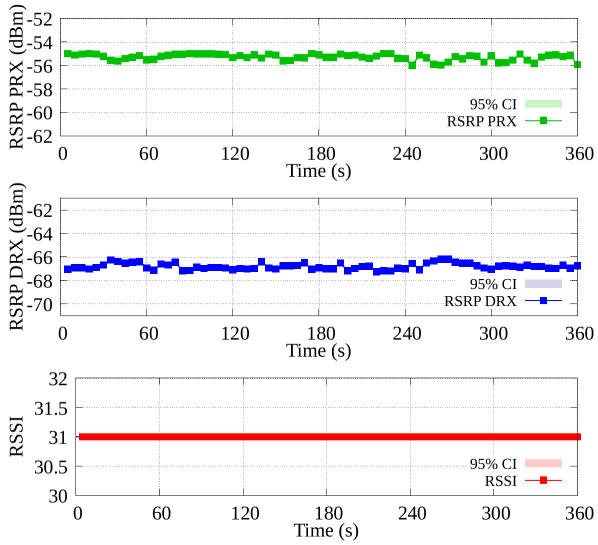

(c) Average values over 5-second windows for the first trial.

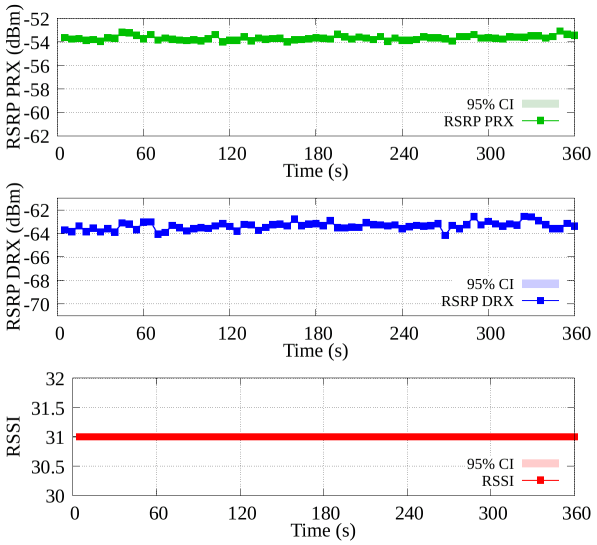

(d) Average values over 5-second windows for the second trial.

Figure 4.7: Results for the 5G fire experiment at $d = 3$ meters. The x-axis indicates the time in seconds and the y-axis is the value for each metric.

slightly when we started and ended the recording. The environment remains static during each trial. Thus, the difference between different trials of the same experiment does not affect the validity of our conclusions. The RSRP PRX appears to be more variable after the stove is turned off at 240 seconds in the first trial but not in the second trial. As for RSRP DRX, the raw data is mostly between -68 and -66 dBm in the first trial and between -65 and -62 dBm in the second trial. We also observe some variations caused by the movement of the person at 60 and 120 seconds while reaching over to the stove. The average values over the 5-second windows for RSRP PRX vary within 1 dBm and the changes in RSRP DRX are within 2 dBm in both trials. However, there are no clear and consistent patterns in RSRP PRX or RSRP DRX that are related to the fire. Again, the RSSI values in both figures are constant throughout the experiment since the signal is above -51 dBm at 3 meters.

Since we are unable to observe any changes in the reported RSSI values so far, we also conduct some experiments at longer distances from the base station in the hope that the RSSI value might fall into the intermediate range. Figure 4.8 shows the results for the experiments conducted at 28 and 60 meters. The raw data is shown in Figure 4.8a and 4.8b for 28 and 60 meters respectively. Then we calculate the average values for every 5 seconds and present them in Figure 4.8c and 4.8d. Although we conducted two trials, we only show one trial for each distance since the results for the two trials are similar in both scenarios. Overall, the RSRP PRX becomes weaker with higher variability due to the attenuation of RF signals as we increase the distance between the 5G device and the base station. The RSRP PRX ranges from -62 to -57 dBm in the 28-meter experiment and ranges from -69 to -66 dBm in the 60-meter experiment. The average values for RSRP PRX are within 2 dBm for both experiments. The RSRP DRX is more variable in the 28-meter experiment, ranging from -71 to -65 dBm, while the values in the 60-meter experiment are between -66 and -65 dBm. We believe this is because the multi-path effects improve the 5G signals, so the 5G device receives stronger signals at a longer distance. The interference brought by the person reaching over to the stove is not visible in any of the graphs. The reported RSSI values are constant in both experiments. There is no clear pattern for any of these metrics that matches the period when the fire is burning.

4.7 Conclusions

In this chapter, we conduct a series of experiments to identify and study potential metrics from our 5G device that might be used for fire detection. We first observe the variations in each metric when a person is walking within the FoV and reduce the candidate metrics to

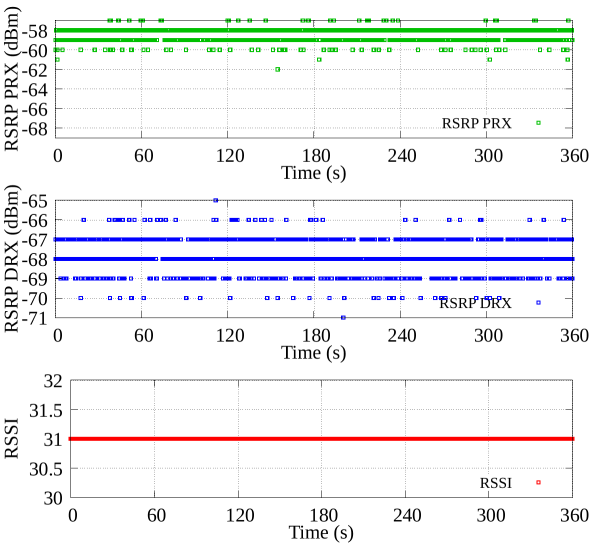

(a) Raw data for the 28-meter experiment.

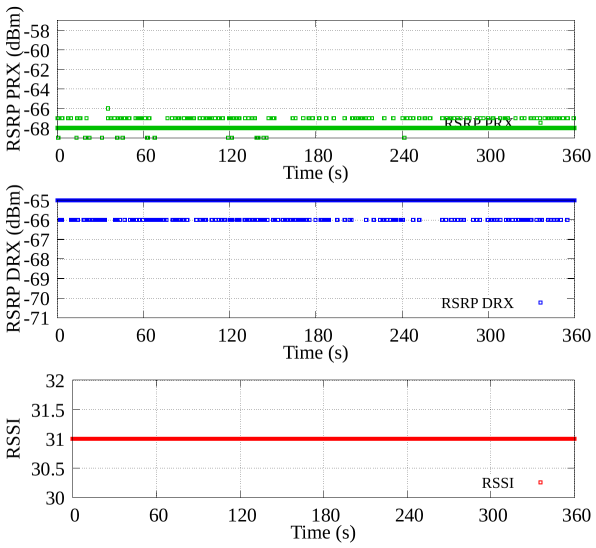

(b) Raw data for the 60-meter experiment

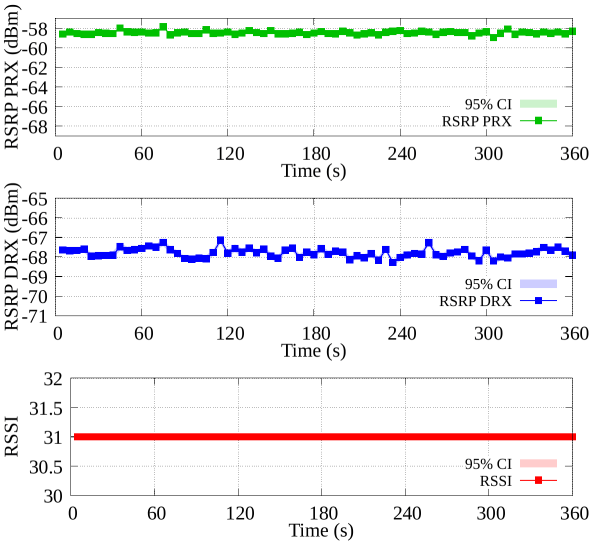

(c) Average values over 5-second windows for the 28-meter experiment.

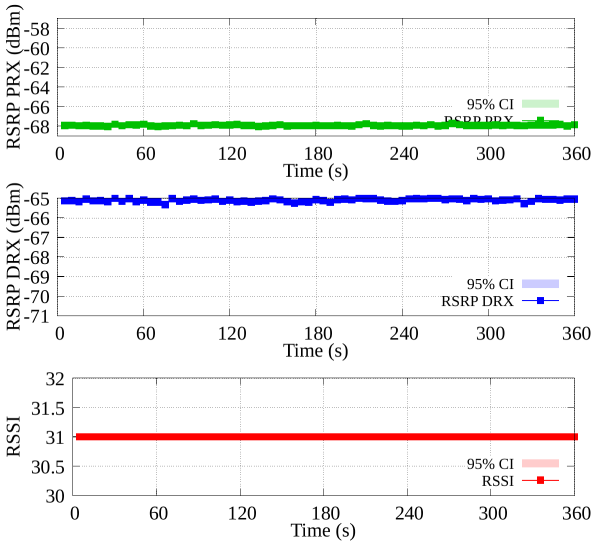

(d) Average values over 5-second windows for the 60-meter experiment

Figure 4.8: Results for the 5G fire experiment at $d = 28$ meters and $d = 60$ meters. The x-axis indicates the time in seconds and the y-axis is the value for each metric.

RSRP and RSSI. Experiments with fire are conducted at 3 different distances (3, 28, and 60 meters) to study the impact of fire on these metrics. The RSSI values remain constant during all experiments due to how RSSI is reported by the 5G device and the real RSSI value is always above -51 dBm. We are unable to see any distinguishable patterns in the changes related to the period of fire burning for any of the candidate metrics. Therefore, we conclude that so far the 5G device used in our experiments is not suitable for fire detection.

Future work could consider different locations where the signal strength is below the threshold of -51 dBm for RSSI so that one could examine the reported RSSI values. However, those distances might be too large to be useful for fire detection in some indoor environments. The size of the fire is another factor that may affect the results we observe. We only use a butane stove to start the fire in our experiments due to the safety regulations. In the future, we may use multiple butane stoves or change the type of fuel to create larger fires. This may have a more measurable impact on the 5G signals. We may also use a device with higher accuracy (e.g., a spectrum analyzer) to further investigate the impact of fire on RF signals in the 28 GHz frequency band.

Chapter 5

Conclusions and Future Work

5.1 Thesis Summary

Structural fires can result in casualties and property damage. Conventional, indoor fire detection devices like smoke detectors and fire alarms are hindered by long response times, the lack of penetration through walls, and nuisance (false-positive) alarms. In this thesis, we explore the feasibility of using wireless signals for fire detection, specifically RF signals in 5 GHz and 28 GHz frequency bands. Our work is motivated by previous work done on wireless fire detection using Wi-Fi and mmWave signals. Devices that use RF signals have the potential to overcome the disadvantages of conventional fire alarms since they would not require fire or smoke to reach the sensor before triggering the alarm, thus resulting in faster fire detection. We conduct a series of experiments using a Vector Network Analyzer (VNA) to study and try to better understand the underlying causes of changes in RF signals when a fire occurs between a pair of transmitting and receiving devices. We also examine the impact of two different fuels and compare the impact of smoke on RF signals. We then study the feasibility of using a 28 GHz mmWave 5G cellular network device for fire detection.

Many of the artifacts created during the completion of this thesis are available on the public repository: https://github.com/k47ma/fire-detection.

5.1.1 Fire Detection with 5 GHz RF Signals

Motivated by previous work on fire detection with 5 GHz Wi-Fi networks [84, 47], we use a VNA device to measure changes in the received signal strength and phase when a fire is

present between the transmitting and receiving antennas. The VNA device is configured to transmit signals in the same frequency range as in one of the previous studies [47] (5.14 - 5.22 GHz to simulate channel 36 with a bandwidth of 80 MHz in an 802.11ac network). We create a fire with two types of fuels: heptane and wood. For heptane fires, we observe only moderate changes in the signal strength and phase when the distance between the two antennas is small (1.3 meters). The received signal strength is slightly stronger when the fire is burning compared to the period when there is no fire. We observe that the magnitude of the changes also varies by frequency. In our experiments, the magnitude of changes in RF signals between 5.16 and 5.18 GHz is larger than those in other frequencies in the spectrum. There is also a very slight decrease in the signal strength near 5.14 GHz in the same experiment. However, the changes in the signals become imperceptible when we conduct the same experiment with a longer distance between the two antennas (3 meters).

As for wood fire (also studied at 3 meters), there are no visible changes that correspond to when the wood is burning. However, we observe a significant decrease in the received signal strength and a shift in the phase of the signal after the fire is extinguished and the wood starts to generate dense smoke. We believe this is because smoke attenuates the signals. It also means that when monitoring RF signals for changes due to fire, smoke might be a better indicator of fire since we can see changes with smoke after the fire is extinguished, but not while the wood fire is burning. This finding may be useful for detecting fire from materials that generate a large amount of smoke while burning in households (e.g., mattress and couch).

5.1.2 Fire Detection with Wi-Fi Devices

In the VNA experiments with heptane fire in Chapter 3, the largest change in signal strength in the VNA experiments is 1.37 dBm when the two antennas are 1.3 meters apart, and becomes imperceptible at 3 meters. Based on the results of the VNA experiments, it is unlikely that one can distinguish the changes caused by fire using Wi-Fi devices, since the VNA device used in our experiments has a much higher degree of accuracy (0.01 dBm [46]) than commodity Wi-Fi devices, which would typically be 1 dB [48]. Therefore, we believe it is unlikely that a Wi-Fi device could be used to detect fire at a useful distance like 3 meters. Because previous work by Zhong et al. [84] only show a very small window of time for the CSI amplitude values close to the start of the fire (1 second before and 1 second after), we believe that what was observed in their work is likely caused by the movement of the person lighting the fire rather than the fire itself. We expect that there is not enough time for the signal strength to stabilize after the person leaves the FoV. We also test this hypothesis by conducting some experiments where a person walks into the FoV

and pretends to light a fire. Our experiments show that the movement of the person can increase the signal strength in some subcarriers and decrease it in others. We expect that such changes could be mistaken for changes caused by fire unless signals were collected and examined for a longer period of time.

5.1.3 Fire detection with mmWave 5G Devices

In the second part of the thesis, we study the impact of fire on 5G network signals. We use the n261 mmWave 5G band in our experiments, with an operating frequency of 28 GHz. We use mmWave devices because previous studies using RF signals [63, 51, 32] report that the signals may be affected by fire. In addition, we hypothesize that 28 GHz signals might be more suitable because they have better propagation properties than the 77 GHz signals used in previous work [63]. Before we start any fire-related experiments, we first conduct experiments to study the impact that someone moving in the FoV might have on the metrics available on the device. The idea is that if the measurements of the signals are not changed by a person's movement, they are not likely to be changed by fire. We determine that the RSRP PRX and RSRP DRX are metrics that might potentially be useful for fire detection. We then use a butane stove to start some controlled fires between the base station and the 5G mobile device at 3 different distances (3, 28, and 60 meters from the mobile device to the base station) to investigate the impact of the fire. The fire is placed next to the mobile device (at a distance of 30 cm) in all scenarios. Unfortunately, we are unable to observe any consistent changes to these metrics that correlate with when the fire is burning. We also find that the RSSI reported is a constant value in all experiments, since the device always reports an RSSI of 31 for any signal strength above a threshold of -51 dBm.

5.2 Future Work

Understanding the Impact of Fire Size on RF Signals

In Chapter 3, we start fires with butane and wood as fuel sources. The heptane fire has a diameter of 12 cm with a height of at least 50 cm. The size of the wood fire is 45×20 cm with a height of at least 30 cm. We believe the sizes of fires in our experiments are as large or larger than those used in the previous Wi-Fi studies [84, 47]. However, structural fires could grow to be much larger than the fires we used in our experiments. In Chapter 4, we create a fire using a butane stove in the direct path between the base station and the 5G

mobile device. We only use a single butane stove to light the fire since the size of the fire is limited by the safety regulations of the building. In the future, we may conduct experiments with multiple butane stoves or other fuels to create larger fires if the environment permits. It would be interesting to conduct experiments with larger fires to determine if they have a more significant impact on RF signals.

Examining the Impact of Fire across a Broader Spectrum

The VNA device used in Chapter 3 is capable of scanning the spectrum from 9 kHz to 20 GHz [46]. The antennas we use operate in a slightly narrower range from 0.5 to 18 GHz. In the future, we may use other antennas that operate at a different range of frequencies to examine the impact of fire at a broader spectrum. One may also use a device that can sweep a broad range of frequencies (e.g., a spectrum analyzer) to determine if some frequencies are impacted by fire more than others.

Investigating the Fidelity of Wi-Fi devices' CSI with Controlled Attenuation

In Wi-Fi networks, Channel State Information (CSI) provides information about the signal strength and phase of the signal on the receiver side, both of which can be measured on the VNA as well. Previous work on Wi-Fi fire detection [84, 47] uses changes in the CSI as an indicator of fire. However, the exact magnitude of changes in signal strength from the Wi-Fi experiments is still unclear due to the lack of a universal standard in CSI. One could measure the sensitivity of the CSI being reported on the Wi-Fi devices being used by replacing the antennas on the Wi-Fi access points with cables that pass through an attenuator that can be used to manually control the amount of attenuation. The cabled connection between the transmitter and receiver minimizes the natural variation in the environment and the only source of attenuation is the cables and the attenuator. In this way, one could slowly increase the attenuation between the two devices until a change in the CSI is observed. This would provide a better understanding of the fidelity of Wi-Fi devices and determine the feasibility of using them to detect the small changes we have observed with the VNA device.

Measuring the Effectiveness of Smoke Detection using RF Signals

In Section 3.4.2, we discover that when the transmitting and receiving antennas are 3 meters apart, the changes in the signal strength and phase are imperceptible while the fire

is burning. However, after the fire is extinguished and the wood starts to generate dense smoke, we observe significant changes in both signal strength and phase. The impact of wood smoke on RF signals is also larger than those from heptane fire at the same distance (as in Section 3.3.2). Therefore, smoke may be a useful indicator of fire for indoor fire detection, especially when there are materials that generate dense smoke while burning (e.g., mattress and couch). It is worth testing the effectiveness of smoke detection using RF signals. Compared to conventional smoke detectors, detectors using RF signals could achieve shorter response times since they can sound an alarm before the smoke reaches the detector.

References

[1] *Electronic Warfare and Radar Systems Engineering Handbook*. Naval Air Warfare Center, 1999.

[2] M. Ali Babar Abbasi, Vincent F. Fusco, and Okan Yurduseven. High directivity beamformer for millimeter-wave 5G base stations. In *2020 IEEE 3rd 5G World Forum (5GWF)*, pages 309–311, 2020.

[3] Hervé Abdi and Lynne J. Williams. Principal component analysis. *WIREs Computational Statistics*, 2(4):433–459, 2010.

[4] Marty Ahrens. Smoke alarms in U.S. home fires. Technical report, National Fire Protection Association, Fire Analysis and Research Division, March 2011.

[5] Marty Ahrens and Radhika Maheshwari. Home structure fires. Technical report, National Fire Protection Association, Fire Analysis and Research Division, 2013.

[6] Naser Al-Falahy and Omar Y. Alani. Technologies for 5G networks: Challenges and opportunities. *IT Professional*, 19(1):12–20, 2017.

[7] Maher Al Naboulsi, Herve Sizun, and Frederique de Fornel. Fog attenuation prediction for optical and infrared waves. *Optical Engineering*, 43(2):319, 2004.

[8] Redhwan Algabri and Mun-Taek Choi. Deep-learning-based indoor human following of mobile robot using color feature. *Sensors*, 20(9):2699, 2020.

[9] Amaanat Ali, Umur Karabulut, Ahmad Awada, Ingo Viering, Olav Tirkkonen, Andre Noll Barreto, and Gerhard P. Fettweis. System model for average downlink SINR in 5G multi-beam networks. In *2019 IEEE 30th Annual International Symposium on Personal, Indoor and Mobile Radio Communications (PIMRC)*, pages 1–6, 2019.

[10] Anum Ali, Jianhua Mo, Boon Loong Ng, Vutha Va, and Jianzhong Charlie Zhang. Orientation-assisted beam management for beyond 5G systems. *IEEE Access*, 9:51832–51846, 2021.

[11] Federico Alimenti, Stefania Bonafoni, Salvatore Leone, Gabriele Tasselli, Patrizia Basili, Luca Roselli, and Klaus Solbach. A low-cost microwave radiometer for the detection of fire in forest environments. *IEEE Transactions on Geoscience and Remote Sensing*, 46(9):2632–2643, 2008.

[12] Federico Alimenti, Luca Roselli, and Stefania Bonafoni. Microwave radiometers for fire detection in trains: Theory and feasibility study. *Sensors*, 16(6), Jun 2016.

[13] Thierry Antoine-Santoni, Jean François Santucci, Emmanuelle de Gentili, Xavier Silvani, and Frederic Morandini. Performance of a protected wireless sensor network in a fire. Analysis of fire spread and data transmission. *Sensors*, 9:5878–5893, Jun 2009.

[14] Panagiotis Barmpoutis, Periklis Papaioannou, Kosmas Dimitropoulos, and Nikos Grammalidis. A review on early forest fire detection systems using optical remote sensing. *Sensors*, 20:1–26, Nov 2020.

[15] H Belcher and Theodore Morris Sugden. Studies on the ionization produced by metallic salts in flames: I. The determination of the collision frequency of electrons in coal-gas/air flames. *Proceedings of the Royal Society of London. Series A. Mathematical and Physical Sciences*, 201(1067):480–488, 1950.

[16] Carlo Bencivenni, Magnus Gustafsson, Abolfazl Haddadi, Ashraf Uz Zaman, and Thomas Emanuelsson. 5G mmWave beam steering antenna development and testing. In *2019 13th European Conference on Antennas and Propagation (EuCAP)*, pages 1–4, 2019.

[17] Leo Breiman. Random forests. *Machine Learning*, 45:5–32, 2001.

[18] Broadcom. BCM43455 Datasheet. https://datasheetspdf.com/datasheet/BCM43455.html, Nov 2015.

[19] Xian-Bin Cao, Hong Qiao, and John Keane. A low-cost pedestrian-detection system with a single optical camera. *IEEE Transactions on Intelligent Transportation Systems*, 9(1):58–67, 2008.

[20] Teng Hooi Chan, Henrik Hesse, and Song Guang Ho. LiDAR-Based 3D SLAM for indoor mapping. In *2021 7th International Conference on Control, Automation and Robotics (ICCAR)*, pages 285–289, 2021.

[21] Robin Chataut and Robert Akl. Massive MIMO systems for 5G and beyond networks - overview, recent trends, challenges, and future research direction. *Sensors*, 20(10), 2020.

[22] Shin Juh Chen, David C. Hovde, Kristen A. Peterson, and André W. Marshall. Fire detection using smoke and gas sensors. *Fire Safety Journal*, 42(8):507–515, 2007.

[23] Thou Ho Chen, Cheng Liang Kao, and Sju Mo Chang. An intelligent real-time fire-detection method based on video processing. *IEEE Annual International Carnahan Conference on Security Technology, Proceedings*, pages 104–111, 2003.

[24] Thomas G. Cleary and Artur Chernovsky. *Smoke Alarm Performance in Kitchen Fires and Nuisance Alarm Scenarios*. US Department of Commerce, National Institute of Standards and Technology, 2013.

[25] Anmol Sheth Daniel Halperin, Wenju Hu and David Wetherall. Tool release: Gathering 802.11n traces with channel state information, 2011.

[26] R. H. Dicke. *The Measurement of Thermal Radiation at Microwave Frequencies*, pages 106–113. Springer Netherlands, Dordrecht, 1982.

[27] Federal Communications Commission. Auction 101: Spectrum Frontiers - 28 GHz. https://www.fcc.gov/auction/101/factsheet, 2018.

[28] David D. Ferris Jr. and Nicholas C. Currie. Microwave and millimeter-wave systems for wall penetration. *Targets and Backgrounds: Characterization and Representation IV*, 3375(July 1998):269–279, 1998.

[29] Lars Ohlsson Fhager, Sebastian Heunisch, Hannes Dahlberg, Anton Evertsson, and Lars-Erik Wernersson. Pulsed millimeter wave radar for hand gesture sensing and classification. *IEEE Sensors Letters*, 3(12):1–4, 2019.

[30] Matthew S. Gast. *802.11 Wireless Networks: The Definitive Guide, 2nd Edition*. O'Reilly, 2013.

[31] Preea Gill and Rebecca V Martin. Smoke inhalation injury. *BJA Education*, 15(3):143–148, 2015.

[32] José-Tomás González-Partida, Pablo Almorox-gonzález, Mateo Burgos-garcía, Blas-Pablo Dorta-Naranjo, and José I. Alonso. Through-the-wall surveillance with millimeter-wave LFMCW radars. *IEEE Transactions on Geoscience and Remote Sensing*, 47(6):1796–1805, 2009.

[33] Francesco Gringoli, Matthias Schulz, Jakob Link, and Matthias Hollick. Free your CSI: A channel state information extraction platform for modern Wi-Fi chipsets. In *Proceedings of the 13th International Workshop on Wireless Network Testbeds, Experimental Evaluation & Characterization*, WiNTECH '19, page 21–28, New York, NY, USA, 2019. Association for Computing Machinery.

[34] Yichen Guo, Chunjing Hu, Tao Peng, Haiming Wang, and Xin Guo. Regression-based uplink interference identification and SINR prediction for 5G ultra-dense network. In *IEEE International Conference on Communications (ICC)*, pages 1–6, 2020.

[35] D. Gutmacher, U. Hoefer, and J. Wöllenstein. Gas sensor technologies for fire detection. *Sensors and Actuators, B: Chemical*, 175:40–45, 2012.

[36] Daniel Halperin, Wenjun Hu, Anmol Sheth, and David Wetherall. Predictable 802.11 packet delivery from wireless channel measurements. *ACM SIGCOMM Computer Communication Review*, 40(4):159–170, 2010.

[37] Congzheng Han and Shu Duan. Impact of atmospheric parameters on the propagated signal power of millimeter-wave bands based on real measurement data. *IEEE Access*, 7:113626–113641, 2019.

[38] Wang Hong, Li Bo, and Li Sikai. The impact of multi-mode on the 5G NR RSRP measurement model. In *2022 IEEE 10th Asia-Pacific Conference on Antennas and Propagation (APCAP)*, pages 1–2, 2022.

[39] Xu Huang, Hasnain Cheena, Abin Thomas, and Joseph KP Tsoi. Indoor detection and tracking of people using mmWave sensor. *Journal of Sensors*, 2021.

[40] Taewon Hwang, Chenyang Yang, Gang Wu, Shaoqian Li, and Geoffrey Ye Li. OFDM and its wireless applications: A survey. *IEEE Transactions on Vehicular Technology*, 58(4):1673–1694, 2009.

[41] Texas Instruments. AWR1642BOOST Evaluation Board. https://www.ti.com/tool/AWR1642BOOST.

[42] Cesar Iovescu and Sandeep Rao. The fundamentals of millimeter wave radar sensors. Technical report, Texas Instruments, Jul 2020. https://www.ti.com/lit/wp/spyy005a/spyy005a.pdf.

[43] Nalini C Iyer, Preeti Pillai, K Bhagyashree, Venkatesh Mane, Raghavendra M Shet, PC Nissimagoudar, G Krishna, and VR Nakul. Millimeter-wave AWR1642 radar for

obstacle detection: autonomous vehicles. In *Innovations in Electronics and Communication Engineering*, pages 87–94. Springer, 2020.

[44] Mohinder Jankiraman. *FMCW Radar Design*. Artech House, 2018.

[45] Thorsten Kempka, Thomas Kaiser, and Klaus Solbach. Microwaves in fire detection. *Fire Safety Journal*, 41(4):327–333, Jun 2006.

[46] Keysight Technologies. E5071C ENA Vector Network Analyzer. https://www.keysight.com/ca/en/assets/7018-01423/brochures/5989-5478.pdf, 2020.

[47] Junye Li, Aryan Sharma, Deepak Mishra, and Aruna Seneviratne. Fire detection using commodity WiFi devices. In *2021 IEEE Global Communications Conference, GLOBECOM 2021 - Proceedings*. Institute of Electrical and Electronics Engineers Inc., 2021.

[48] Mo Li and Yaxiong Xie. Atheros CSI Tool. https://wands.sg/research/wifi/AtherosCSI/.

[49] Ye Geoffrey Li and Gordon L Stuber. *Orthogonal Frequency Division Multiplexing for Wireless Communications*. Springer Science & Business Media, 2006.

[50] Haipeng Liu, Yuheng Wang, Anfu Zhou, Hanyue He, Wei Wang, Kunpeng Wang, Peilin Pan, Yixuan Lu, Liang Liu, and Huadong Ma. Real-time arm gesture recognition in smart home scenarios via millimeter wave sensing. *Proceedings of the ACM on Interactive, Mobile, Wearable and Ubiquitous Technologies*, 4(4):1–28, 2020.

[51] Chris Xiaoxuan Lu, Stefano Rosa, Peijun Zhao, Bing Wang, Changhao Chen, John A. Stankovic, Niki Trigoni, and Andrew Markham. See through smoke: Robust indoor mapping with low-cost mmWave radar. MobiSys '20, page 14–27, New York, NY, USA, 2020. Association for Computing Machinery.

[52] Yongsen Ma, Gang Zhou, and Shuangquan Wang. WiFi sensing with channel state information: A survey. *ACM Computing Surveys (CSUR)*, 52(3), Jun 2019.

[53] Giuseppe Marbach, Markus Loepfe, and Thomas Brupbacher. An image processing technique for fire detection in video images. *Fire Safety Journal*, 41(4):285–289, 2006.

[54] Sarah Masoumi, Thomas C Baum, Amir Ebrahimi, Wayne ST Rowe, and Kamran Ghorbani. Reflection measurement of fire over microwave band: A promising active method for forest fire detection. *IEEE Sensors Journal*, 21(3):2891–2898, 2020.

[55] K. M. Mphale, P. V.C. Luhanga, and M. L. Heron. Microwave attenuation in forest fuel flames. *Combustion and Flame*, 154(4):728–739, 2008.

[56] Kgakgamatso Mphale and Mal Heron. Microwave measurement of electron density and collision frequency of a pine fire. *Journal of Physics D: Applied Physics*, 40(9):2818–2825, May 2007.

[57] National Archives and Records Administration (NARA). 47 CFR Part 15 - Radio Frequency Devices. https://www.ecfr.gov/current/title-47/chapter-I/subchapter-A/part-15.

[58] DoWoo Park and Joon Goo Park. An enhanced ranging scheme using WiFi RSSI measurements for ubiquitous location. In *2011 First ACIS/JNU International Conference on Computers, Networks, Systems and Industrial Engineering*, pages 296–301, 2011.

[59] Raspberry Pi. Raspberry Pi 4 Model B. https://www.raspberrypi.com/products/raspberry-pi-4-model-b/.

[60] Yinan Qi, Mythri Hunukumbure, Hyungju Nam, Hyunil Yoo, and Saidhiraj Amuru. On the phase tracking reference signal (PT-RS) design for 5G new radio (NR). In *2018 IEEE 88th Vehicular Technology Conference (VTC-Fall)*, pages 1–5, 2018.

[61] Quectel Wireless Solutions Co., Ltd. RG50xQ & RM5xxQ Series AT Commands Manual. https://forums.quectel.com/uploads/short-url/avUSxfJeKqWJzAie8wEZCshlXjm.pdf, Oct 2020.

[62] Quectel Wireless Solutions Co., Ltd. Quectel RM510Q-GL 5G Specification. https://www.quectel.com/wp-content/uploads/2021/03/Quectel_RM510Q-GL_5G_Specification_V1.1.pdf, Mar 2021.

[63] David Radke, Omid Abari, Tim Brecht, and Kate Larson. Can future wireless networks detect fires? *BuildSys 2020 - Proceedings of the 7th ACM International Conference on Systems for Energy-Efficient Buildings, Cities, and Transportation*, pages 286–289, 2020.

[64] Anderson R. Ramos, Bruno C. Silva, Marisa S. Lourenço, Emanuel B. Teixeira, and Fernando J. Velez. Mapping between average SINR and supported throughput in 5G new radio small cell networks. In *2019 22nd International Symposium on Wireless Personal Multimedia Communications (WPMC)*, pages 1–6, 2019.

[65] Elizaveta Rastorgueva-Foi, Mário Costa, Mike Koivisto, Kari Leppänen, and Mikko Valkama. User positioning in mmWave 5G networks using beam-RSRP measurements and Kalman filtering. In *2018 21st International Conference on Information Fusion (FUSION)*, pages 1–7, 2018.

[66] Lev S. Sadovnik, Vladimir A. Manasson, Robert E. Chapman, Robert M. Mino, and Vladimir Kiseliov. Remote fire detection using MMW radiometric sensor. In *Passive Millimeter-Wave Imaging Technology II*, volume 3378, pages 73–80. SPIE, Aug 1998.

[67] Seemoo Lab. GitHub repository: seemoo-lab/nexmon. https://github.com/seemoo-lab/nexmon, 2023.

[68] V. I. Semenova. Reflection of electromagnetic waves from an ionization front. *Radiophysics and Quantum Electronics*, 1967.

[69] Jasbir Singh, Brian Ginsburg, Sandeep Rao, and Karthik Ramasubramanian. AWR1642 mmWave sensor: 76–81-GHz radar-on-chip for short-range radar applications. Technical report, Texas Instruments, May 2017. https://www.ti.com/lit/wp/spyy006/spyy006.pdf.

[70] M. Stefanidou, S. Athanaselis, and C. Spiliopoulou. Health impacts of fire smoke inhalation. *Inhalation Toxicology*, 20(8):761–766, 2008. PMID: 18569098.

[71] The MathWorks, Inc. VISA Interface - MATLAB & Simulink. https://www.mathworks.com/help/instrument/visa-interface.html.

[72] Onur Toker and Suleiman Alsweiss. MmWave radar based approach for pedestrian identification in autonomous vehicles. In *2020 SoutheastCon*, pages 1–2, 2020.

[73] Behcet Uğur Töreyin. Fire detection in infrared video using wavelet analysis. *Optical Engineering*, 46(6):067204, 2007.

[74] Pengfei Wang and Yufeng Luo. Research on WiFi indoor location algorithm based on RSSI ranging. In *2017 4th International Conference on Information Science and Control Engineering (ICISCE)*, pages 1694–1698, 2017.

[75] Yun-Ting Wang, Chao-Chung Peng, Ankit A. Ravankar, and Abhijeet Ravankar. A single LiDAR-based feature fusion indoor localization algorithm. *Sensors*, 18(4), 2018.

[76] Zhiqing Wei, Fengkai Zhang, Shuo Chang, Yangyang Liu, Huici Wu, and Zhiyong Feng. MmWave radar and vision fusion for object detection in autonomous driving: A review. *Sensors*, 22(7):2542, 2022.

[77] Widyasmoro, Indar Surahmat, Tony K. Hariadi, and Febian Dwi Putra. Comparative performance analysis of 4G and 5G cellular network technology in Indonesia: Case study in the city of Jakarta. In *2022 2nd International Conference on Electronic and Electrical Engineering and Intelligent System (ICE3IS)*, pages 158–163, 2022.

[78] Chenshu Wu, Zheng Yang, Zimu Zhou, Xuefeng Liu, Yunhao Liu, and Jiannong Cao. Non-invasive detection of moving and stationary human with WiFi. *IEEE Journal on Selected Areas in Communications*, 33(11):2329–2342, 2015.

[79] Yan Wu Li, Hong Yong Yuan, Yang Lu, Ru feng Xu, Ming Fu, Mengqi Yuan, and Ling Han. Experimental studies of electromagnetic wave attenuation by flame and smoke in structure fire. *Fire Technology*, 53(1):5–27, 2017.

[80] Shen Lin Yang, Song Lu, Xudong Cheng, Rong Zheng, and Richard Kwok Kit Yuen. Smoke production and fractal structure properties of soot from n-heptane pool fires under low pressures. *Fire Technology*, 52:1915–1937, Nov 2016.

[81] Norsuzila Ya'acob, Mohammad Syamirza Mohd Najib, Noraisyah Tajudin, Azita Laily Yusof, and Murizah Kassim. Image processing based forest fire detection using infrared camera. *Journal of Physics: Conference Series*, 1768(1):012014, Jan 2021.

[82] Mahnsuk Yoon, Changkyo Lee, Gilhwan Lim, Hyunchul Choi, and Kyucheol Cho. A fire detection scheme using 5G network-based KNN algorithm. In *2022 13th International Conference on Information and Communication Technology Convergence (ICTC)*, pages 2163–2165, 2022.

[83] Zhenwei Zhao and Zhensen Wu. Millimeter-wave attenuation due to fog and clouds. *International Journal of Infrared and Millimeter Waves*, 21(10):1607–1615, 2000.

[84] Shuxin Zhong, Yongzhi Huang, Rukhsana Ruby, Lu Wang, Yu Xuan Qiu, and Kaishun Wu. Wi-fire: Device-free fire detection using WiFi networks. In *IEEE International Conference on Communications*. Institute of Electrical and Electronics Engineers Inc., Jul 2017.

[85] Hai Zhu, Fu Xiao, Lijuan Sun, Ruchuan Wang, and Panlong Yang. R-TTWD: Robust device-free through-the-wall detection of moving human with WiFi. *IEEE Journal on Selected Areas in Communications*, 35(5):1090–1103, 2017.